

University of Montana

ScholarWorks at University of Montana

Graduate Student Theses, Dissertations, &
Professional Papers

Graduate School

1988

Acceleration of point source fire to equilibrium spread

Robert Stanley McAlpine
The University of Montana

Follow this and additional works at: <https://scholarworks.umt.edu/etd>

Let us know how access to this document benefits you.

Recommended Citation

McAlpine, Robert Stanley, "Acceleration of point source fire to equilibrium spread" (1988). *Graduate Student Theses, Dissertations, & Professional Papers*. 1465.
<https://scholarworks.umt.edu/etd/1465>

This Thesis is brought to you for free and open access by the Graduate School at ScholarWorks at University of Montana. It has been accepted for inclusion in Graduate Student Theses, Dissertations, & Professional Papers by an authorized administrator of ScholarWorks at University of Montana. For more information, please contact scholarworks@mso.umt.edu.

COPYRIGHT ACT OF 1976

THIS IS AN UNPUBLISHED MANUSCRIPT IN WHICH COPYRIGHT
SUBSISTS. ANY FURTHER REPRINTING OF ITS CONTENTS MUST BE
APPROVED BY THE AUTHOR.

MANSFIELD LIBRARY
UNIVERSITY OF MONTANA
DATE: 1988

THE ACCELERATION OF POINT SOURCE FIRE
TO
EQUILIBRIUM SPREAD

by

Robert Stanley McAlpine
Hon.B.Sc.F., Lakehead University, 1983

Presented in partial fulfillment of the requirements
for the degree of
MASTER OF SCIENCE
UNIVERSITY OF MONTANA
1988

Approved by


Chairman, Board of Examiners


Dean, Graduate School


Date

UMI Number: EP36561

All rights reserved

INFORMATION TO ALL USERS

The quality of this reproduction is dependent upon the quality of the copy submitted.

In the unlikely event that the author did not send a complete manuscript and there are missing pages, these will be noted. Also, if material had to be removed, a note will indicate the deletion.



UMI EP36561

Published by ProQuest LLC (2012). Copyright in the Dissertation held by the Author.

Microform Edition © ProQuest LLC.

All rights reserved. This work is protected against unauthorized copying under Title 17, United States Code



ProQuest LLC.
789 East Eisenhower Parkway
P.O. Box 1346
Ann Arbor, MI 48106 - 1346

The Acceleration of Point Source Fire to Equilibrium Spread (130 pp.)

Director: Ronald H. Wakimoto



The acceleration phase of a forest fire from ignition to equilibrium Rate-of-Spread (ROS) is perhaps the most important phase of fire behavior, because in many cases it represents the only time period in which suppression efforts could be effective. A total of 29 experimental fires, ignited in a wind tunnel, were conducted to investigate the acceleration of fire from a point source ignition. Two types of fuel, ponderosa pine (Pinus ponderosa Laws.) needles and excelsior fuel beds were burned in wind speeds ranging from 0.0 to 8.0 km/h. The results were analyzed as distance/time data, producing the equation:

$$\text{Distance} = \beta_0 (\text{Time})^{\beta_1}$$

for the acceleration phase of fire growth. The derivative of this equation, which describes the change in ROS with time, is initially, a steeply rising curve that converges with the line of equilibrium ROS.

The first coefficient of the above equation (β_0) was correlated with the observed equilibrium ROS, while the second coefficient (β_1) was correlated (in the form of a natural growth function) with wind speed.

The elapsed time required to reach equilibrium ROS, while different for the two types of fuel, was consistent over the range of wind speeds tested. The change in length-to-breadth ratio, measured over the life of each fire, failed to stabilize for any wind speed condition over 1.6 km/h.

Many aspects of the acceleration phenomenon still require further study. Nevertheless, the results of this initial investigation will find application in elliptical fire growth modelling of wildfires and in designing the grid pattern involved with prescribed fires ignited from single points.

ACKNOWLEDGMENTS

Rarely, if ever, can a thesis be considered a solo effort this being no exception. Thanks are extended to the members of my graduate committee Dr. Don Loftsgaarden and Dick Rothermel who put up with my pestering. I would also like to acknowledge the contribution of my committee chairperson, Dr. Ron Wakimoto, who was prominent in my entire educational experience. The members of the Canadian Forestry Service Fire Danger Group (M.E. Alexander, B.D. Lawson, B.J. Stocks and C.E. Van Wagner) provided valuable comments and inspiration.

The laboratory expertise, dedication and camaraderie of Merlin Brown, Bobbie Hartford, Bob Schutte and Gavriil Xanthopoulos (to name a few) is much appreciated.

I would also like to thank the Canadian Forestry Service, specifically the Northern Forestry Centre and the U.S. Forest Service for the opportunity to conduct the research and support of the study.

Finally I am indebted to my typist, editor, graphics artist and constant supporter; Caroline McAlpine, without whose help this thesis would not have been completed.

TABLE OF CONTENTS

	Page
ABSTRACT	ii
ACKNOWLEDGEMENTS	iii
TABLE OF CONTENTS	iv
LIST OF TABLES	vi
LIST OF FIGURES	vii
1.0 INTRODUCTION	1
1.1 Objectives	4
2.0 LITERATURE REVIEW	6
2.1 Field Observations	6
2.2 Theoretical Approximations	9
3.0 METHODS	21
3.1 Introduction and Experimental Design	21
3.2 Laboratory Facilities	23
3.3 Fuel Collection and Bed Preparation	25
3.4 Preburn Setup and Instrumentation	26
4.0 RESULTS AND DISCUSSION	31
4.1 Occular Time/Distance Results	33
4.1.1 Computation of Equilibrium Rate-of-Spread	37
4.1.2 Acceleration Phase	39
4.1.3 Allometric Equation Coefficient Models	44
4.1.4 Elapsed Time to Equilibrium Rate-of-Spread	64

4.2 Length-to-Breadth Analysis	67
4.3 Backing Fire Spread	71
4.4 Flame Length and Fire Intensity	74
5.0 SUMMARY AND CONCLUSIONS	78
5.1 Further Research Requirements	84
5.2 Equation Summary	86
LITERATURE CITED	87
APPENDICES	
I. Ocular Distance/Time Data	94
II. Fire Perimeter/Time Location Maps	104

LIST OF TABLES

Table	Page
1. An example of the possible differences in elliptical fire growth computations due to acceleration in head fire rate-of-spread (ROS).	4
2. Summary of environmental conditions and fire behavior for all fires.	32
3. Equilibrium head fire ROS values determined three ways for each burning treatment.	40
4. Equilibrium head fire ROS values and regression statistics for each burn conducted.	41
5. Regression coefficients and vital statistics for the allometric model of the acceleration phase weighted by the distance from the ignition point.	44
6. First, second and final predicted B coefficient values for each burning treatment.	50
7. Calculated elapsed time required to reach equilibrium ROS for all burning treatments.	65
8. Average equilibrium backing fire ROS values for each burning treatment.	73
9. Flame lengths by fuel type and burning treatment before and after the fire reached the edge of the fuel bed.	76

LIST OF FIGURES

Figure	Page
1. Head fire spread rate comparison of two concurrent experimental fires of spot and line origin.	10
2. Initial stages of fire development under calm conditions on level ground.	11
3. Idealized acceleration curves proposed by Kerr <u>et al.</u> (1971) and adapted by Pyne (1984).	13
4. Family of acceleration curves proposed by Luke and McArthur (1986) for various environmental conditions.	13
5. Comparison of two mathematical expressions for the theoretical acceleration of wildland fires, assuming 30 minutes to 90 percent of equilibrium ROS.	19
6. Acceleration pattern observed in forest fires (McArthur 1967).	19
7. Observed variation in head fire rate of spread and wind speed with elapsed time since ignition.	20
8. Profile section of the combustion research facilities at the Intermountain Fire Sciences Laboratory, Missoula, Montana (from Rothermel and Anderson 1966).	24
9. Perspective view of fuel bed layout.	28
10. Observed ROS versus Time for a needle fuel bed, with a bulk density of 26.3 kg/m ³ and burned at a wind speed of 4.8 km/h.	34
11. Distance versus time plot for needle fuel beds over the range of wind conditions tested.	35
12. Distance versus time plot for excelsior fuel beds over the range of wind conditions tested. .	36

13.	Allometric function A coefficient value plotted with equilibrium ROS for needle fuels.	45
14.	Allometric function A coefficient value plotted with equilibrium ROS for excelsior fuels.	45
15.	Allometric function A coefficient value plotted with wind speed for needle fuels.	46
16.	Allometric function A coefficient value plotted with wind speed for excelsior fuels.	46
17.	Allometric function B coefficient value plotted with equilibrium ROS.	51
18.	Allometric function B coefficient value plotted with wind speed.	51
19.	Effect of changing the B coefficient value in the allometric function while maintaining a constant A coefficient value of 4.0.	52
20.	Comparison of all observed data (open circles) and prediction line for needle fuel loaded at 26.3 kg/m ³ and burned with a wind speed of 0.0 km/h.	55
21.	Comparison of all observed data (open circles) and prediction line for needle fuel loaded at 26.3 kg/m ³ and burned with a wind speed of 1.6 km/h.	56
22.	Comparison of all observed data (open circles) and prediction line for needle fuel loaded at 26.3 kg/m ³ and burned with a wind speed of 4.8 km/h.	57
23.	Comparison of all observed data (open circles) and prediction line for needle fuel loaded at 26.3 kg/m ³ and burned with a wind speed of 8.0 km/h.	58
24.	Comparison of all observed data (open circles) and prediction line for needle fuel loaded at 13.1 kg/m ³ and burned with a wind speed of 4.8 km/h.	59

25.	Comparison of all observed data (open circles) and prediction line for excelsior fuel loaded at 3.6 kg/m ³ and burned with a wind speed of 0.0 km/h.	60
26.	Comparison of all observed data (open circles) and prediction line for excelsior fuel loaded at 3.6 kg/m ³ and burned with a wind speed of 1.6 km/h.	61
27.	Comparison of all observed data (open circles) and prediction line for excelsior fuel loaded at 3.6 kg/m ³ and burned with a wind speed of 4.8 km/h.	62
28.	Comparison of all observed data (open circles) and prediction line for excelsior fuel loaded at 3.6 kg/m ³ and burned with a wind speed of 8.0 km/h.	63
29.	The effect of wind speed on the elapsed time required to attain equilibrium ROS for all burning treatments.	66
30.	Variation in Length-to-Breadth values over time for needle fuel treatments.	69
31.	Variation in Length-to-Breadth values over time for excelsior fuel treatments.	70
32.	Variation in mean backing fire ROS over the range of wind speeds tested for all burning conditions.	73
33.	Comparison of observed pattern of ROS variation in laboratory tests with theoretical patterns.	79

THE ACCELERATION OF POINT SOURCE FIRE
TO
EQUILIBRIUM SPREAD

1.0 Introduction.

An active forest fire front is said to have three basic characteristics: (1) it spreads, (2) it consumes fuel, and (3) it produces heat energy in a visible flaming combustion reaction (Alexander 1982). This study deals with the spreading characteristics of fire, or more precisely, the rate of acceleration from the time of ignition until an equilibrium spread rate has been achieved. Currently, methods for predicting a fire's rate of spread (ROS) yield only the equilibrium ROS for a given set of fuel-weather conditions. This predicted equilibrium ROS could be compared to the speed limit on a highway (the speed limit assumedly fluctuating with terrain and other conditions). However, just as any particular car on the highway cannot achieve the speed limit instantaneously from a standing start, neither can a forest fire at inception be expected to spread at the same rate as a fully developed fire. Extending this analogy further; the time required for the car to reach the speed limit is

affected by several factors (e.g. engine size, car weight, weather and road conditions, etc.), and similarly, many factors could affect the rate at which a forest fire approaches its equilibrium spread rate.

Experimental endeavors in Canada into the spread of forest fires have been empirical in nature and have mostly been concerned with the equilibrium or maximum spread rate of an established line fire for a particular type of fuel burning in measured weather and fuel moisture conditions. These experiments, with the addition of wildfire documentation, have led to the information contained in recent publications (Alexander et al. 1984, Lawson et al. 1985, McAlpine 1986, 1987) on quantitative fire behavior prediction in Canada. Limited experimental results on point source fires have been reported by Lawson (1972, 1973) and by Alexander et al. (1988). Lawson (1972, 1973) was able to develop a relationship (although fairly weak) to predict ROS of an initiating fire using time since inception and wind speed. Alexander et al. (1988) did not attempt to develop any kind of acceleration function.

In the United States, the fire behavior prediction system is based on physical models of heat transfer (Rothermel 1972, 1983). As in Canada, the predicted

fire behavior parameters (ROS, intensity, etc.) are for equilibrium ROS conditions and although, initiating fire shapes (Anderson 1983, Alexander 1985) are applied to the models to determine perimeter length and area, no consideration is made for differences between initiating and established fire behavior. Some of the current U.S. models have tried to account for acceleration (eg. Fried and Gilless 1987) while others do not (eg. Andrews 1986).

In much of Australia, fire behavior prediction is based on the McArthur Fire Danger Rating System (McArthur 1973). This system predicts fire behavior in much the same way as the Canadian System. Potential fire behavior is predicted from fire danger ratings which are derived from meteorological data (McArthur 1966, 1967, Noble et al. 1980, Luke and McArthur 1986). This system was developed on the basis of over 5000 documented wildfires and 500 prescribed fires (Chandler et al. 1983). The predicted fire behavior is however for established fires, with no provision for incipient fire behavior.

Chandler et al. (1983) notes that "*[all these fire prediction systems] should be used with caution in the initial stages of a fire since they will over predict*

spread rates and do not provide for the increasing fire intensity...". Differences in predicted elliptical fire size with and without an acceleration effect can be considerable (see Table 1).

Table 1. An example of the possible differences in elliptical fire growth computations due to acceleration in head fire rate of spread (ROS). Equilibrium ROS = 14 m/min, elapsed time since ignition = 40 min, and 10-m open wind speed = 20 km/h.

Situation	Forward fire spread distance (m)	Fire area (ha)	Fire perimeter length (m)
A: acceleration ignored	560	16.9	1982
B: acceleration considered ¹	368	8.1	547

¹assuming the fire attains 90% of its final spread rate by 30 min since ignition (Alexander 1987).

1.1 Objectives.

The primary objective of this study is to develop a baseline acceleration function which, in a quantifiable manner, predicts the change in head fire ROS from the time of ignition until equilibrium ROS has been attained. Additionally, the effects of wind speed, fuel moisture, type of fuel, and fuel loading will be evaluated and included in the resulting function. To

eliminate random fluctuations in wind speed, wind direction and other influential environmental factors, a laboratory study with highly controlled burning conditions was conducted.

Secondarily, due to the experimental design, it will be possible to measure other fire attributes as they change over the life of the fire. Backing fire spread rates under various wind speeds in two types of fuel and in two fuel loading conditions will be evaluated. Current models of backing fire spread predict a constant ROS over a variety of wind speeds although few studies of backing fire spread rates have been done in the laboratory. The length-to-breadth (L/B) (or length-to-width) ratio (Anderson 1983, Alexander 1985), a fire shape and consequent fire area and perimeter length prediction model, will be evaluated as it changes over the measurable life of the fire. Current fire shape models are based on a single L/B measurement (for any particular environmental condition) and assume that there is no change over time. Changing fire intensity, based on flame length measurements, will be monitored to compare to an observation recently found by Nelson and Adkins (1986). They noted, in a laboratory study, constant flame lengths regardless of wind speed.

2.0 Literature Review.

2.1 Field Observations of the Acceleration Phenomenon.

Most of the past research in fire behavior has been concerned with the equilibrium ROS. Relatively little work has been devoted expressly to the development phase of fire behavior although, as Albini (1984) notes, "*no theoretical description of the early phase of fire development has been put forward yet, in spite of the fact that in some cases the buildup period is the only time when a fire can be suppressed*". The earliest documented observations of the incipient phase of fire growth are reported by Show (1919) where he notes that once a fire is established, it can create its own draft and increase its growth rate.

Specific field observations of acceleration from an experimental point source fire were noted as early as 1938 by Curry and Fons. They noted that under zero wind speed conditions, acceleration was completed within two minutes, while with higher winds, acceleration was still appreciable after 22 minutes (Curry and Fons 1938; 1940).

Williams (1955) completed a total of 33 fires ignited from a point source in an investigation of fire

hazard abatement. Unfortunately all of the original data has been lost except for the single plot presented as an example in the publication. This plot in Jack Pine (Pinus banksiana Lamb.) slash measured 100 ft. by 100 ft. and the fire was still accelerating as it reached the plot boundary after 10 minutes.

McArthur (1968) found that a fire burning with wind speeds around 9.7 km/h (6 mph) had achieved equilibrium in about 15 minutes, while under similar fuel and weather conditions a fire burning in 25.7 km/h (16 mph) winds was still accelerating after 20 minutes. McArthur (1968) further noted that in many cases "*during the acceleration period] suppression forces have their greatest chance of success*". McArthur (1971), working in 6 year old P. caribea and P. ellioittii plantations in the Fiji Islands found ROS to accelerate in an asymptotic manner, stabilizing in about 20 minutes for two separate fires burning in different fuel-weather conditions.

Lawson (1972, 1973), while working in lodgepole pine (Pinus Contorta Dougl. var. latifolia Engel), found point source fires to accelerate for a period of up to 48 minutes before complete equilibrium ROS was attained. Lawson (1972,1973) also was able to derive a

relationship to predict ROS from time since ignition and wind speed. The actual equation was a log-log transformation of ROS and elapsed time with an additional wind function (Lawson 1972). The function was statistically significant, however the predictive quality ($R^2 = 0.293$) was poor (Lawson 1972).

Kiil (1975) in a Black Spruce (Picea Mariana L.) stand in northern Alberta, Canada, found head fire ROS increased from 0.6 m/min during the first 3 minutes to 6.6 m/min, 10 minutes following ignition.

Comparisons of head fire spread rates for concurrent point and line source ignitions done by Johansen (1987) showed very different results for the two types of fires. Johansen (1987), found equilibrium ROS from a point source was achieved in about 12 minutes; however, this spread rate was much lower than the spread rate exhibited by the simultaneously ignited line origin fire (Fig. 1). Alexander et al. (1988), working in the black spruce - lichen woodland of the Northwest Territories, Canada, conducted two pair of simultaneous point and line source fires, however due to plot size constraints, equilibrium ROS was not attained in either case. A third point source fire, conducted shortly after a line source fire, attained equilibrium ROS after about 20

minutes (Alexander et al. 1988). On a fire control operation in the Northwest Territories of Canada, Lanoville and Schmidt (1985) made the following comparative observations:

"The burnout operation on July 8 also afforded the opportunity to assess the forward rate of spread of a point ignition and an established "line" fire burning under nearly identical environmental conditions. The point ignition originated from an unintentional "drip" from the helitorch device following the line of fire applied during the burnout operation. The resulting 'spot fire' advanced 50 m in 20 min, before being suppressed, for an average spread rate of 2.5 m/min compared to the line fire which progressed 335 m in 21 min for a mean forward rate of spread of 16 m/min."

2.2 Theoretical Approximations of The Acceleration Phenomenon.

In a discussion on the differences between point and line source ignition devices, Rothermel (1985) states:

"Fires lit from point source devices tend to be less intense and of longer duration than those lit as a line of fire ... the fire will gradually expand and grow in intensity ... until the fire reaches an intensity that will just support its flame structure and rate of spread" (i.e. equilibrium).

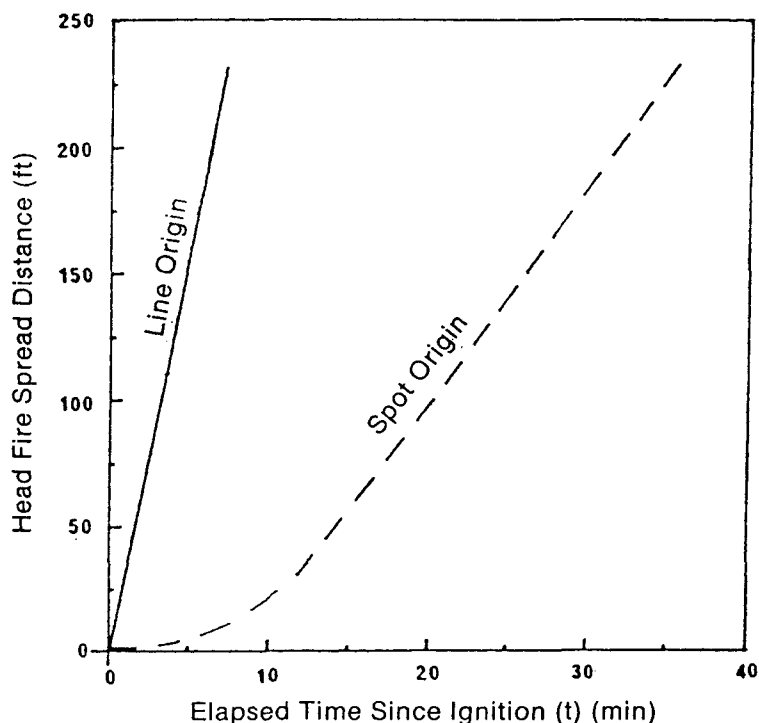


Figure 1. Head fire spread rate comparison of two concurrent experimental fires of spot and line origin (Johansen 1987). The slope of the straight line section in each case is the observed equilibrium ROS.

Most holistic theories of fire growth from a point source divide development into two to three phases, each phase releasing more of the total available potential energy (Chandler et al. 1983, Luke and McArthur 1986, Pyne 1984). Briefly, the first period is initial build-up of heat with the fuel in the center of the fire becoming consumed (Fig. 2) and the fire establishing a surface spread rate. The second stage can be referred to as the transition stage (Luke and McArthur 1986) in

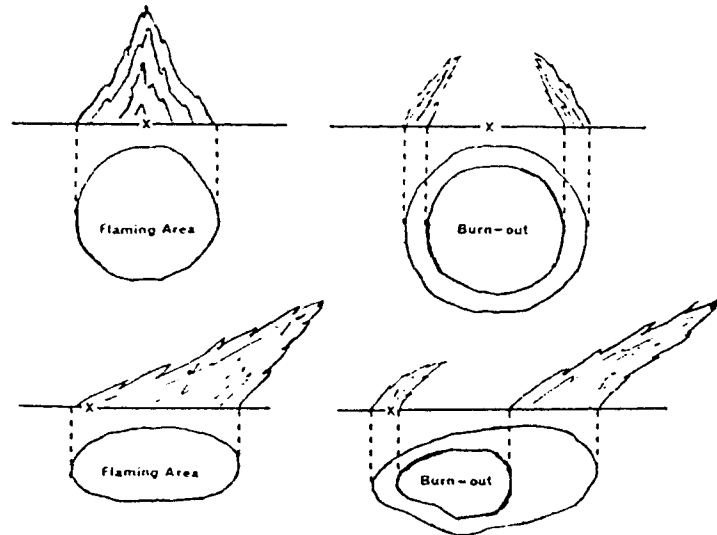


Figure 2. Initial stages of fire development under calm and windy conditions on level ground (Pyne 1984).

which, if conducive environmental conditions exist, the fire will become "three dimensional", develop a convection column and begin to influence wind in the area of the fire (Luke and McArthur 1986). The fire spread models in the U.S., Canada, and Australia will predict ROS following the second stage of development (Chandler et al. 1983). The third phase of development (occurring only if environmental conditions permit) involves a towering convection column which can induce advanced erratic fire behavior characterized by long range spotting, fire whirlwinds, and firestorms (Chandler et al. 1983, Luke and McArthur 1986, Pyne 1984). Generally, the time periods for each phase will vary in length depending on the type of fuel and

loading, and the burning conditions (Brown and Davis 1973, Chandler et al. 1983, Pyne 1984). The present study is restricted to investigation of the first two phases of the holistic view of fire evolution.

Conceptual theories exist to predict acceleration rate but they do not address the problem mathematically. Kerr et al. (1971), for example, provides several idealized acceleration curves (Fig. 3) and identifies 8 principal factors contributing to the acceleration:

1. *fuel moisture content of dead fuels less than 1/4 inch diameter and outer shells of larger materials*
2. *kind, size and distribution of surface fuel*
3. *moisture content gradient in large dead fuels or in depth of litter fuels*
4. *fuel weights*
5. *surface wind speed*
6. *slope - positive or negative*
7. *burnout time of fuel*
8. *convection column - does or does not form.*

Luke and McArthur (1986) also provide a series of possible curve forms (Fig. 4) and identify as factors:

1. *moisture content of fuels less than 6mm (1/4 inch)*

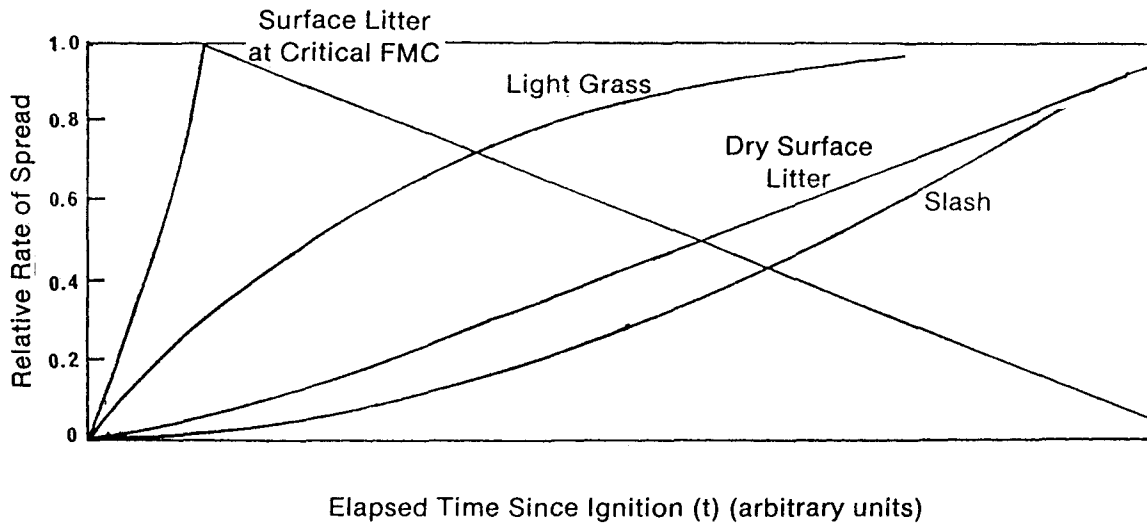


Figure 3. Idealized acceleration curves proposed by Kerr et al. (1971) and adapted by Pyne (1984). Critical fuel moisture content (FMC) indicates that once the fire has passed the initial stage of burning, fuel moisture is too high for sustained combustion.

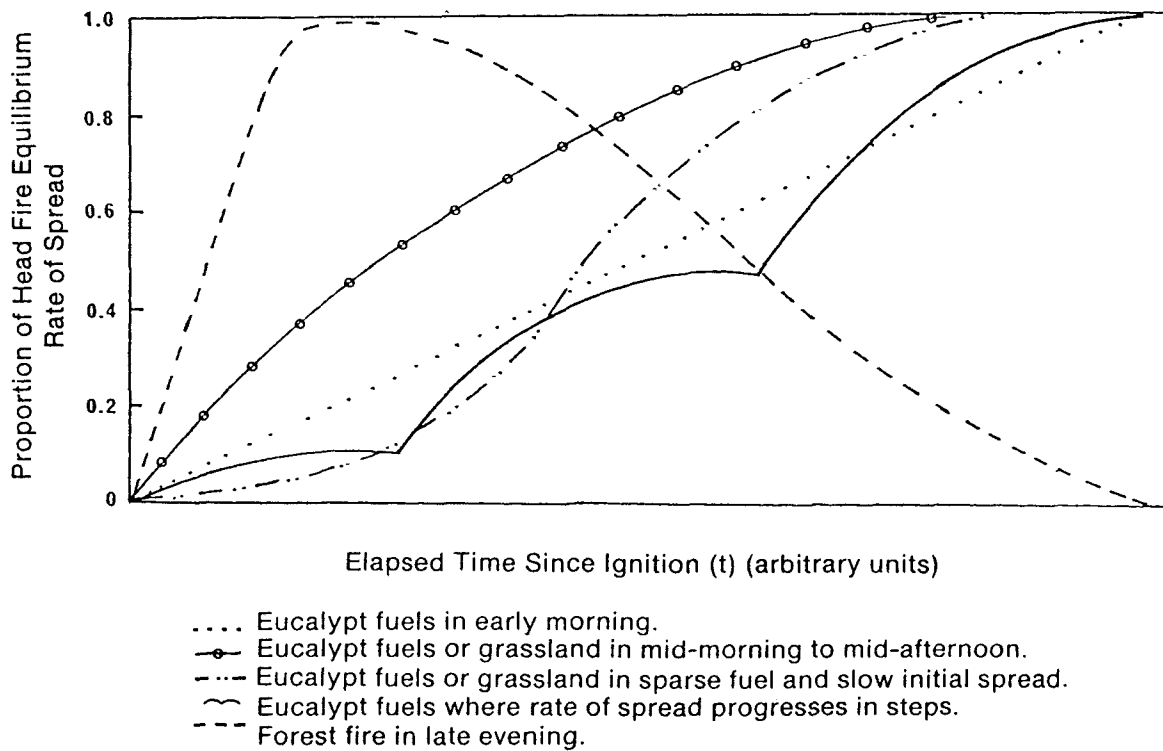


Figure 4. Family of acceleration curves proposed by Luke and McArthur (1986) for various environmental conditions.

2. *moisture content of living vegetation and heavy dead fuels*
3. *fuel surface area and distribution of fuel in the vertical plane*
4. *combustion rate and burn-out time of fuels*
5. *surface wind speed*
6. *atmospheric instability*
7. *slope*
8. *spotting process.*

The two lists are suspiciously similar with most of the major points repeated and some minor disagreements on a few of the principle factors.

Catchpole (1982), in an attempt to statistically analyze the acceleration of several experimental fires in grassland with sparse eucalyptus trees, found that:

"... the rate of spread in different fires changes linearly in different ways with time, but on the average, over all fires, the rate of spread does not vary linearly with time, as the changes in spread rate with time over all fires cancel out."

Cheney (1981) suggests an equation for acceleration in standing timber of the form:

$$\text{ROS} = \text{Re} * e^{-a/t} \quad [1]$$

where: ROS = head fire rate of spread at time t
 Re = equilibrium spread rate
 t = elapsed time since ignition
 a is a constant.

Consideration is not made of specific types of fuel (other than the broad grouping of standing timber), fuel moisture content, or concurrent weather.

Catchpole and Catchpole (1983) found that both equation [1] as well as a power law model:

$$\text{ROS} = a * t^b \quad [2]$$

where: ROS = head fire rate of spread at time t
 t = elapsed time since ignition
 a and b are constants,

fit observed field data for acceleration. Although the power law model [2] fit the data better, the fact that the asymptotic model [1] predicted an eventual steady state, made it the preferred model. In this study it was also observed that "the acceleration of the fires thus appears to be affected by environmental conditions" (Catchpole and Catchpole 1983).

Factors calculated by Cheney and Bary (1969) for a fire in standing eucalypt forest produced an equation similar to [1]:

$$\text{ROS} = 70.13 e^{-2.1645/t} \quad [3]$$

where: ROS = head fire ROS at time t (ft/min)
t = elapsed time since ignition (min).

The curves produced from equation [1] and the more definitive variant [3] are asymptotic to the final equilibrium ROS. Further, in equation [3] the time required to attain 90 percent of the final ROS is equal to 20 minutes, 32 seconds. All of the model equations ([1] - [3]) can be mathematically integrated to give the forward spread distance at any given elapsed time. Backing fire spread distance can be approximated to determine the total spread distance (and, using an elliptical fire growth model, perimeter length and area) by using the head fire/backfire spread ratio (H/B) derived by Alexander (1985).

Van Wagner (1985) suggests that acceleration is independent of the prevailing burning conditions and suggests the equation:

$$\text{ROS} = \text{Re} (1 - e^{-at}) \quad [4]$$

where: ROS = head fire rate of spread at time t
 Re = the equilibrium spread rate
 t = the elapsed time since ignition
 a is a constant.

Van Wagner (1985) suggested that, in the absence of data, 30 min. to reach 90 percent of the equilibrium ROS might be a reasonable first estimate and using this assumption, provided an "a" coefficient value of 0.0768. Both equations, [1] and [4], produce steeply rising curves attaining 50 percent or better of the equilibrium spread rate within ten minutes of ignition (Fig. 5) (assuming 30 minutes to 90%). Equation [4] presented here in its integrated form provides forward or downwind spread distances for any given elapsed time (after Van Wagner 1985):

$$D = \text{Re} \left(t + \frac{e^{-0.0768t}}{0.0768} - \frac{1}{0.0768} \right) \quad [5]$$

where: D = head fire spread distance at time t
 Re = equilibrium spread rate
 t = elapsed time since ignition.

Weber (1988), in a mathematical analysis of the physics of accelerating fire spread theorized that acceleration to equilibrium spread was a function of the curvature of the fire front; the greater the curvature, the faster rate of acceleration. This hypothesis therefore links the changing length-to-breadth ratio (Alexander 1985) of an incipient fire with the acceleration to equilibrium spread. The curve produced from this physical model is similar to those suggested by Van Wagner (1985), and Cheney (1981) (Fig. 5).

McArthur (1966, 1967) suggests a step-like progression for acceleration in grasslands and standing timber where, as the heat output of a fire front increases, thresholds of further fuel involvement are achieved, thus beginning further acceleration (Fig. 6) (Anon. 1975; Chandler et al. 1983). Thus far the limited experimental evidence supports the step-like progression (McArthur 1966, 1967), the asymptotic curve (Cheney and Bary 1969; Van Wagner 1985), and the power law model (Catchpole and Catchpole 1983). A typical plot of head fire rate-of-spread (ROS) versus time as shown in Figure 7, using data from Big Fish Lake Experimental Burning Site, shows the variable nature of the empirical field data and tends to confuse the

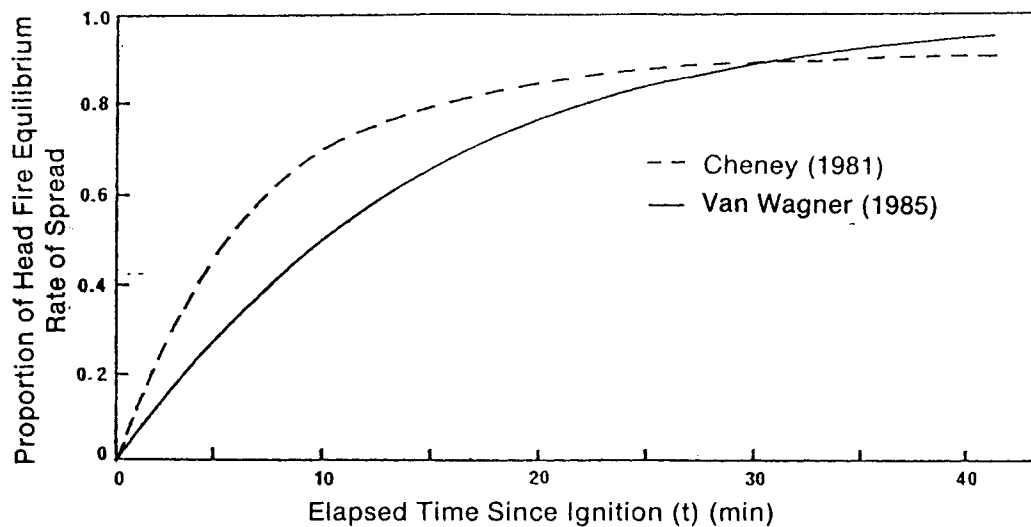


Figure 5. Comparison of two mathematical expressions for the theoretical acceleration in wildland fires, assuming 30 minutes to 90% of equilibrium ROS.

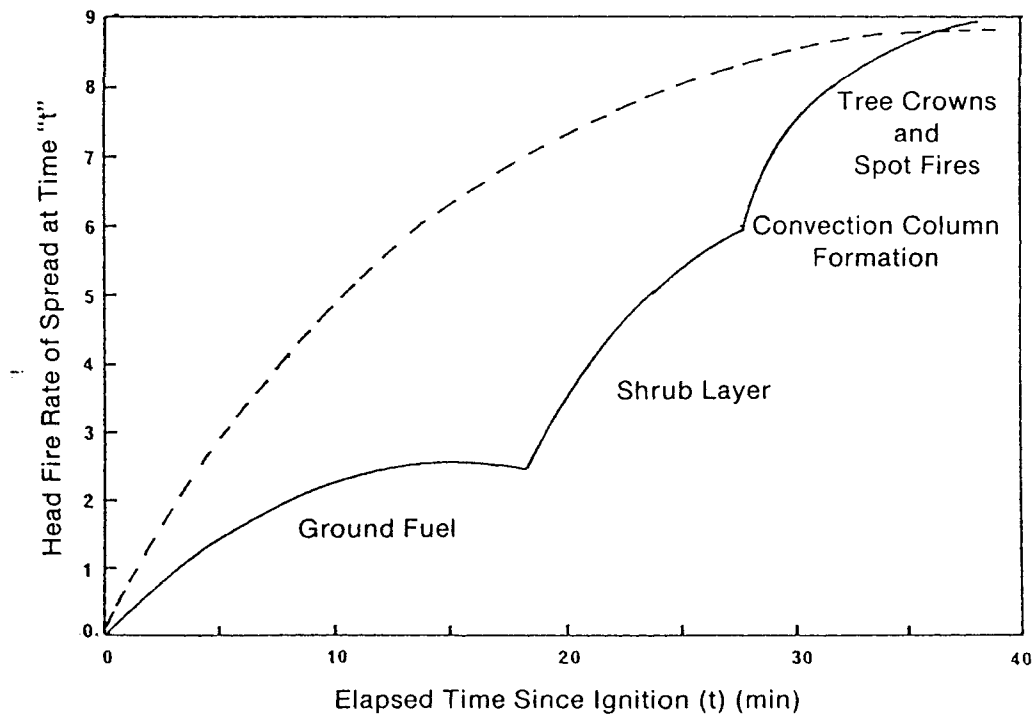


Figure 6. Acceleration pattern observed in forest fires (after McArthur 1967). This particular example illustrates the successive stages in the acceleration of a fire burning in a southeastern Australian eucalypt forest fuel type containing a well-developed shrub layer. Note the generalized curve shape and the step-like acceleration pattern.

issue¹. Cheney (1981) suggests that the two models (step-wise and the asymptotic curve) are not mutually exclusive; the asymptotic curve represents uniform fuel, weather and topographic conditions, whereas the step-wise progression is characteristic of a heterogeneous fire environment (Fig. 6).

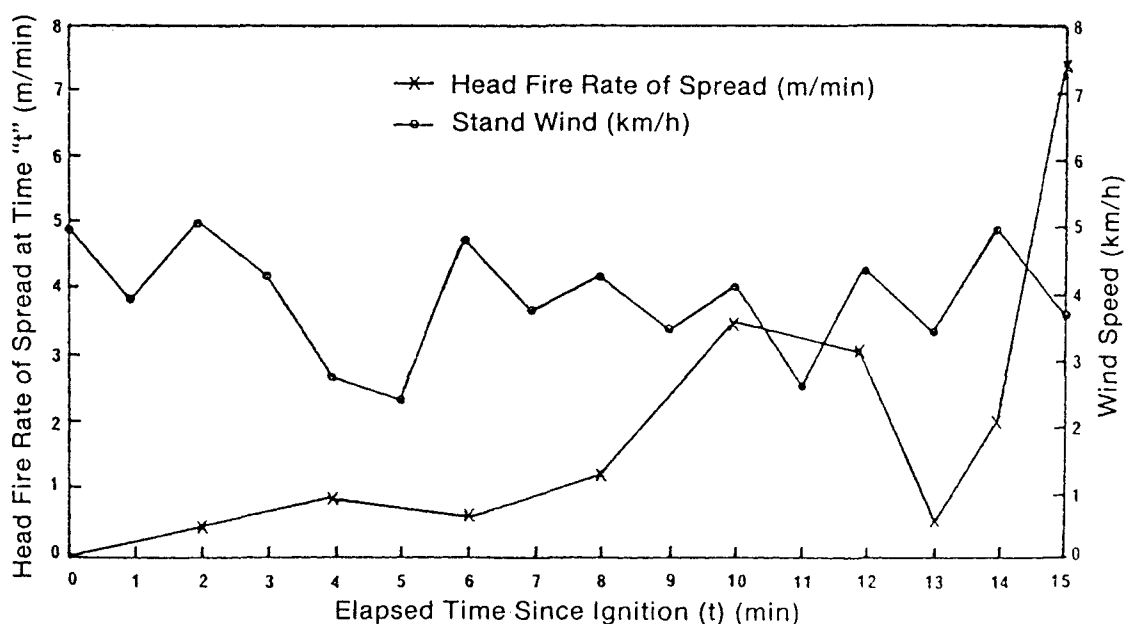


Figure 7. Observed variation in head fire ROS and wind speed with elapsed time since ignition. Points marked represent average value for the previous two minute time period. Wind speed is measured at 1.4 m above ground level in the forest stand. (Experimental fire plot 14, July 25, 1987, Big Fish Lake, Alberta).

¹Big Fish Lake Experimental Burning Project is a cooperative project between the Canadian Forestry Service and the Alberta Forest Service taking place 100 km northeast of High Level, Alberta, in the lowland boreal spruce (*Picea mariana* L.) fuel type. For more information see Alexander and McAlpine (1986).

3.0 Methods:

3.1 Introduction and Experimental Design.

With the primary objective of this study to provide a baseline acceleration model and evaluate the effect of wind speed, fuel moisture, fuel loading (packing ratio), and type of fuel on this function, the following experimental design was adopted. Two types of fuel were tested; recently cast ponderosa pine (Pinus ponderosa Laws.) needles and excelsior. These fuels were chosen for three reasons; the collection (needles) or purchase (excelsior) is relatively simple, the relative ease with which a reproducible fuel bed is made, and they are the most commonly used fuels in past research for comparison purposes.

Fuel loading effects were evaluated by burning ponderosa pine needles at 2 different loadings: 2.0 kg/m², and 1.0 kg/m², packed to a depth of 7.6 cm (3 inches). This yielded fuel bulk densities of 26.3 kg/m³ (1.64 lb/ft³), and 13.12 kg/m³ (0.82 lb/ft³) respectively. A single excelsior fuel loading, set at 0.277 kg/m², and 7.6 cm (3 inches) deep (yielding a fuel bulk density of 3.635 kg/m³ or 0.227 lb/ft³), was chosen

to give the maximum reaction velocity in the zero wind case (Rothermel 1972).

Fuel beds in this experiment simulate a single layer fuel in a forest setting. Multiple fuel layers were not considered, however extrapolation to include multilayered fuels may be possible once an acceleration function is developed.

The effect of wind was evaluated at four different wind speeds; 0.0, 1.6, 4.8, and 8.0 km/h (8.0 km/h being the upper limit of the wind tunnel's capability). Pine needle fuel beds, loaded at 26.3 kg/m³, and all excelsior fuel beds were burned at all possible wind speeds with a minimum of three replications. Pine needle fuel beds loaded at the 13.1 kg/m³ were burned at 4.8 km/h wind speeds with three replications. Since this particular loading was not tested over a range of wind speeds, no interactive effects of wind speed and fuel loading were tested.

Wind tunnel wind speeds tend to be laminar with little or no vertical variation above the surface boundary layer (Rothermel 1967). The boundary layer being the layer of air directly above the fuel bed. A forest setting has a vertically heterogeneous wind speed profile which depends on a variety of environmental

factors (eg. tree form, tree crown density, basal area, density and location of understorey, etc.). The preset wind tunnel wind speed approximates a mid flame wind speed (Rothermel 1972). The international 10 m open standard wind measurements would therefore not be equivalent to the tested wind tunnel wind speeds, however estimations are possible with consideration of the type of fuel in question.

3.2 Laboratory Facilities.

The wind tunnel combustion facilities at the Intermountain Fire Sciences Laboratory in Missoula, Montana are described in detail elsewhere (Rothermel 1967, Rothermel and Anderson 1966); however, a brief description follows. There are two wind tunnels; one large, low speed tunnel and one smaller, high speed tunnel (Fig. 8). The large wind tunnel has a 3.05 m by 3.05 m (10 ft. by 10 ft.) cross-section and is capable of velocities up to 8 km/h. The small wind tunnel has a 0.91 m by 0.91 m (3.0 ft. by 3.0 ft) square cross-section, and is capable of wind speeds up to 80 km/h. The air circulated through the wind tunnels is conditioned to the desired temperature and humidity in a series of heaters, chillers and water spray nozzles

(Rothermel and Anderson 1966). All of the experimental burning conducted for this study was done in the large wind tunnel.

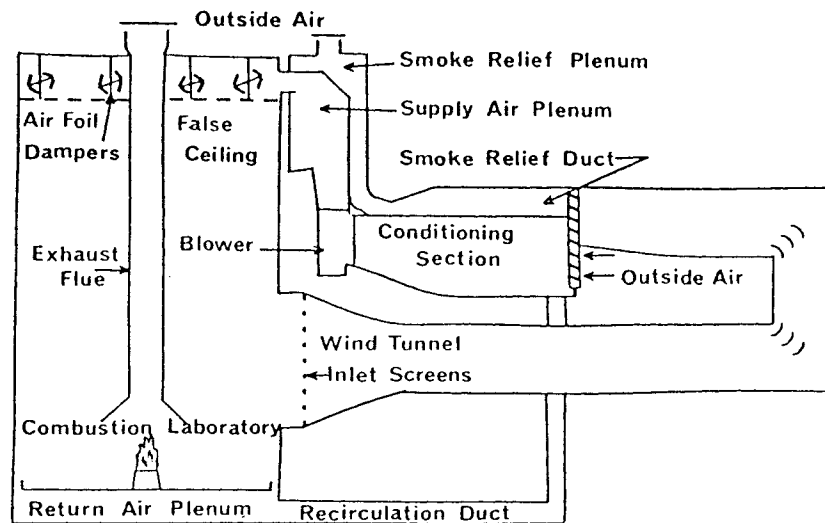


Figure 8. Profile section of the combustion research facilities at the Intermountain Fire Sciences Laboratory, Missoula, Montana (from Rothermel and Anderson 1966).

3.3 Fuel Collection and Bed Preparation.

During the fall of 1987, needles were collected from pure stands of ponderosa pine surrounding Missoula, Montana. These needles were cleaned to remove any extraneous material (grass, leaves, cones, etc.) which may have been inadvertently combined with the needles during the collection process. The needles were then stored overwinter in an unheated storage structure in open air bins. One week prior to burning, the needles were moved into the combustion laboratory to bring them into equilibrium moisture conditions with the laboratory atmosphere.

All experiments were conducted on two fuel beds (each measuring 0.915 m by 2.515 m) placed end to end, with two additional smaller sections (0.20 m, and 1.0 m) added on to the downwind end. This provided a total fuel bed length of 6.15 m. The fuel beds were constructed of an aluminum framework overlaid with wire mesh, aluminum foil, and lastly, ceramic cloth.

Ponderosa pine needle fuel was loaded to a depth of 4.62 cm and to the prescribed density following procedures initially outlined by Anderson (1964) and more definitively by Schutte (1965). Briefly, a known weight (wet weight) of fuel was spread over a known area

of the fuel bed. In practice, the fuel bed was divided into 1.0 m² sections (or part thereof as in the case at the end of the bed) and half the required weight of fuel spread evenly over the section. Once the entire bed had a single layer of fuel, a second layer of fuel was placed on top to fill out the required loading. Lastly, extraneous vertical needles were clipped down to the prescribed 4.62 cm depth for the fuel bed. Due to the light loading of the excelsior fuel, multiple layers were not necessary. The required weight of excelsior was spread evenly over the fuel bed, fluffed to several times the required volume to remove tightly packed concentrations, and lightly and uniformly pressed down to the final fuel depth (Wilson 1982). Extraneous vertical strands above the bed surface were clipped as in the case of the ponderosa pine needle fuel beds.

3.4 Preburn Setup and Instrumentation.

Immediately following the packing of each bed, three fuel moisture tins were filled with the respective type of fuel (needles or excelsior) for eventual moisture content determination. These tins stayed with the bed until just prior to ignition when they were removed from the tunnel, weighed, and placed in a drying oven at

105°C for 24 hours and reweighed.

For burning, the beds were placed end to end on the floor of the wind tunnel and the needles at the fuel bed junctions sufficiently mixed and clipped down to the three inch height to ensure a transparent joint between beds. A trip fence or air spoiler was placed upwind of the beds and wire mesh spread over the floor of the tunnel (also upwind) to allow equally turbulent air flow over the entire length of the fuel bed (Rothermel and Anderson 1966). Once the fuel beds were in place, strings were placed across the fuel bed at 15 cm intervals and sequentially numbered (Fig. 9). A precise estimate of the fire's location was obtained ocularly by recording the time that the base of the flame reached the string and the string's respective number, giving downwind spread distance (hereafter these observations will be referred to as Ocular Distance/Time (D/T) data). After two fires it was found that this scale was too coarse for the period immediately following ignition. To alleviate this situation, strings were placed every 5 cm, from 1.2 m downwind of the front of the bed (the ignition point) to 1.5 m.

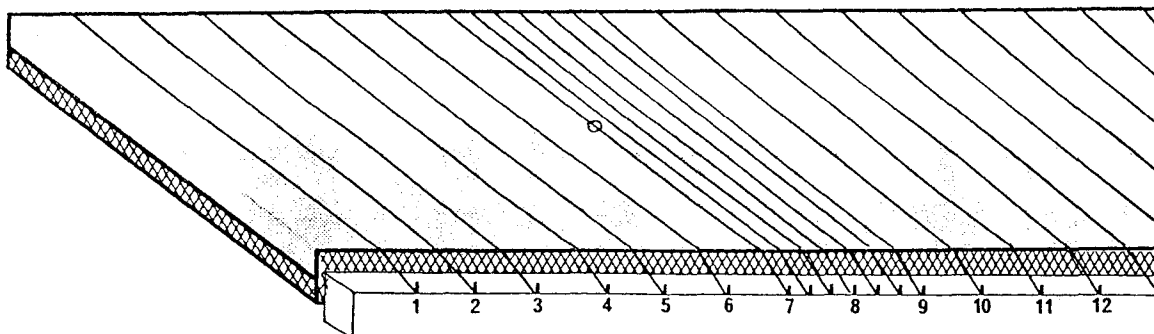


Figure 9. Perspective view of fuel bed layout. Numbers are the respective string numbers for ocular D/T observations, and the circle designates the ignition point.

A 35mm camera with a 28-80mm zoom lens (locked at 28mm), motor drive, and data back capable of imprinting the precise time (hours, minutes and seconds) was bolted to the roof of the wind tunnel directly above the ignition point. This camera was remotely operated with pictures taken every 15 seconds unless the fire behavior warranted more or less rapid exposures. Standard slide film (200 or 64 ASA) was used for all fires. A small sign was placed on the floor of the tunnel, in the field of view of the 35mm camera, to indicate the date, burn number, and wind speed. The developed slides were then projected onto a piece of paper and a map made of the

fire's progress, with the recorded times and fire front locations. The string grid proved an invaluable aid in the scaling of the diagram and establishing the head fire front location.

All fires were documented with video equipment for later image analysis (McMahon, Adkins, and Rodgers 1986). The field of view of the video camera was restricted by structural components of the wind tunnel and did not include the ignition point, or the downwind end of the fuel bed. However, much of the accelerating fire was documented.

Prior to ignition, the environmental conditions in the wind tunnel were stabilized at the desired level. Wind speed was measured using a hot wire anemometer protruding from the roof of the tunnel, upwind of the fuel bed. Temperature and relative humidity in the tunnel, maintained at 26.7°C (80°F), and 20 percent, respectively, were measured with an electronic thermistor.

Ignition was done with an electrically heated coil which contacted 3 kitchen matches. The matches provided a source of flaming combustion for the ignition. Ignition took place 1.05 m from the upwind end of the fuel bed, along the longitudinal centre line of the fuel

bed (Fig. 9). At the first sign of flame at ignition (there was about a 15 second delay from the time the current was applied to the heated coil until the matches ignited); the 35mm overhead camera took a picture to calibrate the subsequent sequence of slides, the timer on the video camera was started and a stopwatch was started for the ocular distance/time estimates.

Additional instrumentation for another study investigating crown fire initiation was placed on all fires. Briefly, instrumentation included four thermocouples in the fuel bed for ROS, thermocouple "trees" to measure temperature above the fuel bed, and an electronic balance to measure a weight loss section of fuel bed near the downwind end.

4.0 Results and Discussion.

A total of 29 fires were conducted over a two week period in March, 1988 (Table 2). The complete set of ocular distance/time (D/T) observations are listed by treatment (type of fuel, loading and wind speed) in Appendix I. In some cases, times were not obtained at all distance markers along the fuel bed because the fire was moving too rapidly. Additionally, the first two fires (fire numbers 1 and 2) had no distance markers in place at the 5, 10, 20, and 25 cm points.

Fire perimeter locations, mapped from overhead 35mm slides, are presented in Appendix II. Head fire perimeter locations were difficult to determine from the overhead imagery alone, as flames obscured the view from above. However, the head fire perimeter location was accurately estimated from the combination of slides and ocular D/T data. Due to camera failure, fire numbers 21, 22, 28, 29 have no perimeter data. Several fires were missing an initial calibration photo of the ignition, due either to camera or operator failure. In these cases, elapsed time was calibrated using the information from the ocular D/T observations.

Table 2. Summary of all burns.

Burn #	Date M/D/Y	Time	Type ¹ of Fuel	Bulk Density (kg/m ³)	Wind speed (km/h)	Temp °C	R.H. %	Fuel moist. %	Head fire ² equil. ROS (m/min)	Backing fire ROS (m/min)	Flame ³ length (m)
1	3.18.88	11:41	N	26.3	1.6	27.6	20.9	8.2	0.46	0.20	--
2	3.18.88	14:07	N	26.3	8.0	27.1	19.8	7.9	4.50	0.25	1.16
3	3.21.88	09:58	N	26.3	4.8	27.3	20.9	8.4	1.45	0.23	1.18
4	3.21.88	11:56	N	26.3	1.6	27.1	20.9	8.1	0.48	0.20	0.97
5	3.21.88	14:32	N	26.3	1.6	26.9	20.5	8.2	0.60	0.19	1.00
6	3.21.88	16:00	N	26.3	4.8	27.3	20.0	7.7	1.73	0.12	1.08
7	3.22.88	10:00	N	26.3	4.8	26.9	19.9	8.8	1.48	0.17	0.83
8	3.22.88	14:37	N	26.3	8.0	27.0	21.3	8.4	2.16	0.20	1.15
9	3.22.88	16:11	N	26.3	8.0	27.8	19.7	8.3	3.03	0.22	1.12
10	3.23.88	11:32	E	3.6	1.6	27.2	21.3	7.1	2.21	0.84	0.87
11	3.23.88	15:02	E	3.6	4.8	27.0	20.4	6.4	6.54	1.29	0.84
12	3.23.88	15:59	E	3.6	8.0	27.2	19.9	6.4	11.69	1.08	1.06
13	3.24.88	09:07	E	3.6	1.6	27.3	21.3	6.6	2.05	0.53	0.65
14	3.24.88	10:30	E	3.6	1.6	27.9	20.1	5.6	3.11	0.64	0.72*
15	3.24.88	11:46	E	3.6	4.8	27.3	20.4	6.2	6.94	0.63	0.89
16	3.24.88	13:44	E	3.6	4.8	27.4	20.8	5.5	6.29	0.71	0.85
17	3.24.88	15:51	E	3.6	8.0	27.3	19.6	5.4	11.90	1.34	0.92
18	3.24.88	16:39	E	3.6	8.0	27.6	19.9	6.7	11.14	0.56	1.04
19	3.25.88	09:47	E	3.6	0.0	27.6	20.8	5.5	1.32	0.70	0.57*
20	3.25.88	13:18	E	3.6	0.0	26.9	20.8	6.9	1.02	0.58	--
21	3.25.88	14:08	N	13.1	4.8	27.1	19.7	8.9	2.09	--	0.73*
22	3.28.88	09:44	N	13.1	4.8	27.2	20.6	8.9	2.19	--	0.76*
23	3.28.88	11:41	N	13.1	4.8	27.6	21.2	8.7	2.52	0.24	0.97
24	3.28.88	13:21	N	26.3	0.0	27.4	20.4	9.97	0.38	0.23	0.82*
25	3.28.88	15:07	N	26.3	0.0	27.1	20.9	9.4	0.37	0.23	0.82*
26	3.29.88	09:16	E	3.6	0.0	27.3	21.0	8.6	1.05	0.65	0.60*
27	3.29.88	10:22	N	26.3	0.0	27.0	21.4	8.7	0.37	0.25	0.68*
28	3.30.88	14:25	N	26.3	4.8	27.5	20.8	9.2	1.25	--	0.81*
29	3.30.88	16:12	N	26.3	4.8	27.0	20.0	8.8	1.30	--	0.71*

¹ N refers to ponderosa pine needles, and E refers to excelsior.

²Regression results using spread data from 2.0 to 4.95 m downwind of the ignition point.

³*--Indicates flame lengths measured after the flanking fire had reached the edge of the fuel bed.

The overhead photos were used to measure changing length-to-breadth (L/B) ratios over the life of the fire, however this assessment of fire shape was not measurable after the fire reached the edge of the fuel bed. In fact, immediately after the edge of the fuel bed was encountered by the flanking fire, the fire moved very quickly up the edge of the fuel bed to catch up to, or even pass the forward progress of the head fire. Following this initial "pulse" of rapid spread, a straight line of fire across the fuel bed was usually achieved. This phenomenon of rapid spread up the fuel bed edge is documented by the overhead photos, which, in many cases, display the perimeter just prior to, and after this effect.

The overhead photos were also used to evaluate backing fire spread rate over the range of conditions tested. Backing fire spread rates proved to be very consistent for each type of fuel regardless of wind speed or fuel loading.

4.1 Ocular Distance/Time (D/T) Results.

The ocular D/T measurements provided the major bulk of the data for determining fire acceleration. Data was initially divided into groups by treatment (type of

fuel, wind speed, and fuel loading) and each group analyzed separately. Originally, the raw D/T data was manipulated to produce ROS values for each time period measured. This data was then plotted on a ROS versus Time graph (Fig. 10). This approach proved to be awkward as slight errors in measurement of time values (or small fluctuations in fuel bed characteristics causing uneven spread) caused large perturbations in the observed ROS. To rectify this problem the data was analyzed as it had been measured - as D/T information. Figures 11 and 12 show lines of average time for each measured distance for needles and excelsior.

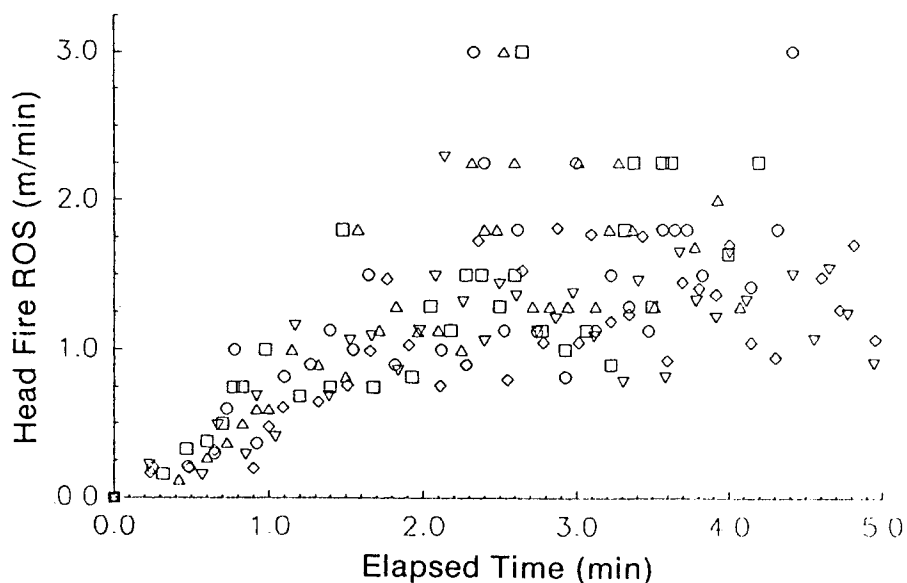


Figure 10. Observed ROS versus Time for a needle fuel bed, with a bulk density of 26.3 kg/m^3 and burned at a wind speed of 4.8 km/h . Five replications are shown.

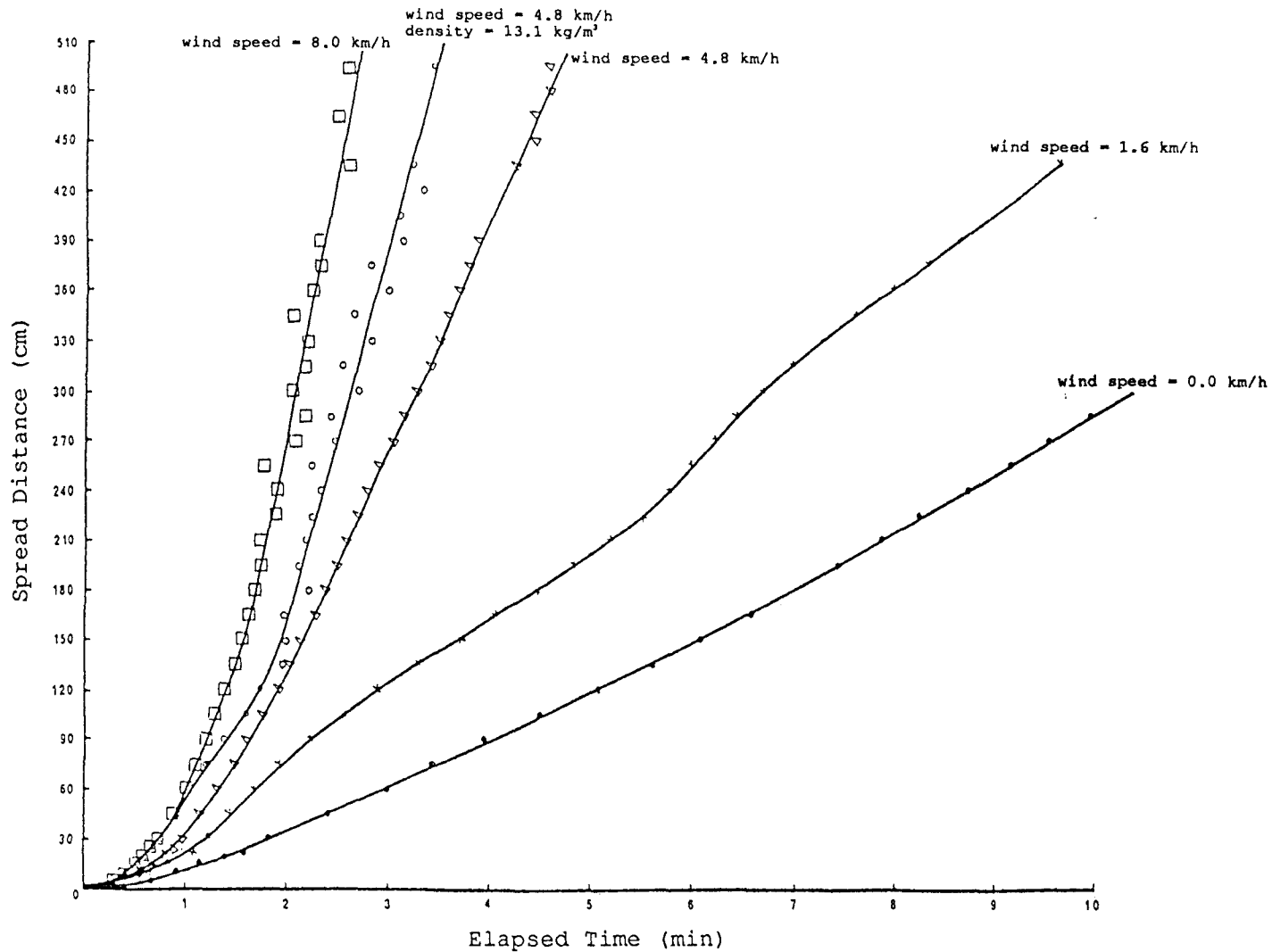


Figure 11. Distance versus time plot for needle fuel beds over the range of wind conditions tested. Points plotted are averages of time for each set of replications.

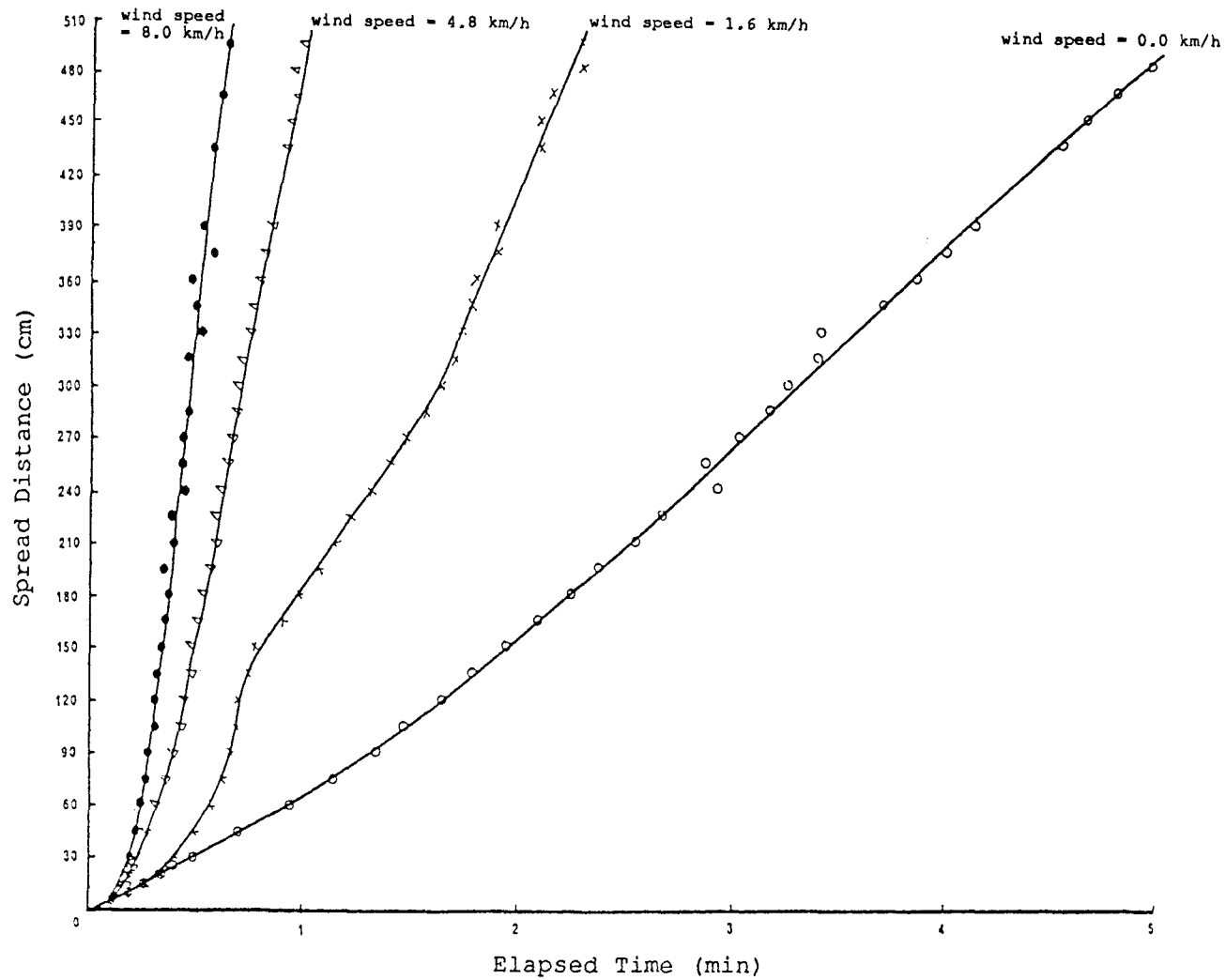


Figure 12. Distance versus time plot for excelsior fuel beds over the range of wind conditions tested. Points plotted are averages of time for each set of replications.

The initial step in analysis was the determination of equilibrium ROS. The D/T graphs were divided into two zones; the accelerating fire phase (the initial, curved part of the line) and the equilibrium ROS zone (the approximately straight part of the line). The two line segments connect at the point where the first derivative of the curved line segment (the slope of the tangent to the line) equals the equilibrium ROS (the slope of the straight segment of line). Using this method of analysis, the first derivative of the entire line (change in ROS over time) will produce a steeply rising curve similar to those suggested by Cheney (1981), Van Wagner (1985) and Weber (1988) (Fig. 5), but instead of becoming asymptotic to the final equilibrium ROS, will intersect it.

4.1.1 Computation of Equilibrium ROS.

In all cases of data analysis, the equilibrium ROS zone was assumed to start after 2.0 metres of forward fire spread. This eliminated usable data in some cases, but prevented distortion of the line caused by the acceleration section. To determine equilibrium ROS from the straight line section of the graph, three methods were compared; 1) net distance/time, 2) grouped simple

linear regression, and 3) individual simple linear regression. For both regression procedures, the constant or "Y" intercept was ignored as only the ROS (slope of the line) was of interest.

The net distance/time method approximates the results which might be obtained with thermocouple data. Essentially, the first and last data points are used to measure spread rate for each fire and the resultant ROS values are averaged for each treatment. The ROS values provided by this method were eventually discarded because the method ignored the intermediate data and relied totally on the accuracy of the first and last observations.

The grouped simple linear regression method places the equilibrium spread D/T data from all of the fires (with the same treatment) in a single data set and a regression line is run through the points. Results from the grouped simple linear regression procedure predicted lower ROS values than were observed in any individual contributing fire. This problem was caused by two factors; the data stratification that had existed during the experiment was removed and the regression forced the line through a common intercept value (common to all fires included), which distorted the slope.

Individual simple linear regression is the regression of each individual fire using the available equilibrium spread data and the resulting spread rates are averaged for each treatment. Resulting ROS values from the individual simple linear regression procedure were in line with any single fire ROS and the procedure eliminated the problems encountered with the first two methods.

Calculated ROS values from all three methods are displayed in Table 3 with regression statistics. Individual fire ROS values (calculated using simple linear regression) along with pertinent regression statistics are presented in Table 4.

4.1.2 Acceleration Phase.

Once an equilibrium head fire spread rate had been defined, the job of describing the acceleration phase (curved section of the D/T graph) began. Once again, data for each treatment was analyzed separately, however for this phase all the D/T data from ignition to completion was used. After several trials with linear transformations and nonlinear models, it was decided to use a simple log-log transformation of the data modeled as a simple linear regression. Once transformed back

Table 3. Equilibrium head fire ROS values determined three ways for each burning treatment. Values shown (except in the case of the grouped simple linear regression) represent averages for each burning treatment.

Type of fuel ¹	Bulk density (kg/m ³)	Wind speed (km/h)	ROS ² (m/min)	ROS ³ (m/min)	SEE ⁴	R ²	ROS ⁵ (m/min)
N	26.3	0.0	0.37	0.35	0.21	.95	0.37
N	26.3	1.6	0.52	0.49	0.17	.97	0.51
N	26.3	4.8	1.47	1.16	0.33	.86	1.44
N	26.3	8.0	3.64	2.45	0.43	.75	3.23
N	13.1	4.8	2.29	1.81	0.39	.82	2.27
E	3.6	0.0	1.12	0.96	0.35	.86	1.13
E	3.6	1.6	2.39	1.28	0.64	.51	2.46
E	3.6	4.8	6.78	6.56	0.14	.98	6.59
E	3.6	8.0	13.95	10.24	0.34	.88	11.58

¹ N - ponderosa pine needles, E - excelsior.

² Determined with net distance/time method.

³ Determined by grouped simple linear regression.

⁴ Standard Error of the Estimate.

⁵ Determined by individual simple linear regression.

from the logarithmic model, this equation takes on the familiar allometric functional form (power curve) (Parton and Innis 1972):

$$D = A * T^B \quad [6]$$

Where D = head fire spread distance

T = elapsed time since ignition

A and B are equation coefficients.

Table 4. Equilibrium ROS measurements for each individual fire determined by simple linear regression. Note: Fires are grouped by treatment.

Fire #	Type of Fuel	Bulk density (kg/m ²)	Wind speed (km/h)	ROS (m/min)	SE ¹ ROS	SEE ²	R ²
24	N	26.3	0.0	0.38	0.26	0.03	.999
25	N	26.3	0.0	0.37	0.00	0.02	.999
27	N	26.3	0.0	0.37	0.00	0.04	.998
1	N	26.3	1.6	0.47	0.01	0.08	.992
4	N	26.3	1.6	0.48	0.07	0.05	.997
5	N	26.3	1.6	0.59	0.01	0.06	.996
3	N	26.3	4.8	1.45	0.03	0.08	.992
6	N	26.3	4.8	1.73	0.03	0.06	.996
7	N	26.3	4.8	1.48	0.05	0.10	.986
28	N	26.3	4.8	1.25	0.02	0.06	.996
29	N	26.3	4.8	1.30	0.01	0.02	.999
2	N	26.3	8.0	4.50	0.16	0.09	.993
8	N	26.3	8.0	2.15	0.29	0.29	.872
9	N	26.3	8.0	3.03	0.21	0.15	.965
21	N	13.1	4.8	2.09	0.02	0.04	.998
22	N	13.1	4.8	2.19	0.04	0.06	.997
23	N	13.1	4.8	2.52	0.06	0.07	.995
19	E	3.6	0.0	1.31	0.02	0.06	.995
20	E	3.6	0.0	1.02	0.01	0.03	.999
26	E	3.6	0.0	1.05	0.01	0.02	.999
10	E	3.6	1.6	2.21	0.07	0.08	.992
13	E	3.6	1.6	2.06	0.05	0.09	.991
14	E	3.6	1.6	3.11	0.17	0.20	.957
11	E	3.6	4.8	6.54	0.12	0.07	.915
15	E	3.6	4.8	6.94	0.15	0.07	.994
16	E	3.6	4.8	6.28	0.22	0.11	.983
12	E	3.6	8.0	11.69	0.29	0.07	.996
17	E	3.6	8.0	11.90	0.40	0.08	.994
18	E	3.6	8.0	11.14	0.29	0.05	.997

¹ Standard error of the slope (ROS).

² Standard error of the estimate.

In equation [6] the A value represents the spread distance when the value of the independent variable (time) is equal to one. The B coefficient is a curve form control parameter (Parton and Innis 1972). The derivative of this equation would describe the change in ROS over time. The derivative takes the form:

$$\text{ROS} = A * B * T^{(B - 1)} \quad [7]$$

Where ROS = head fire ROS at time T
 T = elapsed time since ignition
 A and B are equation coefficients.

This equation form proved to be very versatile for the range of D/T curves being modelled. One problem that did arise was a failure to adequately describe the upper part of the curve where it meets the straight line. When a standard regression analysis was used, the predicted line fell consistently below the data. This was deemed important as an under prediction in spread distance (as was the case) at this juncture would be carried forward throughout the final model. To rectify the under prediction problem a weighted regression (weighted by distance travelled in cm) was done to place more emphasis on the latter section of the line and less

on the initial. The weighting procedure simply multiplied the number of observations by the respective distance (in cm), consequently artificially increasing the sample size. This procedure allowed continued use of the relatively simple allometric function (equation [6]) rather than a more complex nonlinear model.

In the original analysis only the acceleration section of the D/T curve was used to produce a regression line. However the resulting coefficient values were unstable because they depended on the number of data points included. This was solved by using the full data set in most cases. Whether or not to use the full data set was determined graphically by judging how the resulting prediction line compared with the observed data. The case in which the full data set was not used (excelsior at 1.6 km/h) had an unusual D/T curve (Fig. 25). Table 5 contains a list of burning treatments, associated calculated regression coefficients (for the weighted model) and vital statistics for the allometric model of the D/T graphs.

Table 5. Regression coefficients and vital statistics for the allometric model of the acceleration phase weighted by the distance (in cm) from the ignition point.

Type of fuel	Bulk density (kg/m ³)	Wind speed (km/h)	A	B	N	R ² *	SEE*	P-Val*
N	26.3	0.0	0.156	1.263	103	.98	0.09	0.000
N	26.3	1.6	0.234	1.420	99	.86	0.19	0.000
N	26.3	4.8	0.434	1.611	159	.95	0.13	0.000
N	26.3	8.0	0.650	2.055	73	.94	0.16	0.000
N	13.1	4.8	0.548	1.759	87	.92	0.17	0.000
E	3.6	0.0	0.725	1.177	100	.97	0.11	0.000
E	3.6	1.6	1.896	1.700	92	.80	0.30	0.000
E	3.6	4.8	5.317	1.792	97	.97	0.11	0.000
E	3.6	8.0	12.327	1.865	62	.94	0.18	0.000

*Note - Quoted statistics are for the weighted log-log transformed linear model used to derive the allometric equation values shown. N shown is the original number of data points before weighting process.

4.1.3 Allometric Coefficient Predictive Models.

The next step in producing a model was to predict the calculated A and B values (equation [6]) from the varying environmental factors in which the fires were conducted (wind speed, type of fuel and fuel loading) and/or from the equilibrium fire behavior characteristics (ROS).

To develop an equation to predict A, it was plotted against possible independent variables. Two variables; wind speed and ROS were highly correlated with the A coefficient values as can be seen in Figures 13-16. Obviously ROS is highly dependent on wind speed so

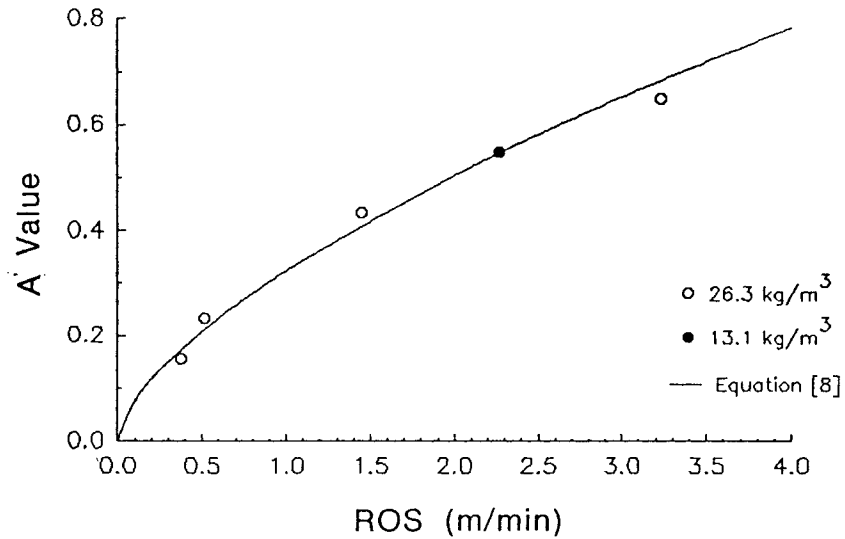


Figure 13. Allometric function A coefficient values plotted with equilibrium ROS for needle fuel beds. The plotted line represents equation [8].

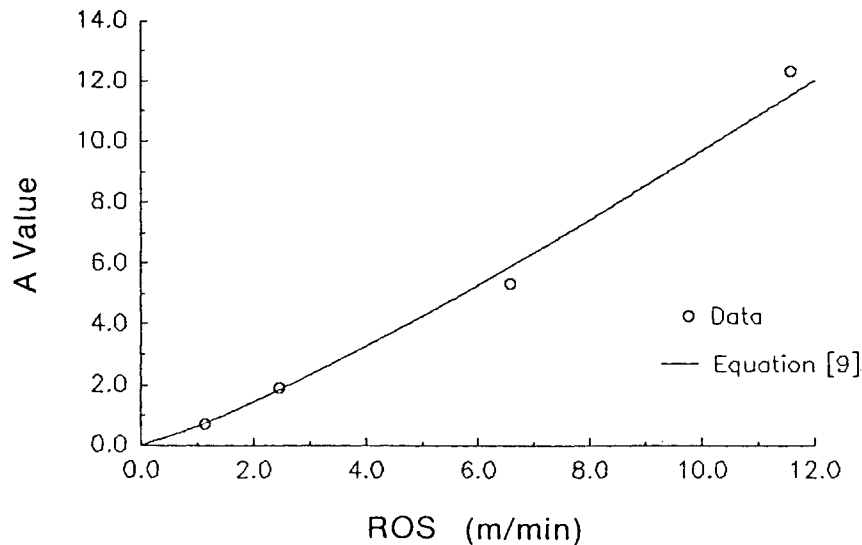


Figure 14. Allometric function A coefficient values plotted with equilibrium ROS for excelsior fuel beds. The plotted line represents equation [9].

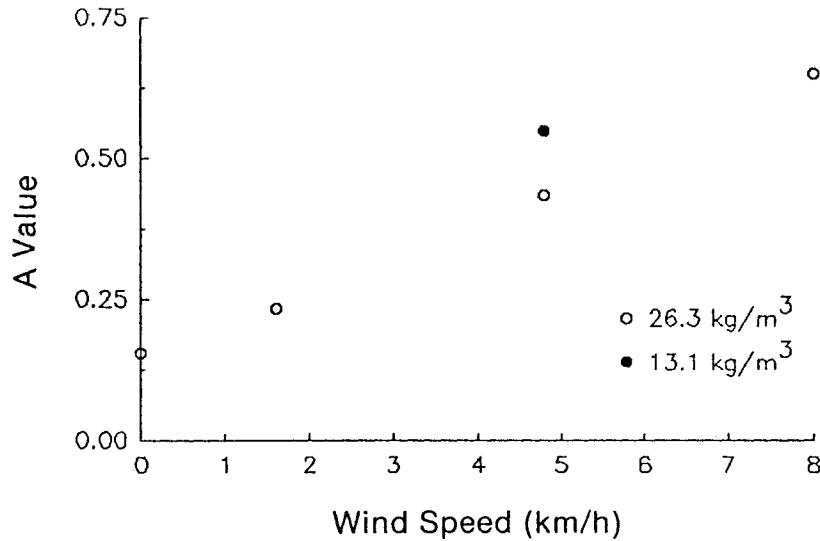


Figure 15. Allometric function A coefficient values plotted with wind speed for needle fuel beds.

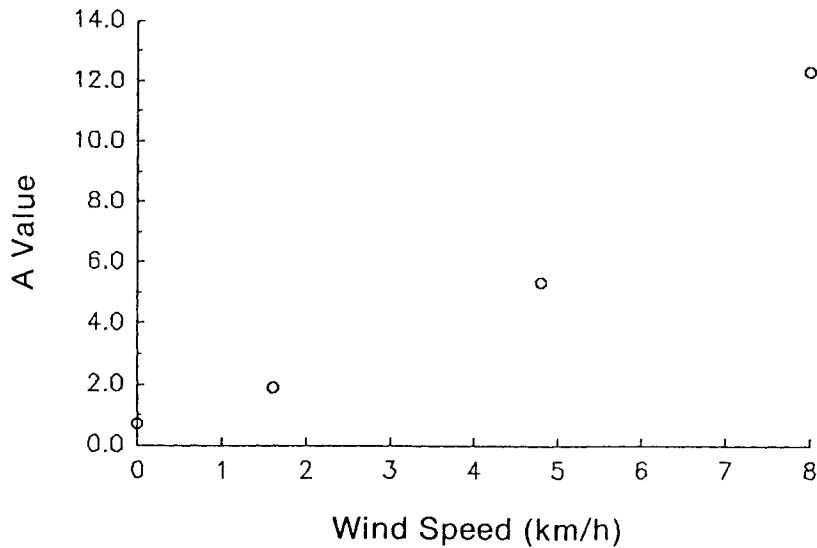


Figure 16. Allometric function A coefficient values plotted with wind speed for excelsior fuel beds.

inclusion of both variables would cause multicollinearity. While ROS did not have the highest correlation for both types of fuel, it proved to be the best compromise as it eliminated the need to account for fuel bulk density effects in the needle fuels and served as an integrator for all other burning condition variables that may have affected the value of A. Thus, equilibrium ROS was chosen as the independent variable. Coefficient values for the two types of fuel were so radically different (a factor of 10) that they had to be separated into two regressions.

On first inspection a linear regression for each type of fuel predicting A coefficient values from equilibrium ROS might be considered. However the overall model (equation [6]) is highly sensitive to errors in the value of the A coefficient, especially at the low end. The errors introduced by the linear model proved too large to be acceptable. To select an appropriate equation form, Figures 13 and 15 were analyzed. The two types of fuel also did not exhibit the same pattern of A coefficient value fluctuation, forcing the choice of either an adaptable model or two separate equations. It was decided to use a single adaptable equation form with a minimum of coefficients.

Again the allometric function was chosen as a highly adaptable equation form and separate equations for each type of fuel were produced. Figures 13 and 15 show the derived regression line for each type of fuel along with the A coefficient values. Regression equations [8] and [9], for needles and excelsior respectively, are listed below along with pertinent regression statistics.

Needles:

$$A = 0.3243 * ROSeq^{0.637} \quad [8]$$

$r^2 = .98$	$SE B_0 = 0.043$
$SEE = 0.094$	$SE B_1 = 0.050$
$P\text{-Value} = 0.001$	
$n = 5$	

Excelsior:

$$A = 0.628 * ROSeq^{1.188} \quad [9]$$

$r^2 = .996$	$SE B_0 = 0.082$
$SEE = 0.091$	$SE B_1 = 0.051$
$P\text{-Value} = 0.002$	
$n = 4$	

Note: Statistics quoted for equations [8] and [9] are from the log-log linear regression model used to derive the allometric model.

Equations [8] and [9] describe separate functions for the A coefficient value for the two types of fuel. The two type of fuel differ in two major respects: Firstly, the physical characteristic most commonly measured for fire behavior analysis is the surface area to volume ratio (Rothermel 1972). Values for this parameter are $57.6 \text{ cm}^2/\text{cm}^3$ and $81.3 \text{ cm}^2/\text{cm}^3$ for needles and excelsior respectively (Anderson et al. 1978; Wilson 1982, 1985). Secondly, thermochemical heat of combustion figures also differ between the two fuels with values of 22,910 kW/kg and 19,600 kW/kg for needles and excelsior respectively (Susot 1982). The two patterns observed in the A coefficient value plots are attributed to these physical and thermochemical differences. Fuel bulk density is not considered because of the close agreement of the lower loading of needles with the prediction line (Fig. 13).

In an effort to reduce the errors in the overall model caused by errors in the prediction of the A coefficient, the predicted A coefficient values from equations [8] and [9] were forced back into the original allometric equation and the analysis redone to produce new B coefficient values. Differences in the original and the adjusted B coefficient values are minor in most cases (Table 6).

Table 6. First approximation, second approximation and predicted B coefficient values for all burning conditions.

Fuel type	Bulk Density (kg/m ³)	Wind speed (km/h)	Original B value	Adjusted B value	Predicted [*] B value
N	26.3	0.0	1.263	1.223	1.204
N	26.3	1.6	1.420	1.360	1.501
N	26.3	4.8	1.611	1.610	1.784
N	26.3	8.0	2.055	1.991	1.886
N	13.1	4.8	1.759	1.761	1.784
E	3.6	0.0	1.177	1.176	1.204
E	3.6	1.6	1.700	1.656	1.501
E	3.6	4.8	1.792	1.953	1.784
E	3.6	8.0	1.865	1.800	1.886

* From equation [11].

Figures 17 and 18 show the B trends for the two types of fuel over the tested wind speeds and observed equilibrium ROS respectively. Wind speed, rather than equilibrium ROS appeared as a better predictor of B values indicating that wind speed is the main controlling factor in the rate of acceleration. It was also decided that, since the data was closely grouped together, a single regression line would be used to maintain simplicity. Either one of two approaches could be taken in the modelling effort for the B coefficient values; a straight line regression or a non-linear natural growth function.

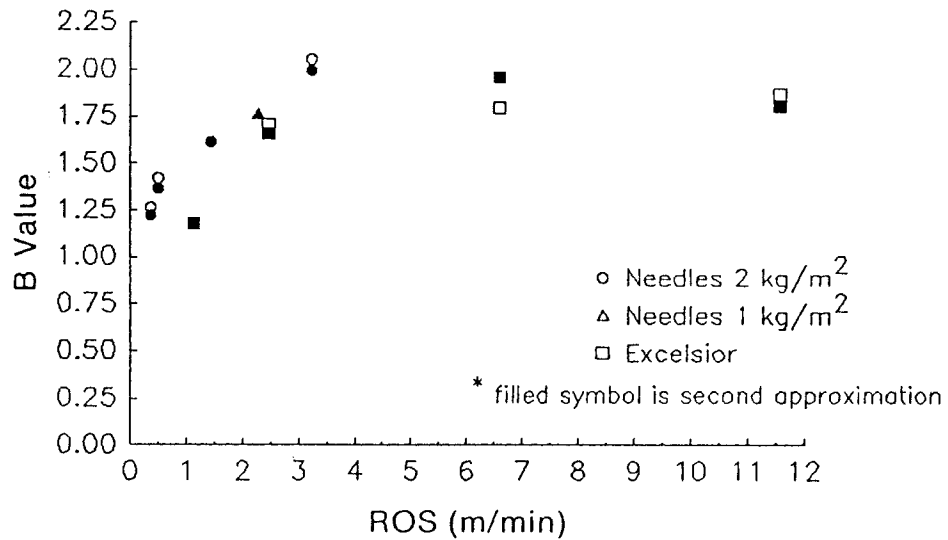


Figure 17. Allometric function B coefficient value plotted with equilibrium ROS. All burning treatments are displayed.

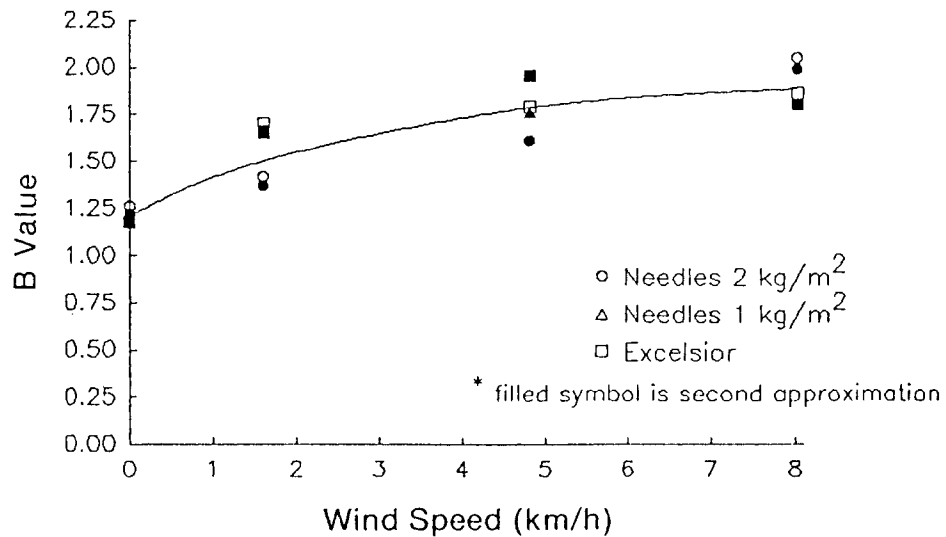


Figure 18. Allometric function B coefficient value plotted with wind speed. All burning treatments are displayed.

Either equation form (linear or natural growth) would probably produce an equally good predictor with the limited data available. In fact, the needle data seemed to lend itself more to a straight line function while the excelsior data was more of a curve form. The decision fell back to the function of the B value in the original allometric function. The B value, as previously stated, controls the shape of the curve. As the value of B increases, the time required to reach equilibrium ROS is reduced (Fig. 19). It was decided that there must be some limit to the rapidity with which

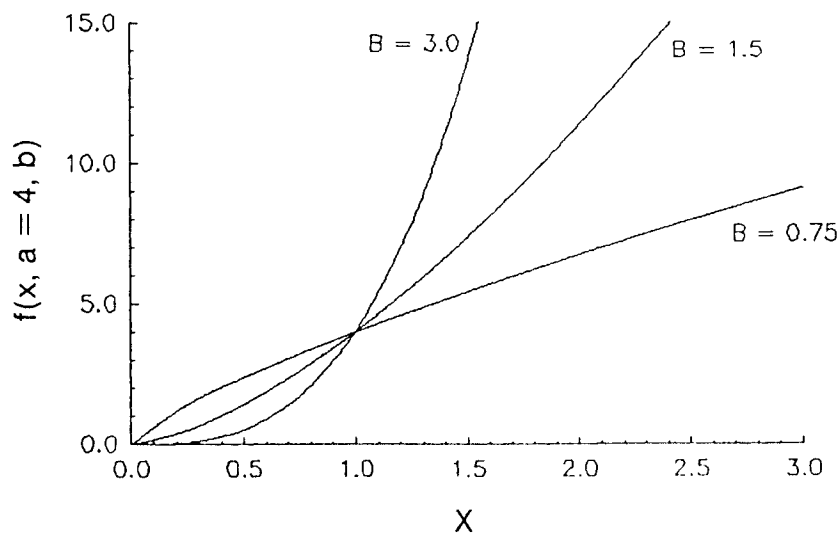


Figure 19. Effect of changing "B" coefficient value in the allometric function while maintaining a constant "A" coefficient value of 4.0.

the fire accelerated and therefore a limit on the B coefficient value. Thus, an exponential growth equation was selected of the form:

$$B = B_0 + B_1 * (1 - e^{-B_2 * WS}) \quad [10]$$

Where B = B value in the allometric model
 WS = Wind speed (km/h)
 B₀, B₁, B₂, are constants.

The B₀ constant (Y intercept) term was added to the standard exponential equation to prevent the B value in the allometric function from taking on a zero value when the wind speed was zero. This equation was fitted to both excelsior and needle data in a nonlinear computer software regression package yielding the following equation :

$$B = 1.204 + 0.740 * (1 - e^{-0.319 * WS}) \quad [11]$$

Where B = B value in the allometric model
 WS = Wind speed (km/h)

SEE = 0.155	SE B ₀ = 0.099
R ² = .83	SE B ₁ = 0.186
P-value = .025	SE B ₂ = 0.209

Equation [11] produces a curve with a minimum B coefficient value of 1.204 and a maximum of 1.944 as the

wind speed increases towards infinity. Predicted B coefficient values for the wind speeds tested are shown in Table 6.

The functions to compute the A and B values for the allometric equation ([6]) are used until the derivative of the allometric equation (equation [7]) approximately equals the equilibrium ROS, at which point the equilibrium ROS is used to compute spread distance. The results of this procedure were plotted with the original data sets to check the prediction accuracy. Figures 20 - 28 are plots of observed data with the appropriate prediction line for all treatment conditions. Two plots are shown for each burning treatment; the first displays all the data and the second is an enlargement of the acceleration phase. The plotted prediction lines in Figures 20 - 28 used the calculated ROS values (from Table 3) to compute the A coefficient values used in equation [6] and [7] for each treatment in the computation.

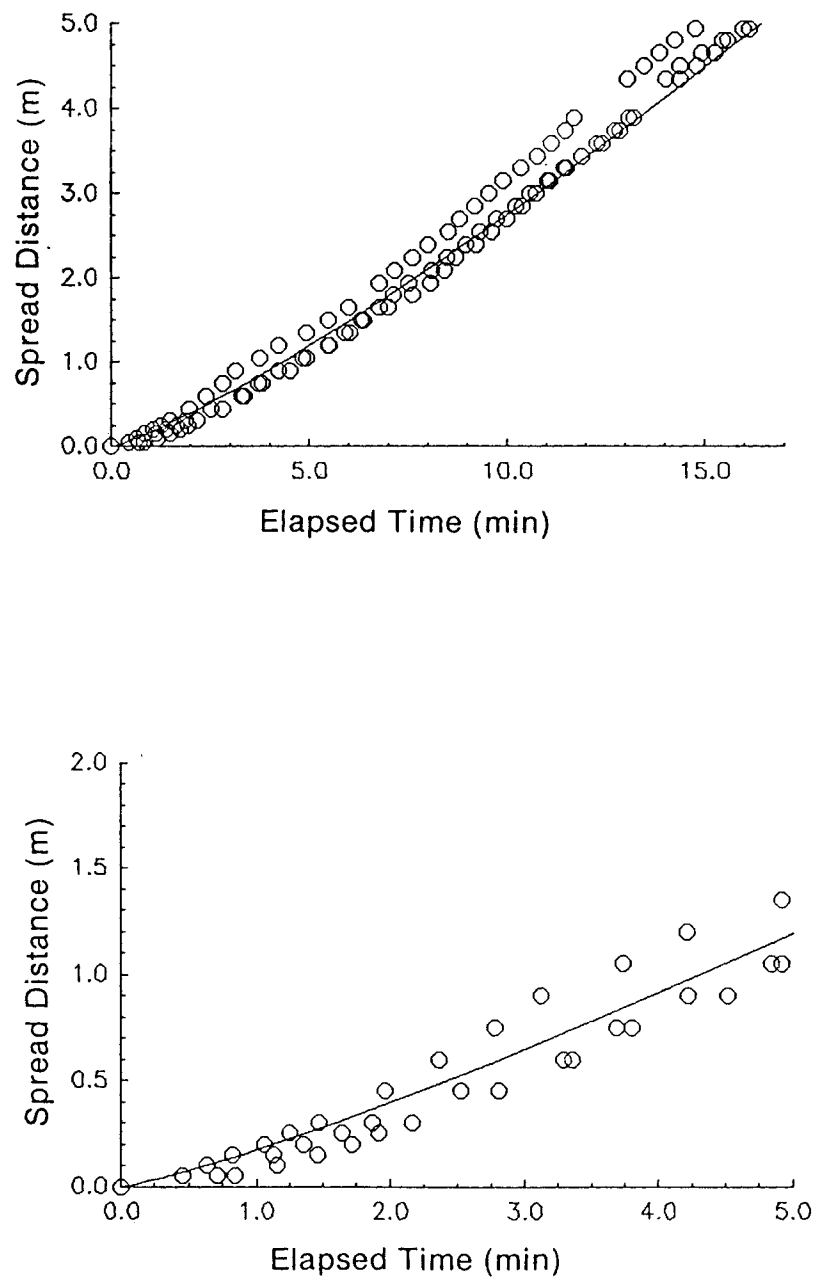


Figure 20. Comparison of all observed data (open circles) and prediction line for needle fuel loaded at 26.3 kg/m^3 and burned with a wind speed of 0.0 km/h . The upper plot shows the full data set, while the lower plot shows only the acceleration portion of the fire.

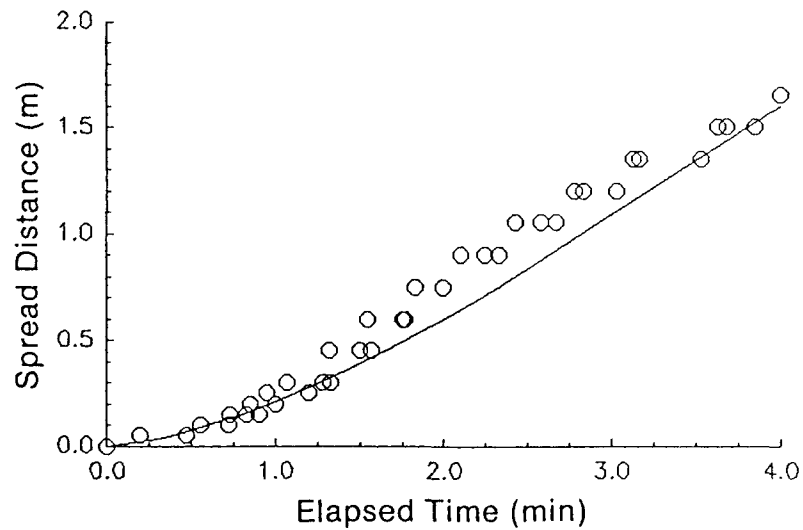
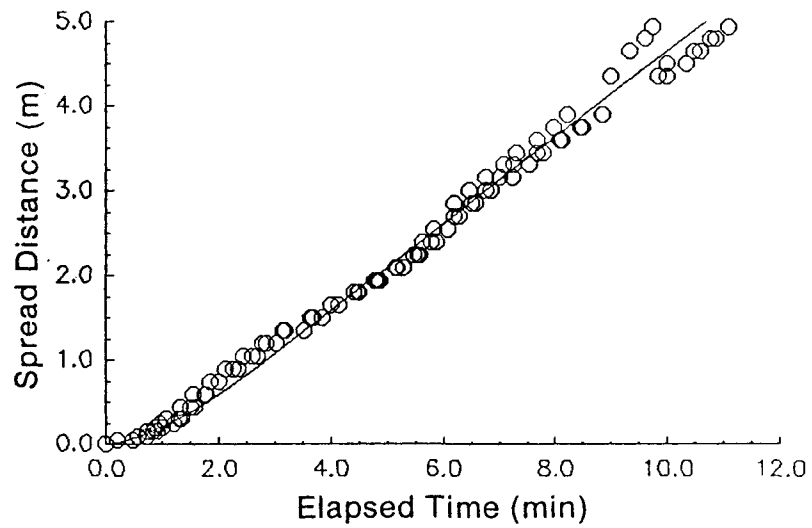


Figure 21. Comparison of all observed data (open circles) and prediction line for needle fuel loaded at 26.3 kg/m^3 and burned with a wind speed of 1.6 km/h . The upper plot shows the full data set, while the lower plot shows only the acceleration portion of the fire.

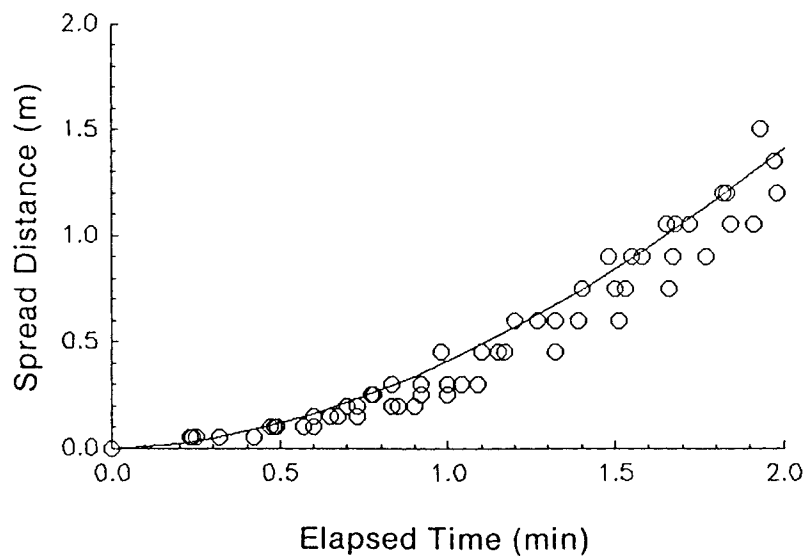
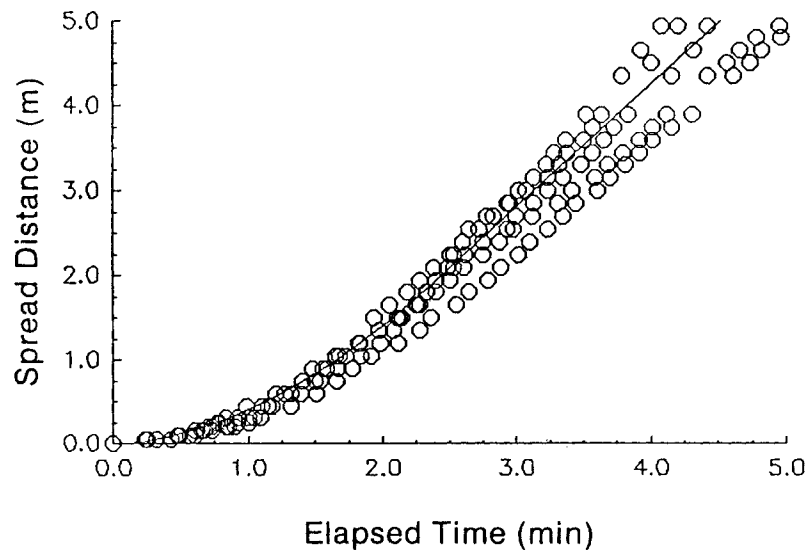


Figure 22. Comparison of all observed data (open circles) and prediction line for needle fuel loaded at 26.3 kg/m^3 and burned with a wind speed of 4.8 km/h . The upper plot shows the full data set, while the lower plot shows only the acceleration portion of the fire.

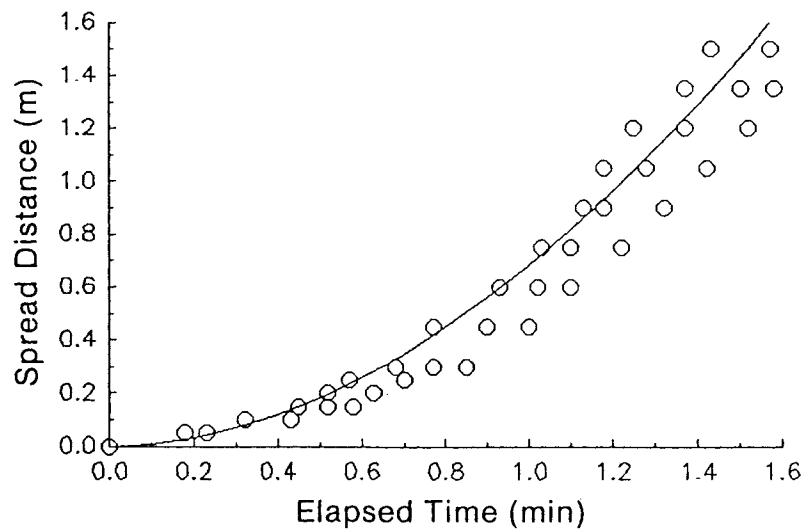
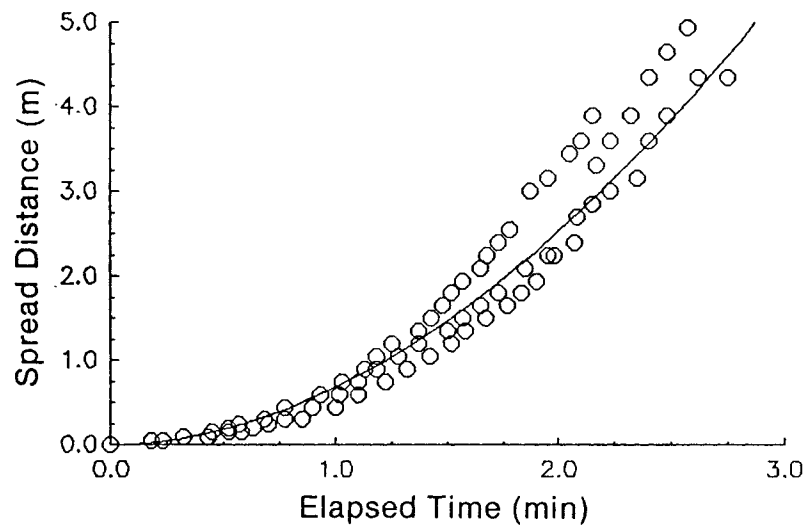


Figure 23. Comparison of all observed data (open circles) and prediction line for needle fuel loaded at 26.3 kg/m^3 and burned with a wind speed of 8.0 km/h . The upper plot shows the full data set, while the lower plot shows only the acceleration portion of the fire.

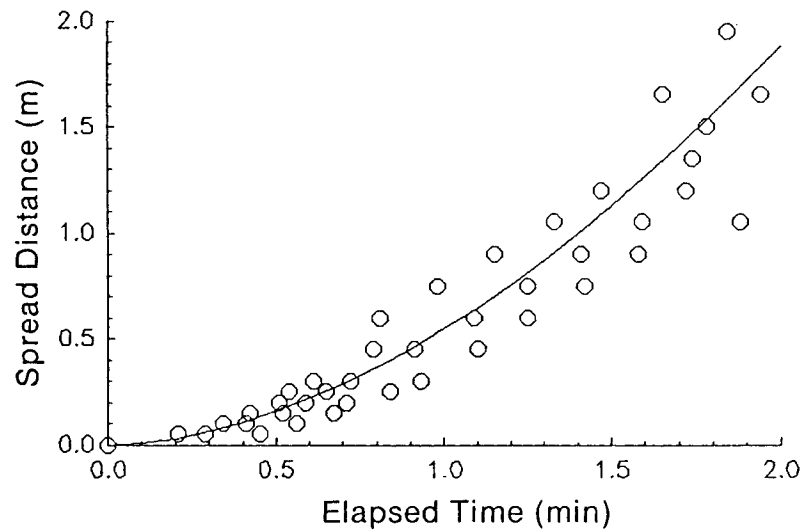
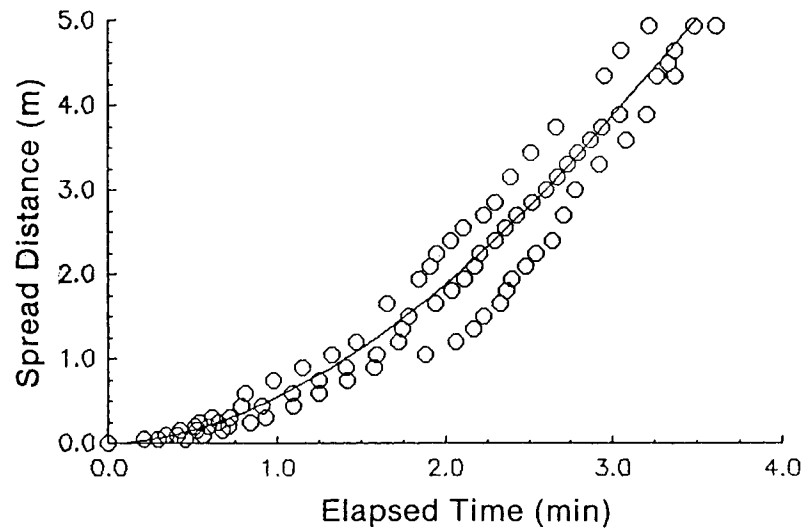


Figure 24. Comparison of all observed data (open circles) and prediction line for needle fuel loaded at 13.1 kg/m^3 and burned with a wind speed of 4.8 km/h . The upper plot shows the full data set, while the lower plot shows only the acceleration portion of the fire.

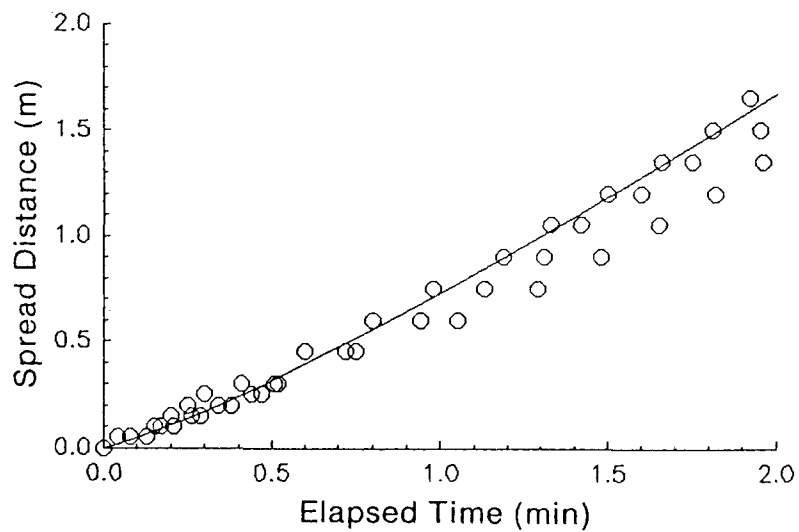
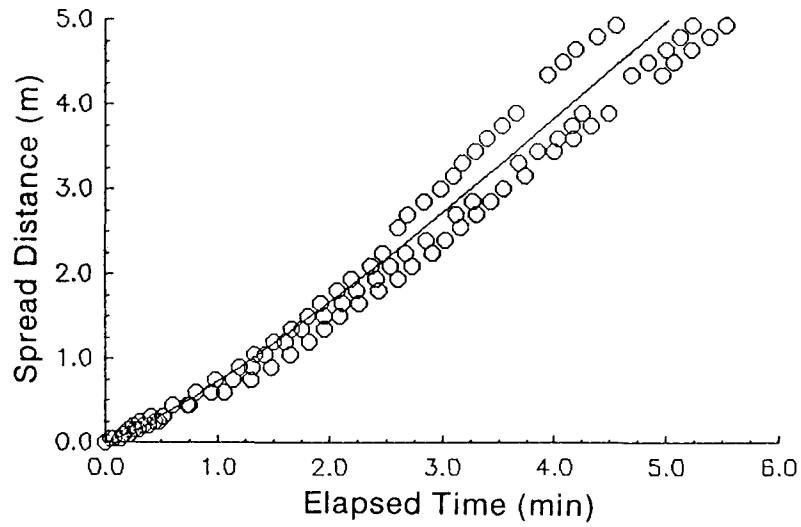


Figure 25. Comparison of all observed data (open circles) and prediction line for excelsior fuel loaded at 3.6 kg/m^3 and burned with a wind speed of 0.0 km/h . The upper plot shows the full data set, while the lower plot shows only the acceleration portion of the fire.

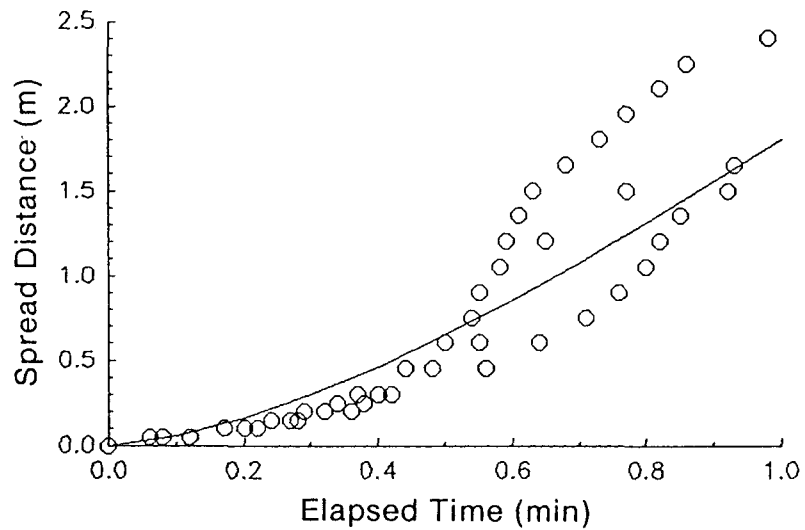
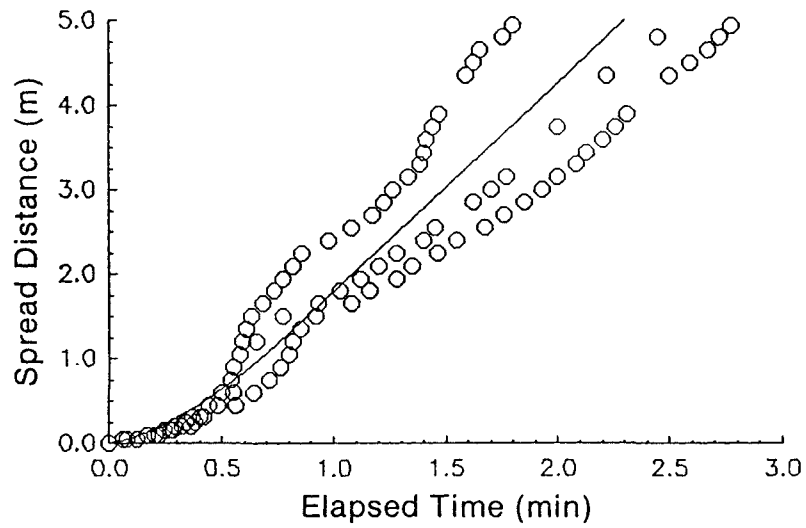


Figure 26. Comparison of all observed data (open circles) and prediction line for excelsior fuel loaded at 3.6 kg/m^3 and burned with a wind speed of 1.6 km/h . The upper plot shows the full data set, while the lower plot shows only the acceleration portion of the fire.

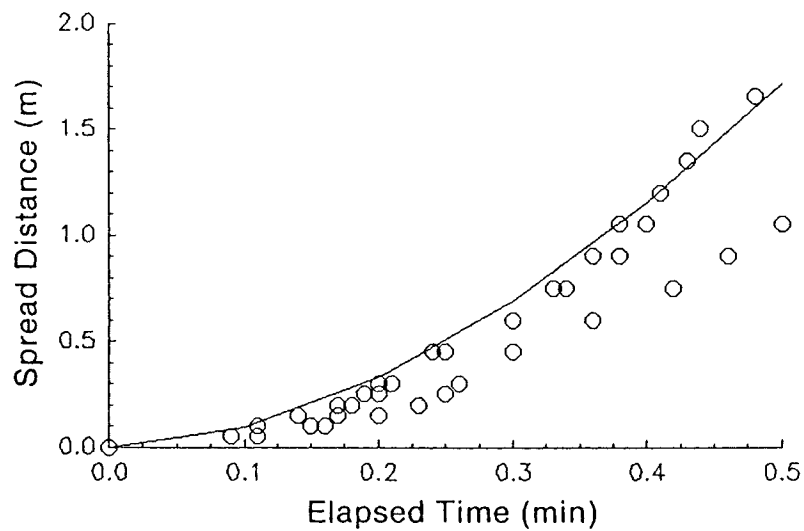
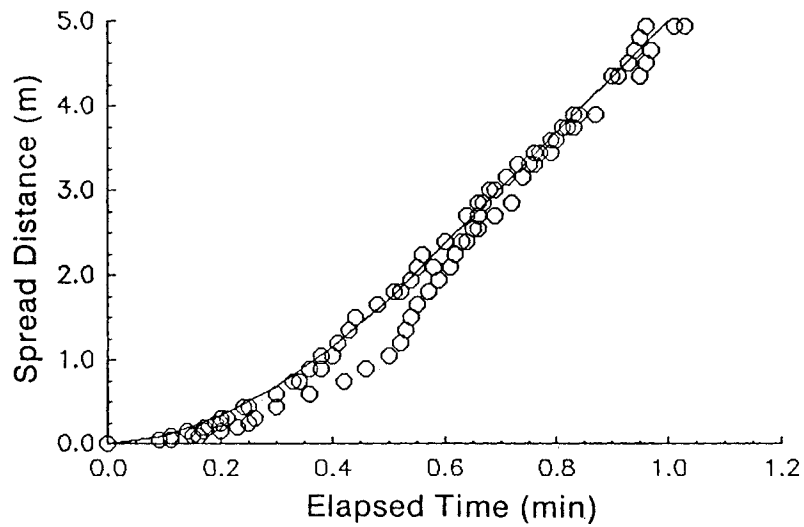


Figure 27. Comparison of all observed data (open circles) and prediction line for excelsior fuel loaded at 3.6 kg/m^3 and burned with a wind speed of 4.8 km/h . The upper plot shows the full data set, while the lower plot shows only the acceleration portion of the fire.

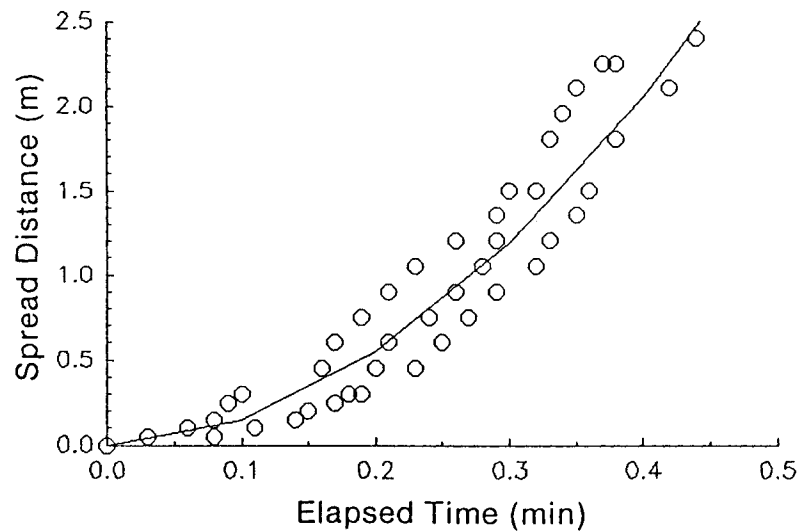
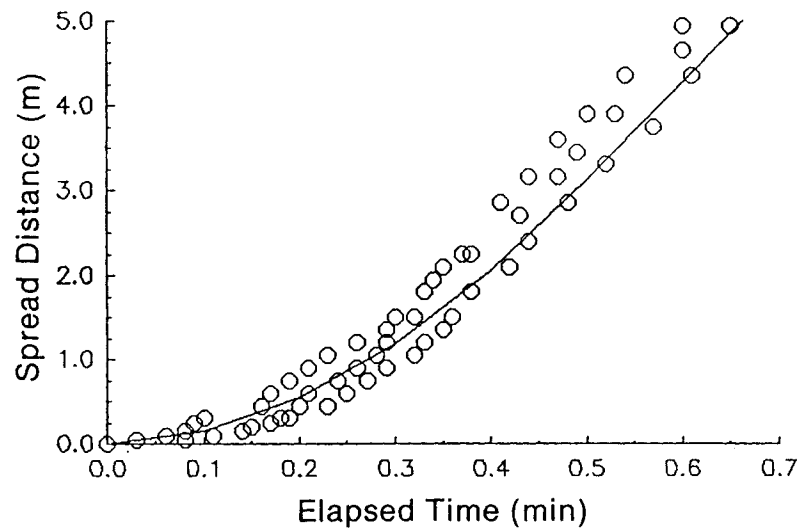


Figure 28. Comparison of all observed data (open circles) and prediction line for excelsior fuel loaded at 3.6 kg/m^3 and burned with a wind speed of 8.0 km/h . The upper plot shows the full data set, while the lower plot shows only the acceleration portion of the fire.

4.1.4 Elapsed Time to Equilibrium ROS.

The precise time required for the fire to complete the acceleration phase is difficult to determine directly from the observed data. A precise time can be determined mathematically from equation [7]. As stated previously, equation [7] describes the ROS at any time during the acceleration phase. If the ROS in equation [7] is set to equal the equilibrium ROS, the time required to reach equilibrium ROS can be solved for. Equation [12] shows the rearranged form of equation [7].

$$T_e = \left(\frac{ROSeq}{A * B} \right)^{\frac{1}{B-1}} \quad [12]$$

Where T_e = Time required to reach ROSeq (min)
 ROSeq = Equilibrium ROS (m/min) (from Table 3)
 A and B are coefficients (from Table 4).

Table 7 presents the calculated elapsed time to equilibrium values for all burning treatments over the range of wind speeds tested. Two values for the elapsed time to equilibrium ROS are presented in Table 7; the first being computed based on the original A and B coefficient values from the allometric equation (Table 5) and the second computed based on the predicted A and

B values from equations [8], [9], and [11]. The two elapsed time to equilibrium values are very similar in all cases demonstrating that the introduction of the regression lines to predict A and B coefficient values (equations [8], [9], and [11]) causes only a minor amount of error in this value. Figure 29 shows the plot of elapsed time to equilibrium ROS versus wind speed. It can be seen that the elapsed time to equilibrium ROS is static for each type of fuel over the range of wind speeds tested.

Table 7. Calculated elapsed time (Te) required to reach equilibrium ROS for all burning conditions.

Type of Fuel	Bulk density (kg/m ³)	Wind speed (km/h)	ROSeq ¹ (m/min)	A ²	B ²	Te (min)	
						(1) ³	(2) ⁴
N	26.3	0.0	0.37	0.156	1.263	10.9	17.2
N	26.3	1.6	0.51	0.234	1.420	2.8	2.6
N	26.3	4.8	1.44	0.434	1.611	3.3	2.4
N	26.3	8.0	3.23	0.650	2.055	2.3	2.8
N	13.1	4.8	2.27	0.548	1.759	3.1	2.9
E	3.6	0.0	1.13	0.725	1.177	4.9	3.5
E	3.6	1.6	2.46	1.896	1.700	0.7	0.8
E	3.6	4.8	6.59	5.317	1.792	0.6	0.6
E	3.6	8.0	11.58	12.327	1.865	0.5	0.5

¹ from Table 3

² from Table 5

³ computed using A and B coefficient values from Table 5

⁴ computed using A and B coefficient values calculated from equations [8], [9], and [11].

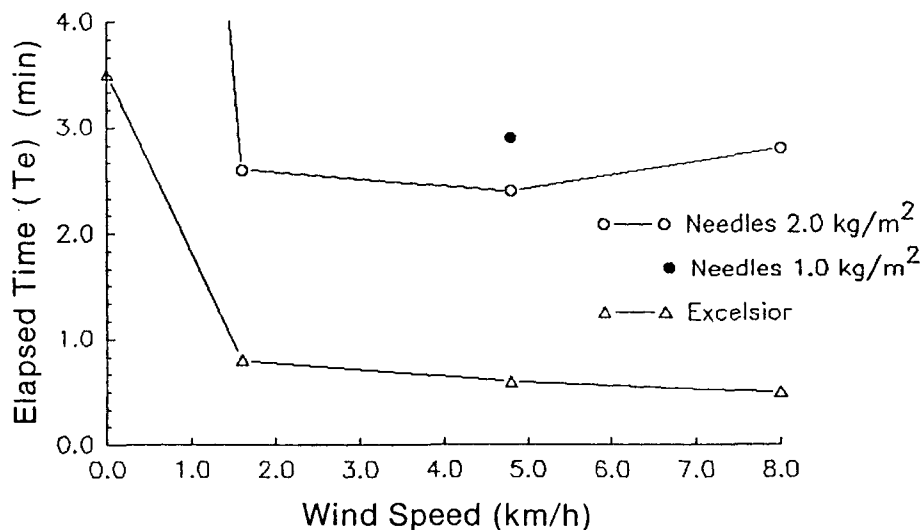


Figure 29. Calculated elapsed time (T_e) (from the final column in Table 6) required to attain equilibrium ROS versus wind speed. Note that the zero wind speed case for needles is off the graph.

The observed values for elapsed time to equilibrium ROS (T_e) and the past field observations of point source fires (Curry and Fons 1938, 1940; McArthur 1968, 1971; Lawson 1972, 1973; Johansen 1987; Alexander *et al.* 1988) are different. Observations from field point source ignition studies not only found much longer values for T_e but also that the T_e was dependent on wind speed. The longer time periods required to reach equilibrium ROS are likely a simple problem of scaling the small laboratory fires to the normal wildland fire situation. The historical observations of varying T_e with wind speed may be more difficult to quantify but the factors

likely linked are; 1) the vertical wind profiles for the fuel type in question and 2) the characteristics of the vertical fuel continuity (multilayered fuels). Further field research is required to definitively quantify the solution. Multilayered fuel types may require special consideration as the same acceleration pattern may be exhibited in each fuel layer.

4.2 Length-to-Breadth Analysis.

Length-to-Breadth (L/B) as described by Alexander (1985) or Length-to-Width as described by Anderson (1983) assumes fire shape to be that of an ellipse (or double ellipse in the case of Anderson (1983)) and the value of the L/B is a measure of the eccentricity of that ellipse. A value of 2 would mean the fire is twice as long as it is wide. L/B values, measured from perimeter plots developed from the overhead photos (Appendix II), showed some predictable results. For low wind speed trials (0.0 and 1.6 km/h) there was little or no observable trend in the L/B values over time. However, as the wind speed increased (to 4.8 and 8.0 km/h), so did the markedness of the trend, starting from a value of 1 (circular growth) and becoming progressively elongated until the edge of the fuel bed

was encountered (Fig. 30 and 31). The trend in L/B value showed no indication of stabilizing over the measurable life of the fire for the 8.0 km/h trials and debatable stabilization for the 4.8 km/h trials. Thus, for this experiment, a final L/B value for the type of fuel and wind speed is undeterminable in wind speeds beyond 1.6 km/h. At wind speeds of 0.0 and 1.6 km/h, L/B stabilized at about 1.0 and 1.3 respectively for both types of fuel.

In some cases, as can be seen in Figures 30 and 31, length-to-breadth values of less than 1.0 are observed, most notably in the zero wind case. This would seem to be an impossibility if the length-to-breadth were measured at any one time, the longest axis always being the numerator. However, if a series of length-to-breadth measurements are taken over time, a single common axis should be used, to avoid skewing the data to a value above 1.0.

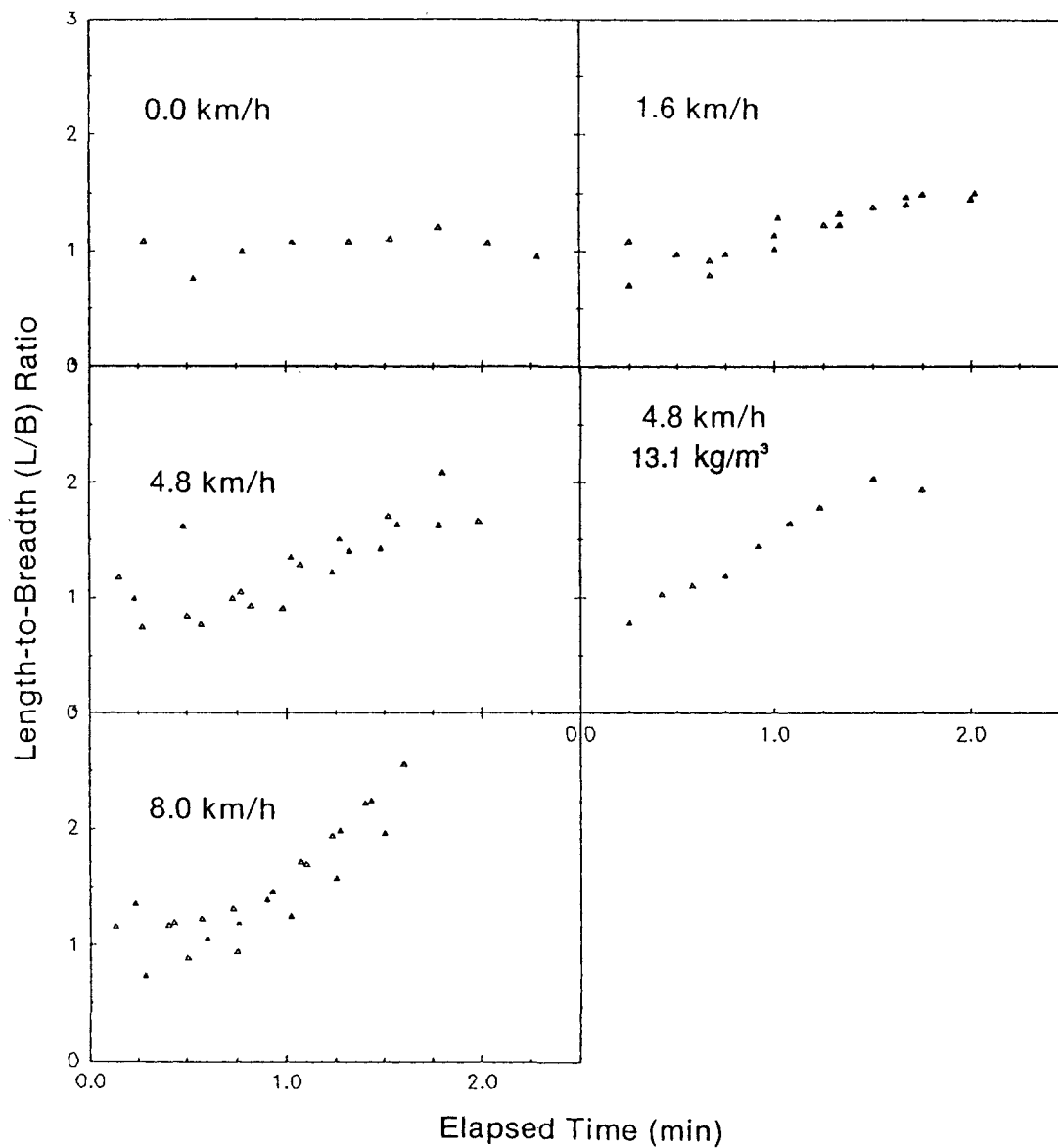


Figure 30. Variation in Length-to-Breadth ratio values over time for needle fuel treatments. Only the measurable period before the flanking fire reached the edge of the fuel bed is displayed. Treatment wind speeds are displayed for each respective plot. All fuel bulk densities are 26.3 kg/m³ unless noted otherwise.

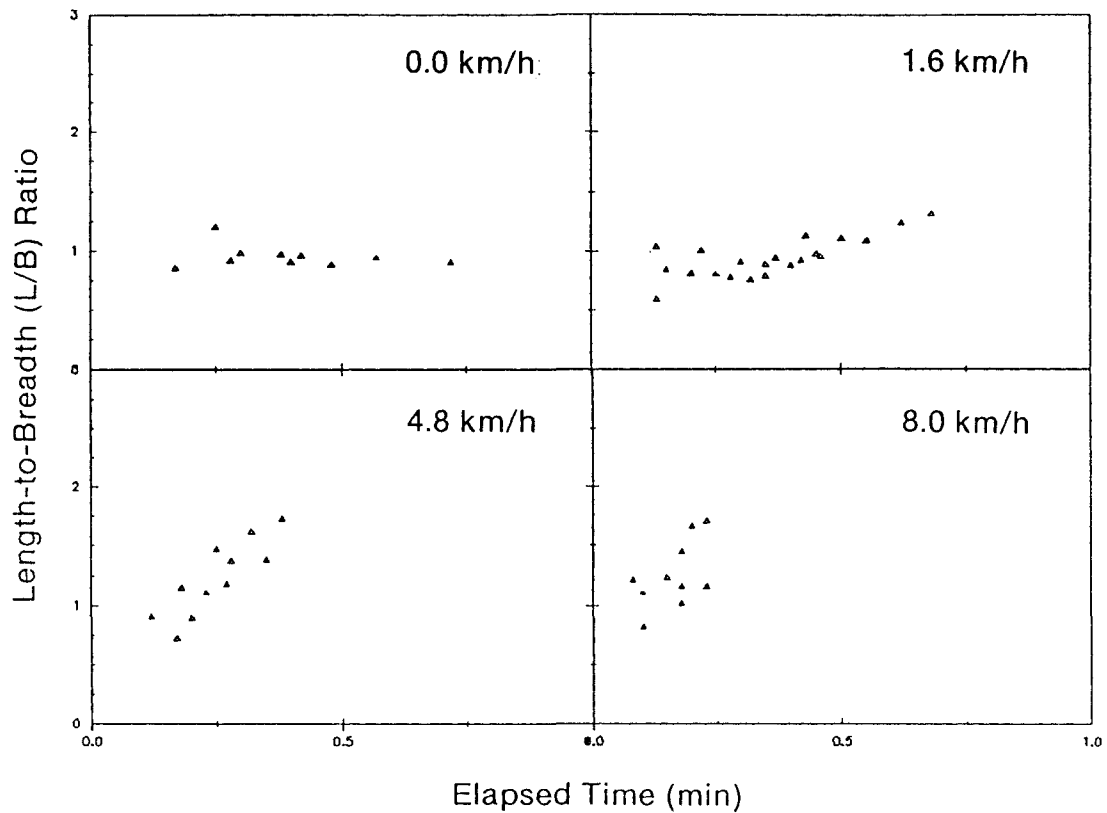


Figure 31. Variation in Length-to-Breadth ratio values over time for excelsior fuel treatments. Only the measurable period before the flanking fire reached the edge of the fuel bed is displayed. Treatment wind speeds are displayed for each respective plot.

4.3 Backing Fire Spread.

Backing fire spread was consistent for each type of fuel over the range of wind speeds and fuel loadings tested. Average backing fire ROS values, for all treatments, calculated using net distance spread / elapsed time, are presented in Table 8. This calculated ROS was not based on the full spread distance to the upwind end of the fuel bed (a total of 1.05 m), rather it was limited to the first 80 cm¹ of travel. By limiting the length of the backing fire spread distance in this way, it was hoped to avoid any anomalies caused by an unformed boundary layer wind condition. The boundary layer of air above the fuel bed is not stabilized at the upwind end of the fuel bed because the wind has met a new horizontal surface, raised 6.2 cm above the floor of the tunnel. The air flow at the extreme upwind end of the fuel bed tended to curl over the front of the fuel bed and establish a stable boundary layer some distance downwind from the end of the bed. For the purposes of this investigation the distance required to establish a uniform boundary layer air flow condition was assumed to be 25 cm.

¹Approximately - since the backing fire D/T information is based on images from the overhead camera, taken at certain time intervals, a precise time is not available for 80 cm upwind from the ignition point.

Figure 32 shows a scatterplot of the backing fire ROS versus wind speed for all fires. Two ROS values are evident over the range of wind speeds reflecting the different backing fire characteristics of the two types of fuel. Backing fire spread rate results for pine needles were very similar to results reported by Beaufait (1965)² who found consistent spread rates of 0.152 m/min over a range of wind speeds (2.4 - 12.8 km/h). A slight upward trend (as wind speed increased) in backing fire spread rates for excelsior fuels is detectable in Figure 32. Whether this trend is real or an anomaly of the data is difficult to determine due to the increasing variability in the observed spread rate data (Fig. 32). More experimentation is required to confirm the apparent trend.

²Burning environmental conditions differed for the current experiment, accounting for the difference in the observed ROS.

Table 8. Average equilibrium backing fire ROS values for each burning treatment.

Type of fuel	Bulk density (kg/m ³)	Wind speed (km/h)	Average backing fire ROS (m/min)	SE
Needles	26.3	0.0	0.23	0.017
Needles	26.3	1.6	0.19	0.003
Needles	26.3	4.8	0.19	0.031
Needles	26.3	8.0	0.22	--- ²
Needles	13.1	4.8	0.24	0.026
Excelsior	3.6	0.0	0.67	0.054
Excelsior	3.6	1.6	0.63	0.130
Excelsior	3.6	4.8	0.85	0.362
Excelsior	3.6	8.0	1.06 ¹	0.470

¹Highly variable spread rate data. As the wind speed escalated for the excelsior fuels, variability also increased.

²Data from only one fire was available.

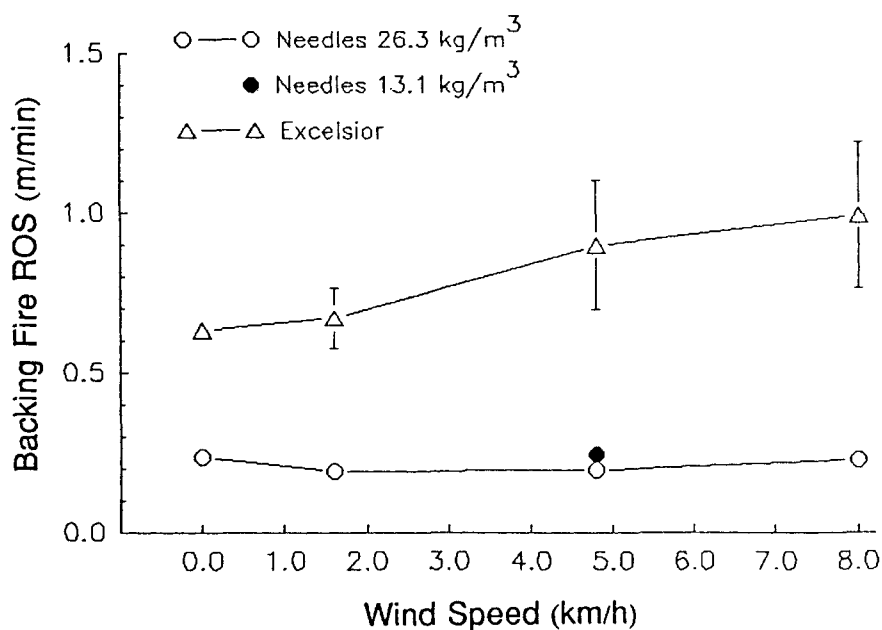


Figure 32. Variation in mean backing fire ROS over the range of wind speeds tested for all burning treatments. Points plotted are average ROS values with standard errors shown for each treatment. Note that at the current resolution of the graph, the error bars for the needle fuels are not visible.

4.4 Flame Length and Fire Intensity.

Flame length was measured on all fires with the use of the video image analysis system (McMahon, Adkins, and Rodgers 1986). The analysis system provides temporal and spatial values for flame height, depth, length, and cross-sectional area measured from video still frame images (Adkins 1988). Due to obstructions in the field of view the ignition point was not visible, in fact, the fire was not visible initially until it had travelled over 20 cm, and in most cases a full flame (suitable for digitizing) was visible only after 45 cm. Flame lengths measured after the fire had established a line across the fuel bed were constant over the range of wind speeds tested. This consistency in flame length measurements is in agreement with observation by Nelson and Adkins (1986) and invalidates any estimates of fire intensity based on flame length measurements (Byram 1959, Alexander 1982, Nelson and Adkins 1986). Frontal fire intensity based on heat of combustion, fuel consumption and head fire ROS is not possible as the quantity of fuel consumed by the head fire is not determinable.

In this investigation, during the study of the video imagery it was noted that a change in flame length occurred over the life of the fire. Flame length being

the distance from the center of the flame base to the furthest most tip of flame. Two phases of the fire were noted and the flame lengths were separated into groups. The first phase took place before the flanking fire had reached the edge of the fuel bed (while the head fire still retained a characteristic elliptical shape). The second phase occurred after the fire had spread along the fuel bed edges (the phenomenon noted in the overhead photos) to produce a straight line of fire across the fuel bed. The field of view severely limited the time available for analysis of the first phase of the fire, and in some cases (particularly the 0.0 km/h wind cases) precluded any measurement at all.

Flame lengths before and after the fuel bed "edge effect" are presented in Table 9. To contrast the two flame length values, a paired comparison T-test was set up using three flame length measurements before and after from each fire. Results from this test, grouping all data together, showed (P-value 0.000) that flame length before the edge effect was greater than the flame length after. The difference between the two values was 0.23 m (with a standard error of 0.027). When divided into the two types of fuel (needles and excelsior) the difference became more pronounced in the needle fuels

(0.34 m with a standard error of 0.028) but less pronounced in the excelsior fuels (0.10 m with a standard error of 0.031). The flame length difference was contrasted by the fact that no difference in flame height between the two groups was found. Flame height being the vertical distance from the surface of the fuel bed to the highest point of flame.

Table 9. Flame lengths by type of fuel and burning treatment before and after the fire reached the edge of the fuel bed.

Type of Fuel	Bulk density (kg/m ³)	Wind speed (km/h)	Flame length before (m)	Flame length after (m)
N	26.3	0.0	no data	0.767(0.025)
N	26.3	1.6	0.987(0.019)	0.617(0.022)
N	26.3	4.8	1.033(0.068)	0.613(0.059)
N	26.3	8.0	1.142(0.048)	0.847(0.039)
N	13.1	4.8	0.969(0.059)	0.766(0.055)
E	3.6	0.0	no data	0.584(0.017)
E	3.6	1.6	0.759(0.063)	0.751(0.029)
E	3.6	4.8	0.859(0.035)	0.754(0.040)
E	3.6	8.0	1.009(0.031)	0.856(0.062)

Note: Standard errors are given in parentheses.

The observed difference in observed flame lengths may have been due to measurement error. Measurement error in the flame length measurements before the edge effect are caused by a misinterpretation of the head fire flame depth. The flame depth measurement is

increased by including the flank fire flame which lags behind the head fire. It may also have been caused by a concentration of the convective force of the fire while the elliptical curvature of the head fire remained intact. This may be caused by the heat energy released by the flank fire being drafted forward into the head fire. This effect would break down once the line of fire across the fuel bed was established. Further investigation into this phenomenon is required.

5.0 Summary and Conclusions.

The present study represents the most complete empirical analysis of forest fire acceleration to date. Previous studies of point source ignition have been deficient in either intermediate perimeter location data (Fons 1940) or a well controlled burning environment (de Mestre 1982).

The theoretical models of fire acceleration proposed by Cheney (1981), Van Wagner (1985) and Weber (1988), which follow a natural growth function were generally supported by the experimental evidence (Fig 33). However, due to inherently high variability in observed ROS values when plotted with time, it was impossible to choose between the existing theoretical models. In order to circumvent the highly variable ROS problem the experimental data was analyzed as distance/time data and an allometric equation (power curve) fitted to the data. This equation form was easily differentiated producing an equation describing the change in ROS over time until the equilibrium spread rate had been achieved (Fig 33). The allometric equation is therefore used until the ROS value (from the differentiated equation) equals the equilibrium ROS. The differentiated equation can also be manipulated to estimate the length of time required to attain equilibrium ROS.

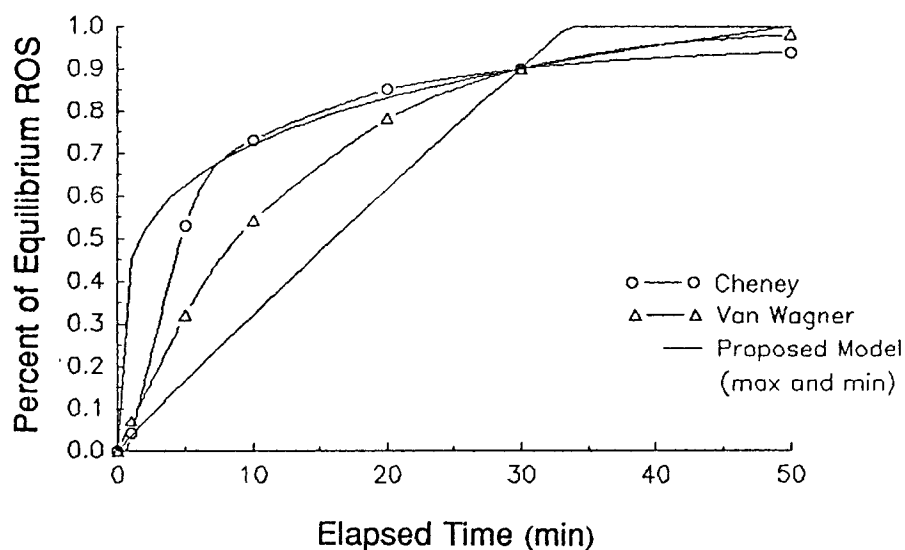


Figure 33. Comparison of the ROS pattern from the proposed model and the theoretical models suggested by Cheney (1981) and Van Wagner (1985). The proposed model has been scaled to the Van Wagner (1985) assumption of 30 min. to 90 percent of equilibrium ROS. The proposed model illustrates the two extreme values of the B coefficient value (1.204, and 1.944) with A coefficient values computed to satisfy the Van Wagner (1985) assumption.

The coefficient values, resulting from the regression of the distance/time data for each burning treatment, were in turn regressed on the variables which separated the original burning treatments (type of fuel, wind speed, equilibrium ROS, packing ratio). From these regressions it was found that the A coefficient value in the allometric equation was correlated with the equilibrium ROS, however the values for the two types of fuel were so vastly different the equations had to be separated by type of fuel. This difference in

coefficient values was attributed to the different physical and thermochemical properties of the two types of fuel. The B coefficient values from the allometric equation were fitted to a single natural growth equation with wind speed. No separation was made for type of fuel for the B coefficient regression. The derived equations for all parameters follow at the end of this chapter.

Inherent limitations of wind tunnel burning restrict the direct operational application of the results from this study. Estimates of midflame wind speed from 10 m open wind speed observations can be done with a variety of available models (eg. Cooper 1965, Berglund and Barney 1977, Albini and Baughman 1979). Modifications are required to allow for the different wind profile characteristics encountered in the field and a procedure must be established to allow for multiple layer fuel types.

Multilayer fuels could be approached in the same manner as the Van Wagner (1977) crown fire model; as the intensity output from the lowest fuel layer increases, at some point it will ignite the next fuel layer, starting the process again. Should the maximum intensity output from any lower fuel layer be

insufficient to ignite the subsequent fuel layer, no further fuel layer involvement will occur. This follows the stepwise acceleration proposal suggested by McArthur (1967), however by applying the derived acceleration function and a variation of the Van Wagner (1977) crown fire model, these successive acceleration steps of fuel layer involvement could be quantified.

A constant elapsed time to equilibrium spread (T_e) for each type of fuel (2.7 min and 0.6 min for needles and excelsior respectively) over the range of wind speeds tested (above 0.0 km/h) was also observed. This would indicate that while wind speed affects the rate of acceleration, T_e is dependent on the fuel bed characteristics and independent of other environmental factors. The observed constant T_e over a range of wind speeds appears to be at odds with field observations of increased T_e with increased wind speed (Curry and Fons 1938, 1940; McArthur 1968) but in agreement with theoretical models (Cheney 1981, Van Wagner 1985, Weber 1988). This apparent disparity between field and laboratory observations may be explained by the vertically heterogeneous nature of wind speeds in the field as opposed to the laminar wind flow found in the laboratory. Additionally, the presence of a multilayered fuel type may have added effects.

The model presented for acceleration to equilibrium ROS will be used operationally as a model within a model. That is; the equilibrium ROS will be predicted by an existing model (Rothermel 1972, McArthur 1973, Lawson et al. 1985) and the resulting value used as a variable in the acceleration model. "Nested" models of this type can be weak because small initial errors inserted at the start, can compound themselves in the final result. If the original predicted ROS is no where near the actual ROS, the acceleration function cannot hope to operate properly. Nevertheless, once the model has been adapted to operate in the field (through modifications to the A and B coefficient regression equations), application to existing fire behavior prediction systems is straight forward and can be broken into two possible cases:

1: The specified elapsed time of fire activity (starting from ignition) is less than the computed T_e value for the fuel type and weather conditions. In this case fire size calculations are based on equation [6] while fire behavior estimates can begin with the predicted head fire ROS from equation [7].

2: The specified elapsed time of fire activity (starting from ignition) is greater than the computed T_e value for the fuel type and weather conditions. In this case there would be no modification to the fire behavior estimates (the fire has reach equilibrium) but fire size computations would be modified as follows:

$$T_f = T - T_e \quad [13]$$

$$D_1 = A * T_e^B \quad [14]$$

$$D_2 = T_f * ROSeq \quad [15]$$

$$D = D_1 + D_2 \quad [16]$$

Where T = specified elapsed time of fire activity
 T_e = computed elapsed time to equilibrium
 ROS (equation [12])
 T_f = elapsed time of fire activity at
 the predicted equilibrium ROS
 D₁ = distance spread during the acceleration
 phase
 D₂ = distance spread during the equilibrium
 ROS phase
 A, B = constant regression coefficients
 described by equations [8], [9], and [11]
 ROSeq = equilibrium ROS
 D = total head fire spread distance for the
 specified elapsed time (T).

The Length-to-Breadth ratio of the fires failed to stabilize over the measurable life of the fire in all cases with wind speeds over 1.6 km/h. To properly analyze the effect of wind speed on the L/B ratio in wind tunnel experiments, wider fuel beds will be required. The use of wider fuel beds will in turn require a wind tunnel of larger proportions.

Backing fire spread rates were constant over the range of wind speeds tested. Needle fuel backing fire

spread rates varied about a mean of 0.211 m/min while excelsior varied about a mean of 0.80 m/min. As wind speed increased in the excelsior fuels, variability of the backing fire spread rate also increased. Results for needle fuel backing fire spread rates compared well with other reported backing fire spread data.

Flame lengths measured before the flanking fire encountered the edge of the fuel bed (while the elliptical head fire shape was still intact) were longer than flame lengths measured after the fire had formed a straight line across the fuel bed. The flame length difference was contrasted by the fact that the measured flame heights were the same. While it was obvious from viewing the video documentation that the two phases of fire spread were different in flame character, the difference was difficult to quantify.

5.1 Further Research Requirements.

While this study is not a definitive analysis of the acceleration of fire to equilibrium spread, it is an important first step. Extended laboratory study might include a more complete analysis of the effects of fuel bulk density and fuel moisture. Development of the workable theory on successive fuel layer involvement may

not only relate to fire acceleration but also lead to an indication of possible crown fire initiation.

Investigation into field application of the fire acceleration theories presented herein is required to further probe the disparities in field and laboratory differences in elapsed time to equilibrium ROS. This research would also provide a more accurate model for current fire behavior prediction systems to use.

Further investigation into Length-to-Breadth ratios in the wind tunnel is required to verify current operational models. Past studies on L/B ratios in the wind tunnel were not able to evaluate change over time, thereby not able to determine if the final stabilized L/B ratio had been achieved.

The difference observed in flame lengths between the elliptical fire front and the line of fire remains, as yet, not completely quantified. Although an obvious difference was observed, further study of this curiosity may reveal some interesting results.

5.2 Equation Summary

$$D = A * T^B \quad [6]$$

$$ROS = A * B * T^{(B - 1)} \quad [7]$$

$$T_e = \left(\frac{ROSeq}{A * B} \right)^{\frac{1}{B-1}} \quad [12]$$

$$B = 1.204 + 0.740 * (1 - e^{(-0.319 * WS)}) \quad [11]$$

Needles: $A = 0.324 * ROSeq^{0.637} \quad [8]$

Excelsior: $A = 0.628 * ROSeq^{1.188} \quad [9]$

$$T_f = T - T_e \quad [13]$$

$$D_1 = A * T_e^B \quad [14]$$

$$D_2 = T_f * ROSeq \quad [15]$$

$$D = D_1 + D_2 \quad [16]$$

Where D = head fire spread distance (m)
 T = elapsed time since ignition (min)
 ROS = head fire ROS at time T (m/min)
 WS = wind speed (km/h)
 T_e = elapsed time to reach ROSeq (min)
 ROSeq = equilibrium ROS (m/min)
 T_f = elapsed time of fire activity at the predicted equilibrium ROS (min)
 D₁ = distance spread during the acceleration phase (m)
 D₂ = distance spread during the ROSeq phase (m)
 A and B are allometric equation coefficients

REFERENCES CITED

- Adkins, C.W. 1988. Fire image analysis system version 4.0. USDA For. Serv. [report in prep.]
- Albini, F.A. 1984. Wildland fires. Amer. Sci. 72: 590-597.
- Albini, F.A. and R.G. Baughman. 1979. Estimating windspeeds for predicting wildland fire behavior. USDA For. Serv., Intermt. For. and Range Exp. Stn., Ogden, Utah. Res. Pap. INT-221. 12 p.
- Alexander, M.E. 1982. Calculating and interpreting forest fire intensities. Can. J. Bot. 60:349-357, 2185.
- Alexander, M.E. 1985. Estimating the length-to-breadth ratio of elliptical forest fire patterns. Pages 287-304 In Proc. Eighth Conf. Fire and For. Meteor. (Apr. 29 - May 2, Detroit, Mich.) Soc. Am. For., Bethesda, Md. SAF Publ. 85-04.
- Alexander, M.E. 1987. Personal Communication.
- Alexander, M.E., and R.S. McAlpine. 1986. Fire behavior in the black spruce-Labrador tea - Cladonia fuel complex: the Big Fish Lake Project ... a progress report. In Proc. Third West. Reg. Fire Weather Comm. Sci. and Tech. Seminar (Feb. 4, Edmonton, Alta.). Govt. Can., Can. For. Serv., West. and North. Reg., North. For. Cent., Edmonton, Alta. Study NOR-5-05 (NOR-5-101) File Rep. No. 15.
- Alexander, M.E., B.D. Lawson, B.J. Stocks, and C.E. Van Wagner 1984. User guide to the Canadian Forest Fire Behavior Prediction System: rate of spread relationships. Interim edition. Environ. Can., Can. For. Serv. Fire Danger Group. 73 p. + Supplements [First Printing - July 1984; Revision & Second Printing - September 1984].
- Alexander, M.E., B.D. Lawson, B.J. Stocks, and C.E. Van Wagner. 1988. Fire behavior in black spruce - lichen woodland: the Porter Lake project. Govt. Can., Can. For. Serv., North. For. Cent., Edmonton Alta. Inf. Rep. NOR-X-000 [in press]

- Anderson, H.E. 1964. Mechanisms of fire spread research progress report NO. 1. USDA For. Serv., Intermt. For. and Range Exp. Stn., Ogden, Utah. 20 p.
- Anderson, H.E. 1983. Predicting wind-driven wild land fire size and shape. USDA For. Serv., Intermt. For. and Range Exp. Stn., Ogden, Utah. Res. Pap. INT-305. 26 p.
- Anderson, H.E., R.D. Schuette, and R.W. Mutch. 1978. Timelag and equilibrium moisture content of ponderosa pine needles. USDA For. Serv., Intermt. For. and Range Exp. Stn., Ogden, Utah. Res. Pap. INT-202. 28 p.
- Andrews, P.L. 1986. BEHAVE: fire behavior prediction and fuel modeling system -- BURN subsystem, Part 1. USDA For. Serv., Intermt. Res. Stn., Ogden, Utah. Gen. Tech. Rep. INT-194. 130 p.
- Anonymous. 1975. Fire behaviour in tropical open forest. Pages 16-17. In Forestry and Timber Bureau Annual Report, 1973-74. Aust. Govt. Publ. Serv., Canberra, A.C.T.
- Beaufait, W.R. 1965. Characteristics of backfires and headfires in a pine needle fuel bed. USDA For. Serv., Intermt. For. Range Exp. Stn., Ogden, Utah. Res Note INT-39. 7 p.
- Berglund, E.R., and R.J. Barney. 1977. Air temperature and wind profiles in an Alaskan lowland black spruce stand. USDA For. Serv., Pac. Northwest For. and Range Exp. Stn., Portland, Oreg. Res. Note PNW-305. 12 p.
- Byram, G.M. 1959. Combustion of forest fuels. Pages 61-89. In Forest Fire: Control and Use, K.P. Davis (ed.). McGraw-Hill, N.Y.
- Catchpole, W.(R). 1982. A statistical analysis of some bushfire data I. Univ. New South Wales, Fac. Military Stud., Dep. Math. Royal Military Coll. Duntroon A.C.T. No. 3/82. 40 p.
- Catchpole, E.A., and W.R. Catchpole. 1983. Analysis of the 1972 Darwin grass fires. Univ. New South Wales, Fac. Military Stud., Royal Military Coll. Duntroon, A.C.T. Rep. No. 3/83. 67 p.

- Chandler, C., P. Cheney, P. Thomas, L. Trabaud, and D. Williams. 1983. Fire in forestry. Volume I: Forest fire behavior and effects. John Wiley & Sons, Inc., New York. N.Y. 450 p.
- Cheney, N.P. 1981. Fire behaviour. Pages 151-175. In Fire and the Australian Biota. Aust. Acad. Sci., Canberra, A.C.T.
- Cheney, N.P. 1983. Behaviour of fire in Australia forests. Paper 'A' In Life Safety and Escape from Fire - Proc. Ninth Natl. Conf. Aust. Fire Prot. Assoc. (Sept. 14-16, Sydney, N.S.W.). 12 p.
- Cheney, N.P. 1985. New approaches to fire danger and fire behaviour. In Proc. Fire Weather Serv. Conf. (May 13-14, Adelaide, S.A.). Aust. Dep. Sci., Bureau Meteor., Melbourne, Vic. 9 p.
- Cheney, N.P., and G.A.V. Bary. 1969. The propagation of mass conflagrations in a standing eucalypt forest by the spotting process. Paper A6. In Collected Papers. Mass Fire Symp. (Feb. 10-12, Canberra, A.C.T.), Vol. I. Commonw. Aust., Defence Standards Lab., Maribyrnong, Vic.
- Cooper, R.W. 1965. Wind movements in pine stands. Georgia For. Res. Coun., Res. Pap. 33. 4 p.
- Curry, J.R., and W.L. Fons. 1938. Rate of spread of surface fires in the ponderosa pine type of California. J. Agric. Res. 57: 239-267.
- Curry, J.R., and W.L. Fons. 1940. Forest-fire behavior studies. Mech. Eng. 62: 219-225.
- de Mestre, N. 1982. Small-scale fire experiments. Univ. New South Wales, Fac. Military Stud., Dep. Math., Royal Military Coll., Duntroon, A.C.T. Rep. No. 81/3. 10 p.
- Fried, J.S., and J.K. Gilles. 1987. California fire economics simulator: initial attack model (CFES-IAM). User's Manual (version 1.11). Univ. Calif., Dep. For. and Resour. Manage., Berkley, Calif. 124 p.

- Fons, W.L. 1940. Forest fuels progress report no. 6, May 20, 1940. Calif. For. and Range Exp. Stn. Unpublished report on file with USDA For. Serv., Pac. Southwest For. and Range Exp. Stn., For. Fire Lab., Riverside, Calif. 47 p.
- Fons, W.L. 1940. An eiffle-type wind tunnel for forest research. J. For. 881-884.
- Fons, W.L. 1946. Analysis of fire spread in light fuels. J. Agric. Res. 72: 93-121.
- Johansen, R.W. 1987. Ignition patterns and prescribed fire behavior in southern pine forests. Georgia For. Comm., Res. Division, Macon, Ga. For. Res. Pap. 72. 6 p.
- Kerr, J.W., C.C. Buck, W.E. Cline, S. Martin, and W.D. Nelson. 1971. Nuclear weapons effects in a forest environment - thermal and fire. Gen. Electric. Co.-TEMPO, DoD Nuclear Inf. and Analysis Cent., Santa Barbara, Calif. Rep. N2: TR 2-70. n.p.
- Kiil, A.D. 1975. Fire spread in a black spruce stand. Can. For. Serv. Bi-mon. Res. Notes 31:2-3.
- Lanoville, R.A., and R.E. Schmidt. 1985. Wildfire documentation in the Northwest Territories: a case study of Fort Simpson-40-1983. Pages 17-22 In Proc. Second West Reg. Fire Weather Comm. Sci. and Tech. Seminar (Mar. 6, 1984, Edmonton, Alta.). Govt. Can./ Can. For. Serv., North. For. Res. Cent., Edmonton, Alta. Study NOR-5-191 File Rep. No. 9.
- Lawson, B.D. 1972. Fire spread in lodgepole pine stands. M.Sc. Thesis, Univ. Mont., Missoula, Mont. 119 p. [also available as: Environ. Can., Can. For. Serv., Pac. For. Res. Cent., Victoria, B.C. Int. Rep. BC-36].
- Lawson, B.D. 1973. Fire behavior in lodgepole pine stands related to the Canadian Forest Fire Weather Index. Dept. Environ., Can. For. Serv., Pacific For. Res. Cent. Inf. Rep. BC-X-76. 26 p.

- Lawson, B.D., B.J. Stocks, M.E. Alexander, and C.E. Van Wagner. 1985. A system for predicting fire behavior in Canadian forests. Pages 6-16. In Proc. Eighth Conf. Fire and For. Meteorol. (Apr. 29-May 2, Detroit, Mich.). Soc. Am. For., Bethesda, Md. SAF Publ. 85-04.
- Luke, R.H., and A.G. McArthur. 1986. Bushfires in Australia. Revision and second printing. Aust. Govt. Publ. Serv., Canberra, A.C.T. 359 p.
- McAlpine, R.S. 1986. Forest fire growth calculator. Govt. Can., Can. For. Serv., North. For. Cent., Edmonton, Alta. For. Manage. Note No. 35. 8 p.
- McAlpine, R.S. 1987. Two BASIC programs for fire danger and fire behavior computations. Govt. Can., Can. For. Serv., North. For. Cent., Edmonton, Alta. For. Manage. Note 43. 4 p.
- McArthur, A.G. 1966. Weather and grassland fire behaviour. Commonw. Aust., Dep. Natl. Develop., For. and Timber Bureau, Canberra, A.C.T. Leaflet No. 100. 23 p.
- McArthur, A.G. 1967. Fire behaviour in eucalypt forests. Commonw. Aust., Dep. Natl. Develop., For. Timb. Bureau, For. Res. Instit., Canberra, A.C.T. Leaflet No. 107. 36 p.
- McArthur, A.G. 1968. The effect of time on fire behaviour and fire suppression problems. S.A. Emergency Fire Serv., Keswick, South Aust. E.F.S. Manual 1968:3-6, 10-13.
- McArthur, A.G. 1971. Aspects of fire control in the P. caribaea and P. ellioittii plantations of north western Viti Levu, Fiji Islands. Commonw. Aust., Dep. Natl. Develop., For. and Timber Bureau, Canberra, A.C.T. Report to Fiji Pine Commission. 38 p. + Appendices.
- McArthur, A.G. 1973. Forest fire danger meter Mk. 5. Forest Research Institute, Forestry and Timber Bureau, Canberra, Australia.
- McMahon, C.K., C.W. Adkins, and S.L. Rodgers. 1986. A video image analysis system for measuring fire behavior. Fire Manage. Notes, 47(1): 10-15.

- Nelson, R.M. and C.W. Adkins. 1986. Flame characteristics of wind-driven surface fires. *Can. J. For. Res.* 16:1293-1300
- Noble, I.R., G.A.V. Bary and A.M. Gill. 1980. McArthur's fire danger meters expressed as equations. *Aust. J. Ecol.* 5, 201-203.
- Parton, W.J. and G.S. Innis. 1972. Some graphs and their functional forms. *Nat. Res. Ecol. Lab. Colorado State Univ. Fort Collins, Colorado. Tech. Rep.* 153. 41 p.
- Pyne, S.J. 1984. *Introduction to wildland fire; fire management in the United States.* John Wiley & Sons, Inc., New York. 455 p.
- Rothermel, R.C. 1967. Airflow characteristics - wind tunnels and combustion facilities Northern Forest Fire Laboratory. USDA For. Serv., Intermt. For. and Range Exp. Stn., Missoula Mt. (unnumbered publ.) 32 p.
- Rothermel, R.C. 1972. A mathematical model for predicting fire spread in wildland fuels. USDA For. Serv., Intermt. For. and Range Exp. Stn., Ogden, Utah. *Res. Pap. INT-115.* 40 p.
- Rothermel, R.C. 1983. How to predict the spread and intensity of forest and range fires. USDA For. Serv., Intermt. For. and Range Exp. Stn., Ogden, Utah. *Gen. Tech. Rep. INT-143.* 161 p.
- Rothermel, R.C. 1985. Fire behavior considerations of aerial ignition. Pages 143-158 In Proc. Workshop Prescribed Fire by Aerial Ignition (Oct. 30 - Nov. 1, 1984, Missoula, Mt.). Intermt. Fire Council., Missoula, Mt.
- Rothermel, R.C., and H.A. Anderson. 1966. Fire spread characteristics determined in the laboratory. USDA For. Serv., Intermt. For. and Range Exp. Stn., Ogden, Utah. *Res. Pap. INT-30.* 34 p.
- Schuetz, R.D. 1965. Preparing reproducible pine needle fuel beds. USDA For. Serv., Intermt. For. and Range Exp. Stn., Ogden, Utah. *Res. Note INT-36.* 7 p.

- Show, S.B. 1919. Climate and forest fires in northern California. *J. For.* 17: 965-979.
- Susot, R.A. 1982. Characterization of the thermal properties of forest fuels by combustible gas analysis. *For. Sci.*, 28(2):404-420.
- Van Wagner, C.E. 1977. Conditions for the start and spread of crown fire. *Can. J. For. Res.* 7:23-34.
- Van Wagner, C.E. 1985. Fire spread from a point source. Govt. Can., Can. For. Serv., Petawawa Natl. For. Instit., Chalk River, Ont. Memo PI-4-20 dated January 14, 1985 to P.H. Kourtz. 2 p. [unpublished].
- Weber, R.O. 1988. Analytical models for fire spread due to radiation. *Combust. Flame* [in press].
- Williams, D.E. 1955. Fire hazard resulting from jack pine slash. Can. Dep. North. Aff. and Natl. Resour., For. Branch, For. Res. Div. Ottawa, Ont. Tech. Note 22. 17 p.
- Wilson, R.A., Jr. 1982. A reexamination of fire spread in free burning porous fuel beds. USDA For. Serv., Intermt. For. and Range Exp. Stn., Ogden, Utah. Res. Pap. INT-289. 28 p.
- Wilson, R.A., Jr. 1985. Observations of extinction and marginal burning states in free burning porous fuel beds. *Combust. Sci. and Tech* 44:179-193.

APPENDIX I

Ocular Distance/Time Data

Fuel: Needles
 Loading: 2.0 kg/m²
 Wind speed: 0.0 km/h

Total Spread Distance (cm)	Elapsed Time (minutes)		
	Burn # 24	Burn # 25	Burn # 27
0.00	0.00	0.00	0.00
5.00	0.45	0.84	0.71
10.00	0.63	1.16	
15.00	0.82	1.46	1.13
20.00	1.06	1.72	1.36
25.00	1.25	1.92	1.64
30.00	1.47	2.16	1.87
45.00	1.96	2.81	2.52
60.00	2.36	3.36	3.29
75.00	2.78	3.69	3.81
90.00	3.12	4.22	4.52
105.00	3.74	4.84	4.92
120.00	4.21	5.46	5.52
135.00	4.92	5.91	6.01
150.00	5.49	6.37	6.30
165.00	6.00	6.98	6.78
180.00		7.59	7.13
195.00	6.76	8.05	7.51
210.00	7.16	8.40	8.09
225.00	7.59	8.69	8.48
240.00	8.00	9.21	8.95
255.00	8.50	9.61	9.33
270.00	8.80	10.00	9.75
285.00	9.18	10.37	10.22
300.00	9.55	10.74	10.56
315.00	9.90	11.08	11.04
330.00	10.35	11.45	11.52
345.00	10.77	11.91	11.91
360.00	11.13	12.41	12.30
375.00	11.49	12.87	12.75
390.00	11.71	13.21	13.11
435.00	13.06	14.40	14.04
450.00	13.49	14.81	14.37
465.00	13.88	15.25	14.93
480.00	14.26	15.57	15.46
495.00	14.76	16.12	15.98

Fuel: Needles
 Loading: 2.0 kg/m²
 Wind Speed: 1.6 km/h

Total Spread Distance (cm)	Elapsed Time (minutes)		
	Burn # 1	Burn # 4	Burn # 5
0.00	0.00	0.00	0.00
5.00		0.20	0.47
10.00		0.55	0.72
15.00	0.83	0.73	0.90
20.00		0.85	1.00
25.00		0.95	1.20
30.00	1.28	1.07	1.33
45.00	1.50	1.32	1.57
60.00	1.77	1.55	1.75
75.00	2.00	1.83	2.00
90.00	2.25	2.10	2.33
105.00	2.67	2.43	2.58
120.00	3.03	2.83	2.78
135.00	3.53	3.13	3.17
150.00	3.85	3.63	3.68
165.00	4.13	4.00	4.00
180.00	4.50	4.42	4.47
195.00	4.87	4.83	4.78
210.00	5.27	5.15	5.17
225.00	5.53	5.58	5.45
240.00	5.78	5.87	5.62
255.00	6.07	6.07	5.83
270.00	6.18	6.28	
285.00	6.50	6.57	6.20
300.00	6.75	6.85	6.47
315.00	7.00	7.23	6.75
330.00	7.25	7.53	7.08
345.00	7.67	7.78	7.30
360.00	8.12	8.08	7.67
375.00	8.45	8.50	7.97
390.00	8.83	8.85	8.22
435.00	10.00	9.83	9.00
450.00	10.33	10.00	
465.00	10.48	10.58	9.33
480.00	10.78	10.85	9.60
495.00	11.08	11.08	9.75

Fuel: Needles
 Loading: 2.0 kg/m²
 Wind speed: 4.8 km/h

Total Spread Distance (cm)	Elapsed Time (minutes)				
	Burn# 3	Burn# 6	Burn# 7	Burn# 28	Burn# 29
0.00	0.00	0.00	0.00	0.00	0.00
5.00	0.25	0.42	0.32	0.23	0.24
10.00	0.48	0.60	0.47	0.57	0.49
15.00	0.65	0.73	0.60	0.67	0.65
20.00	0.73	0.83	0.70	0.85	0.90
25.00	0.78	0.92	0.77	0.92	1.00
30.00	0.92	1.00	0.83	1.04	1.09
45.00	1.10	1.15	0.98	1.17	1.32
60.00	1.27	1.32	1.20	1.39	1.51
75.00	1.40	1.50	1.40	1.53	1.66
90.00	1.55	1.58	1.48	1.67	1.77
105.00	1.65	1.72	1.68	1.84	1.91
120.00	1.82	1.83		1.98	2.11
135.00		1.97	1.75	2.08	2.28
150.00	2.12	2.10	1.93	2.14	2.36
165.00	2.28	2.25	2.05	2.26	2.55
180.00	2.33	2.32	2.18	2.40	2.65
195.00	2.40	2.40	2.28	2.50	2.79
210.00	2.53	2.48	2.38	2.61	2.88
225.00	2.62	2.53	2.50	2.75	3.02
240.00	2.75	2.60	2.60	2.87	3.10
255.00	2.93	2.72	2.65	2.98	3.23
270.00	3.00	2.83	2.78	3.12	3.35
285.00	3.13	2.95	2.93	3.31	3.44
300.00	3.23	3.02	3.07	3.41	3.60
315.00	3.35	3.13	3.23	3.59	3.70
330.00	3.48	3.22	3.32	3.68	3.81
345.00	3.57	3.28	3.38	3.79	3.92
360.00	3.65	3.37	3.50	3.92	4.01
375.00	3.73	3.40	3.57	4.01	4.15
390.00	3.83	3.52	3.63	4.12	4.31
435.00	4.15	3.78		4.42	4.61
450.00			4.00	4.56	4.73
465.00	4.32	3.93		4.66	4.82
480.00		3.97		4.78	4.96
495.00	4.42	4.08	4.20	4.95	5.09

Fuel: Needles
 Loading: 1.0 kg/m²
 Wind speed: 4.8 km/h

Total Spread Distance (cm)	Elapsed Time (minutes)		
	Burn # 21	Burn # 22	Burn # 23
0.00	0.00	0.00	0.00
5.00	0.29	0.21	0.45
10.00	0.41	0.34	0.56
15.00	0.52	0.42	0.67
20.00	0.59	0.51	0.71
25.00	0.65	0.54	0.84
30.00	0.72	0.61	0.93
45.00	0.91	0.79	1.10
60.00	1.09	0.81	1.25
75.00	1.25	0.98	1.42
90.00	1.41	1.15	1.58
105.00	1.59	1.33	1.88
120.00	1.72	1.47	2.06
135.00	1.74		2.17
150.00	1.78		2.23
165.00	1.94	1.65	2.33
180.00	2.04		2.37
195.00	2.12	1.84	2.40
210.00	2.18	1.91	2.48
225.00	2.21	1.95	2.54
240.00	2.30	2.03	2.64
255.00	2.36	2.11	
270.00	2.43	2.23	2.71
285.00	2.52	2.30	
300.00	2.60		2.78
315.00	2.67	2.39	
330.00	2.73		2.92
345.00	2.79	2.51	
360.00	2.87		3.08
375.00	2.94	2.66	
390.00	3.04		3.20
435.00	3.26	2.95	3.37
450.00	3.33		
465.00	3.37	3.05	
495.00	3.48	3.22	3.61

Fuel: Needles
 Loading: 2.0 kg/m²
 Wind speed: 8.0 km/h

Total Spread Distance (cm)	Elapsed Time (minutes)		
	Burn # 2	Burn # 8	Burn# 9
0.00	0.00	0.00	0.00
5.00		0.18	0.23
10.00		0.32	0.43
15.00	0.58	0.45	0.52
20.00		0.52	0.63
25.00		0.57	0.70
30.00	0.85	0.68	0.77
45.00	1.00	0.77	0.90
60.00	1.10	0.93	1.02
75.00	1.22	1.03	1.10
90.00	1.32	1.13	1.18
105.00	1.42	1.18	1.28
120.00	1.52	1.25	1.37
135.00	1.58	1.37	1.50
150.00	1.67	1.43	1.57
165.00	1.77	1.48	1.65
180.00	1.83	1.52	1.73
195.00	1.90	1.57	
210.00		1.65	1.85
225.00	1.95	1.68	1.98
240.00		1.73	2.07
255.00		1.78	
270.00	2.08		
285.00			2.15
300.00		1.87	2.23
315.00		1.95	2.35
330.00	2.17		
345.00		2.05	
360.00	2.23	2.10	2.40
390.00	2.32	2.15	2.48
435.00	2.40	2.75	2.62
465.00	2.48		
495.00	2.57		

Fuel: Excelsior
 Loading: 0.277 kg/m²
 Wind Speed: 0.0 km/h

Total Spread Distance (cm)	Elapsed Time (minutes)		
	Burn # 19	Burn # 20	Burn # 26
0.00	0.00	0.00	0.00
5.00	0.04	0.08	0.13
10.00	0.15	0.17	0.21
15.00	0.20	0.26	0.29
20.00	0.25	0.34	0.38
25.00	0.30	0.44	0.47
30.00	0.41	0.51	0.52
45.00	0.60	0.75	0.72
60.00	0.80	1.05	0.94
75.00	0.98	1.29	1.13
90.00	1.19	1.48	1.31
105.00	1.33	1.65	1.42
120.00	1.50	1.82	1.60
135.00	1.66	1.96	1.75
150.00	1.81	2.09	1.95
165.00	1.92	2.26	2.11
180.00	2.07	2.43	2.24
195.00	2.19	2.60	2.41
210.00	2.36	2.73	2.54
225.00	2.47	2.91	2.67
240.00		3.03	2.86
255.00	2.60	3.16	
270.00	2.69	3.30	3.12
285.00	2.83	3.42	3.27
300.00	2.98	3.54	
315.00	3.09	3.73	
330.00	3.18		3.67
345.00	3.29	3.99	3.85
360.00	3.39	4.17	4.03
375.00	3.53	4.33	4.15
390.00	3.65	4.48	4.25
435.00	3.94	4.96	4.69
450.00	4.07	5.07	4.84
465.00	4.19	5.22	5.00
480.00	4.38	5.38	5.12
495.00	4.55	5.53	5.24

Fuel: Excelsior
 Loading: 0.277 kg/m²
 Wind Speed: 1.6 km/h

Total Spread Distance (cm)	Elapsed Time (minutes)		
	Burn # 10	Burn # 13	Burn # 14
0.00	0.00	0.00	0.00
5.00	0.12	0.08	0.06
10.00	0.20	0.22	0.17
15.00	0.28	0.27	0.24
20.00	0.32	0.36	0.29
25.00		0.38	0.34
30.00	0.40	0.42	0.37
45.00	0.48	0.56	0.44
60.00	0.55	0.64	0.50
75.00		0.71	0.54
90.00		0.76	0.55
105.00		0.80	0.58
120.00	0.65	0.82	0.59
135.00		0.85	0.61
150.00	0.77	0.92	0.63
165.00	0.93	1.08	0.68
180.00	1.03	1.16	0.73
195.00	1.12	1.28	0.77
210.00	1.20	1.35	0.82
225.00	1.28	1.46	0.86
240.00	1.40	1.55	0.98
255.00	1.45	1.67	1.08
270.00		1.76	1.17
285.00	1.62	1.85	1.22
300.00	1.70	1.93	1.26
315.00	1.77	2.00	1.33
330.00		2.08	1.38
345.00		2.13	1.40
360.00		2.20	1.41
375.00	2.00	2.26	1.44
390.00		2.31	1.47
435.00	2.22	2.50	1.59
450.00		2.59	1.62
465.00		2.67	1.65
480.00	2.45	2.72	1.75
495.00		2.77	1.80

Fuel: Excelsior
 Loading: 0.277 kg/m²
 Wind speed: 4.8 km/h

Total Spread Distance (cm)	Elapsed Time (minutes)		
	Burn # 11	Burn # 15	Burn # 16
0.00	0.00	0.00	0.00
5.00	0.11	0.09	0.11
10.00	0.15	0.11	0.16
15.00	0.17	0.14	0.20
20.00	0.18	0.17	0.23
25.00	0.20	0.19	0.25
30.00	0.21	0.20	0.26
45.00	0.24	0.25	0.30
60.00	0.30	0.30	0.36
75.00	0.34	0.33	0.42
90.00	0.38	0.36	0.46
105.00	0.40	0.38	0.50
120.00	0.41	0.41	0.52
135.00		0.43	0.53
150.00	0.44	0.44	0.54
165.00	0.48	0.48	0.55
180.00	0.51	0.52	0.57
195.00	0.54	0.54	0.59
210.00	0.55	0.58	0.61
225.00	0.56	0.62	0.62
240.00	0.60	0.64	0.63
255.00		0.66	0.65
270.00	0.64	0.69	0.66
285.00	0.66	0.72	0.67
300.00	0.68		0.69
315.00	0.71		0.74
330.00	0.73	0.76	0.75
345.00	0.76	0.79	0.77
360.00	0.79	0.80	0.80
375.00	0.81	0.82	0.83
390.00	0.83	0.84	0.87
435.00	0.90	0.91	0.95
450.00	0.93		0.96
465.00	0.94	0.97	
480.00	0.95		
495.00	0.96	1.01	1.03

Fuel: Excelsior
 Loading: 0.277 kg/m²
 Wind speed: 8.0 km/h

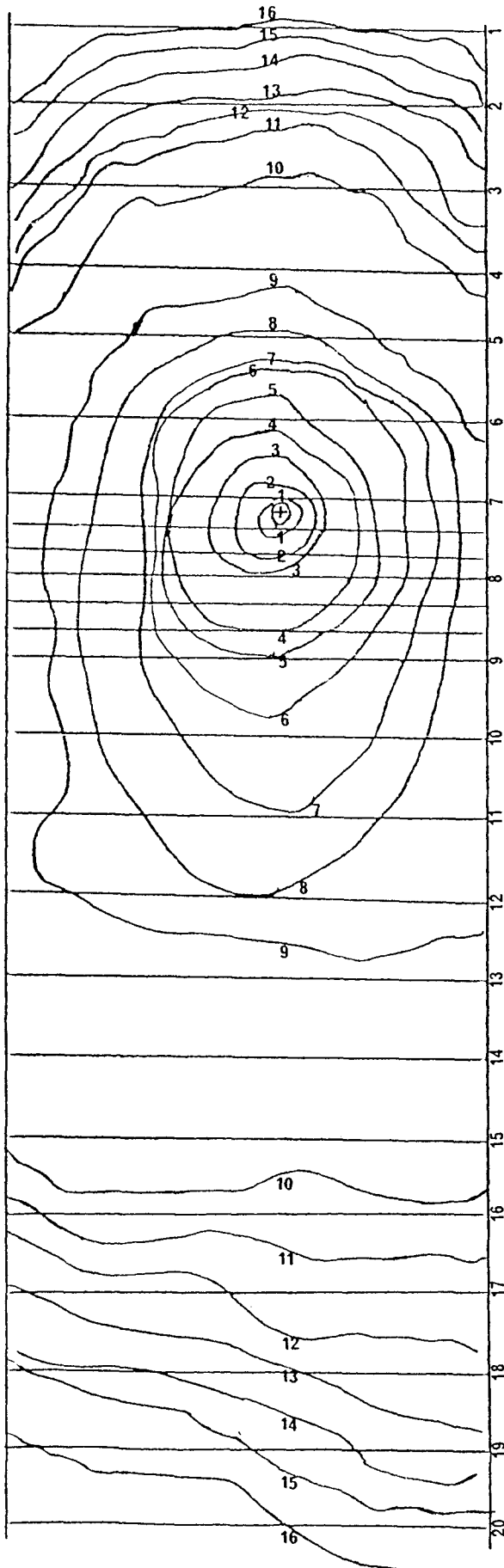
Total Spread Distance (cm)	Elapsed Time (minutes)		
	Burn # 12	Burn # 17	Burn # 18
0.00	0.00	0.00	0.00
5.00		0.08	0.03
10.00		0.11	0.06
15.00	0.08	0.14	0.14
20.00		0.15	0.15
25.00	0.09	0.17	0.17
30.00	0.10	0.19	0.18
45.00	0.16	0.23	0.20
60.00	0.17	0.25	0.21
75.00	0.19	0.27	0.24
90.00	0.21	0.29	0.26
105.00	0.23	0.32	0.28
120.00	0.26	0.33	0.29
135.00	0.29	0.35	
150.00	0.30	0.36	0.32
180.00		0.38	0.33
195.00	0.34		
210.00	0.35	0.42	
225.00	0.37		0.38
240.00		0.44	
270.00			0.43
285.00	0.41	0.48	
315.00	0.44		0.47
330.00		0.52	
345.00			0.49
360.00	0.47		
375.00		0.57	
390.00	0.50		0.53
435.00	0.54	0.61	
465.00			0.60
495.00	0.60	0.65	

APPENDIX II

Fire Perimeter/Time Location Maps

Index to Appendix II.

Fire #	Type of Fuel	Bulk Density (kg/m ³)	Fuel load (kg/m ²)	Wind speed (km/h)	Page No.
24	Needles	26.3	2.0	0.0	127
25	Needles	26.3	2.0	0.0	128
27	Needles	26.3	2.0	0.0	130
1	Needles	26.3	2.0	1.6	106
4	Needles	26.3	2.0	1.6	109
5	Needles	26.3	2.0	1.6	110
3	Needles	26.3	2.0	4.8	108
6	Needles	26.3	2.0	4.8	111
7	Needles	26.3	2.0	4.8	112
2	Needles	26.3	2.0	8.0	107
8	Needles	26.3	2.0	8.0	113
9	Needles	26.3	2.0	8.0	114
23	Needles	13.1	1.0	4.8	126
19	Excelsior	3.6	0.277	0.0	124
20	Excelsior	3.6	0.277	0.0	125
26	Excelsior	3.6	0.277	0.0	129
10	Excelsior	3.6	0.277	1.6	115
13	Excelsior	3.6	0.277	1.6	118
14	Excelsior	3.6	0.277	1.6	119
11	Excelsior	3.6	0.277	4.8	116
15	Excelsior	3.6	0.277	4.8	120
16	Excelsior	3.6	0.277	4.8	121
12	Excelsior	3.6	0.277	8.0	117
17	Excelsior	3.6	0.277	8.0	122
18	Excelsior	3.6	0.277	8.0	123

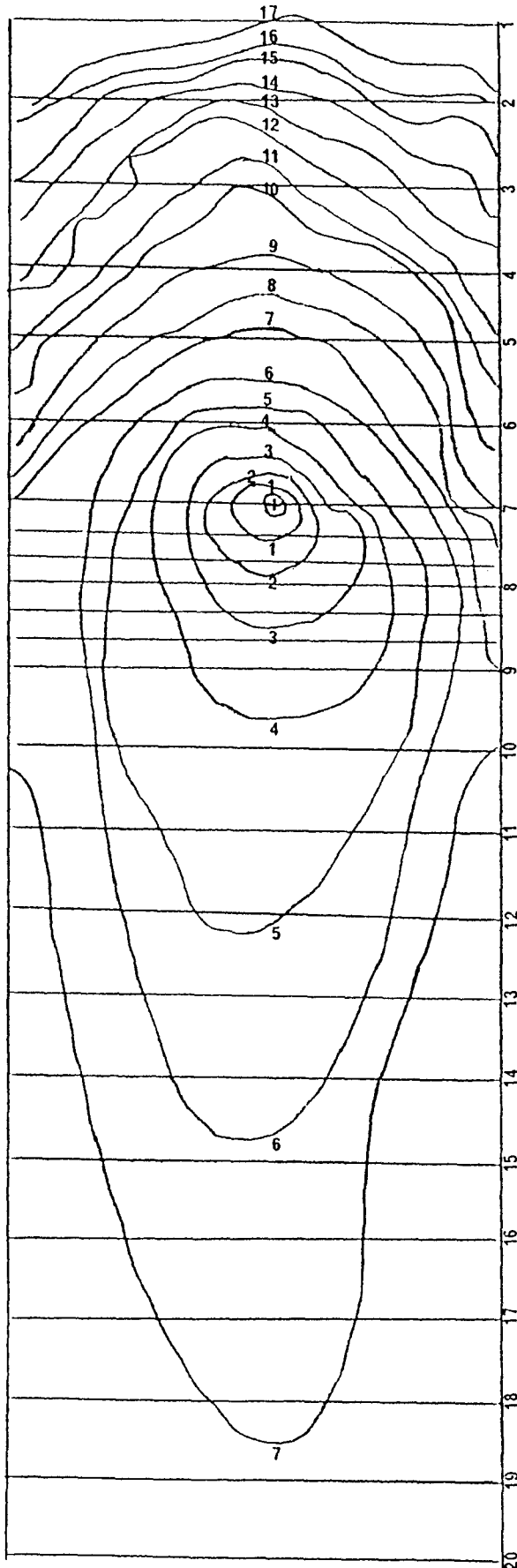


Burn No.: 1
 Fuel: Needles
 Loading: 2 kg/m²
 Wind Speed: 1.6 km/h
 Temp.: 27.6 °C
 % RH: 20.9
 Fuel Moist.: 8.2 %

Perimeter Line Number	Elapsed Time (min:sec)
1	0:15
2	0:30
3	0:45
4	1:00
5	1:15
6	1:30
7	1:45
8	2:01
9	2:15
10	3:28
11	3:45
12	4:00
13	4:15
14	4:31
15	4:45
16	5:00

↓ Wind Direction
 + Ignition Point

Straight, horizontal lines represent string lines stretched across each fuel bed at 15 cm intervals. Between lines 7 and 9, lines are at 5 cm intervals.



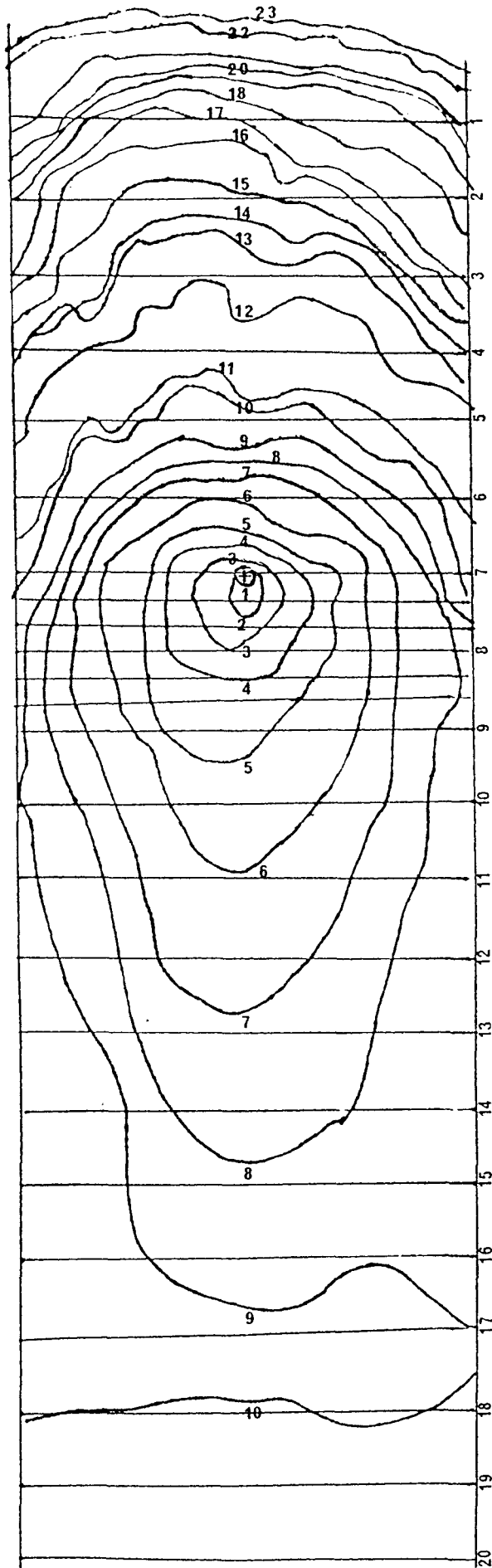
Burn No.: 2
 Fuel: Needles
 Loading: 2 kg/m²
 Wind Speed: 8.0 km/h
 Temp.: 27.6 °C
 % RH: 19.8
 Fuel Moist.: 7.9 %

Perimeter Line Number	Elapsed Time (min:sec)
1	0:17
2	0:30
3	0:45
4	1:01
5	1:15
6	1:30
7	1:45
8	2:00
9	2:17
10	2:30
11	2:45
12	3:00
13	3:14
14	3:30
15	3:45
16	4:01
17	4:23

↓
 Wind Direction

+ Ignition Point

Straight, horizontal lines represent string lines stretched across each fuel bed at 15 cm intervals. Between lines 7 and 9, lines are at 5 cm intervals.

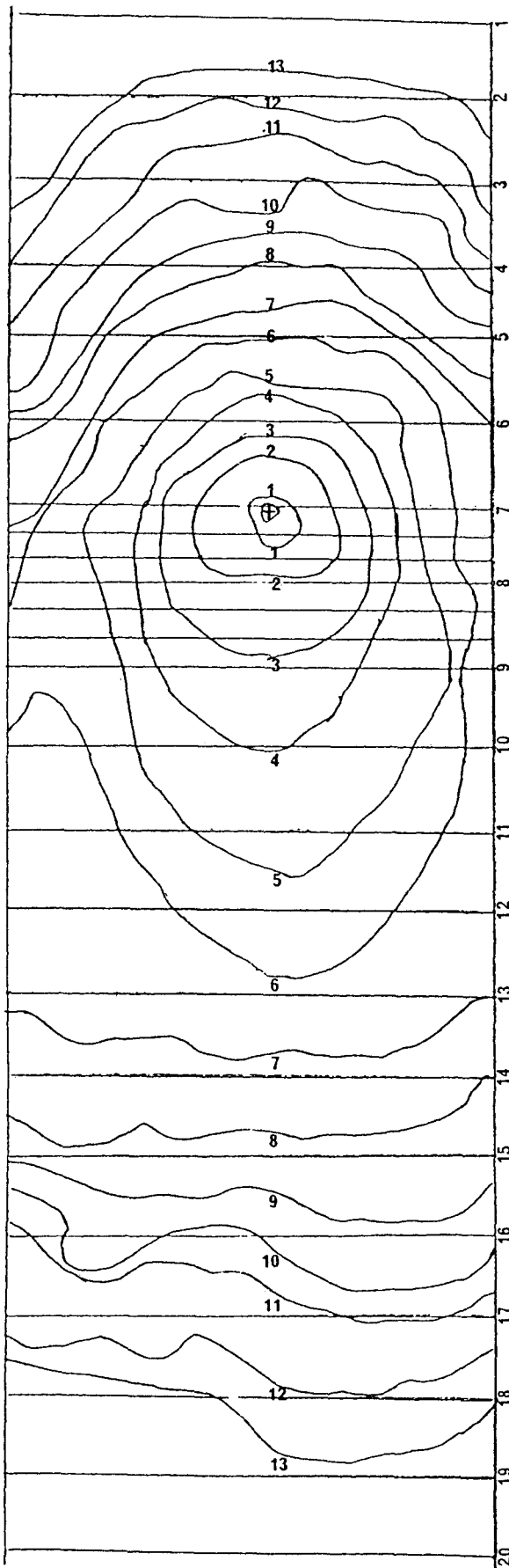


Burn No.: 3
 Fuel: Needles
 Loading: 2 kg/m²
 Wind Speed: 4.8 km/h
 Temp.: 27.3 °C
 % RH: 20.9
 Fuel Moist.: 8.4 %

Perimeter Line Number	Elapsed Time (min:sec)
1	0:14
2	0:29
3	0:44
4	0:59
5	1:14
6	1:29
7	1:47
8	1:59
9	2:15
10	2:29
11	2:44
12	2:59
13	3:14
14	3:30
15	3:44
16	3:59
17	4:14
18	4:29
19	4:44
20	4:59
21	5:15
22	5:29
23	5:44

↓ Wind Direction
 + Ignition Point

Straight, horizontal lines represent string lines stretched across each fuel bed at 15 cm intervals. Between lines 7 and 9, lines are at 5 cm intervals.



Burn No.: 4
 Fuel: Needles
 Loading: 2 kg/m²
 Wind Speed: 1.6 km/h
 Temp.: 27.1 °C
 % RH: 20.9
 Fuel Moist.: 8.1 %

Perimeter Line Number	Elapsed Time (min:sec)
1	0:15
2	0:40
3	1:01
4	1:20
5	1:40
6	2:00
7	2:20
8	2:40
9	3:00
10	3:21
11	3:40
12	4:00
13	4:20

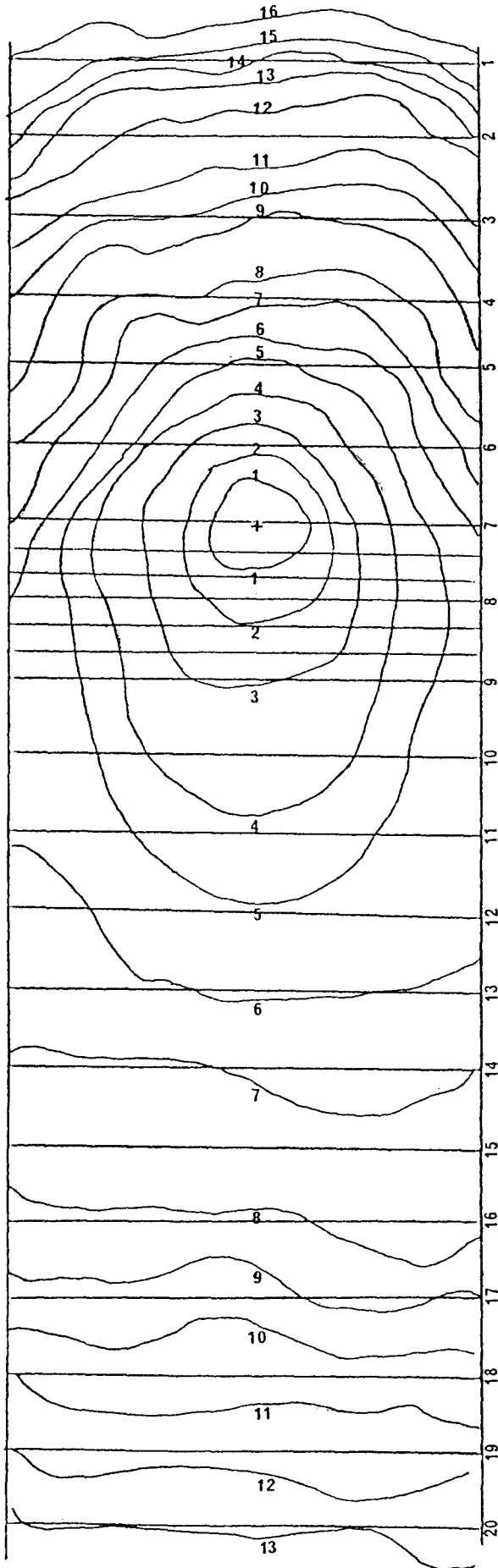
↓
 Wind Direction

+ Ignition Point

Straight, horizontal lines represent string lines stretched across each fuel bed at 15 cm intervals. Between lines 7 and 9, lines are at 5 cm intervals.

Burn No.: 5
 Fuel: Needles
 Loading: 2 kg/m²
 Wind Speed: 1.6 km/h
 Temp.: 26.9 °C
 % RH: 20.5
 Fuel Moist.: 8.2 %

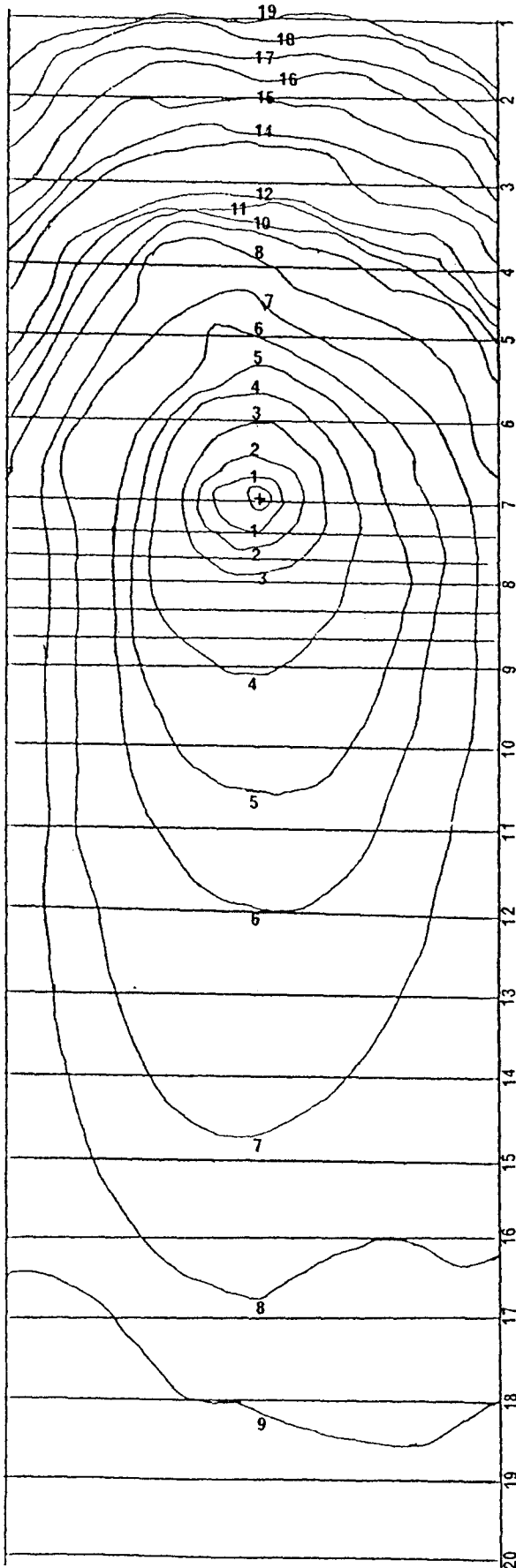
Perimeter Line Number	Elapsed Time (min:sec)
1	0:40
2	1:00
3	1:20
4	1:40
5	2:00
6	2:20
7	2:40
8	3:00
9	3:21
10	3:40
11	4:01
12	4:20
13	4:43
14	5:00
15	5:20
16	5:40



↓ Wind Direction

+ Ignition Point

Straight, horizontal lines represent string lines stretched across each fuel bed at 15 cm intervals. Between lines 7 and 9, lines are at 5 cm intervals.



Burn No.: 6
 Fuel: Needles
 Loading: 2 kg/m²
 Wind Speed: 4.8 km/h
 Temp.: 27.3 °C
 % RH: 20.0
 Fuel Moist.: 7.7 %

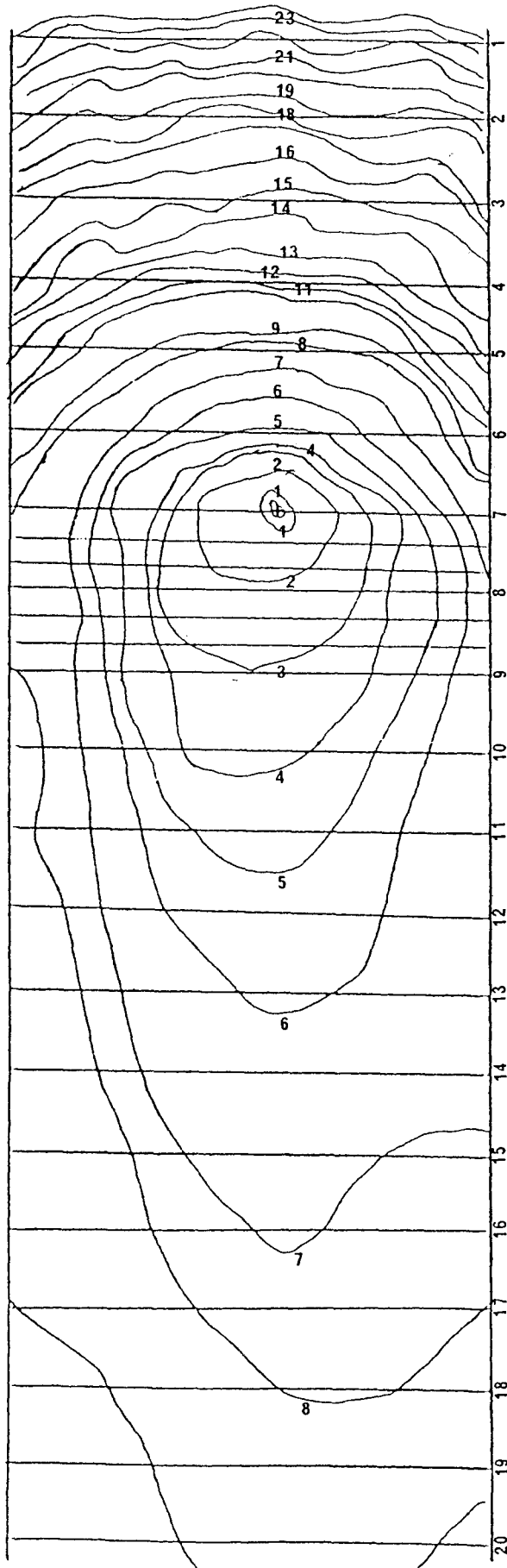
Perimeter Line Number	Elapsed Time (min:sec)
1	0:16
2	0:30
3	0:46
4	1:01
5	1:16
6	1:31
7	1:48
8	2:01
9	2:15
10	2:31
11	2:46
12	3:00
13	3:15
14	3:30
15	3:46
16	4:01
17	4:17
18	4:30
19	4:45

↓ Wind Direction
 + Ignition Point

Straight, horizontal lines represent string lines stretched across each fuel bed at 15 cm intervals. Between lines 7 and 9, lines are at 5 cm intervals.

Burn No.: 7
 Fuel: Needles
 Loading: 2 kg/m²
 Wind Speed: 4.8 km/h
 Temp.: 26.9 °C
 % RH: 19.9
 Fuel Moist.: 8.8 %

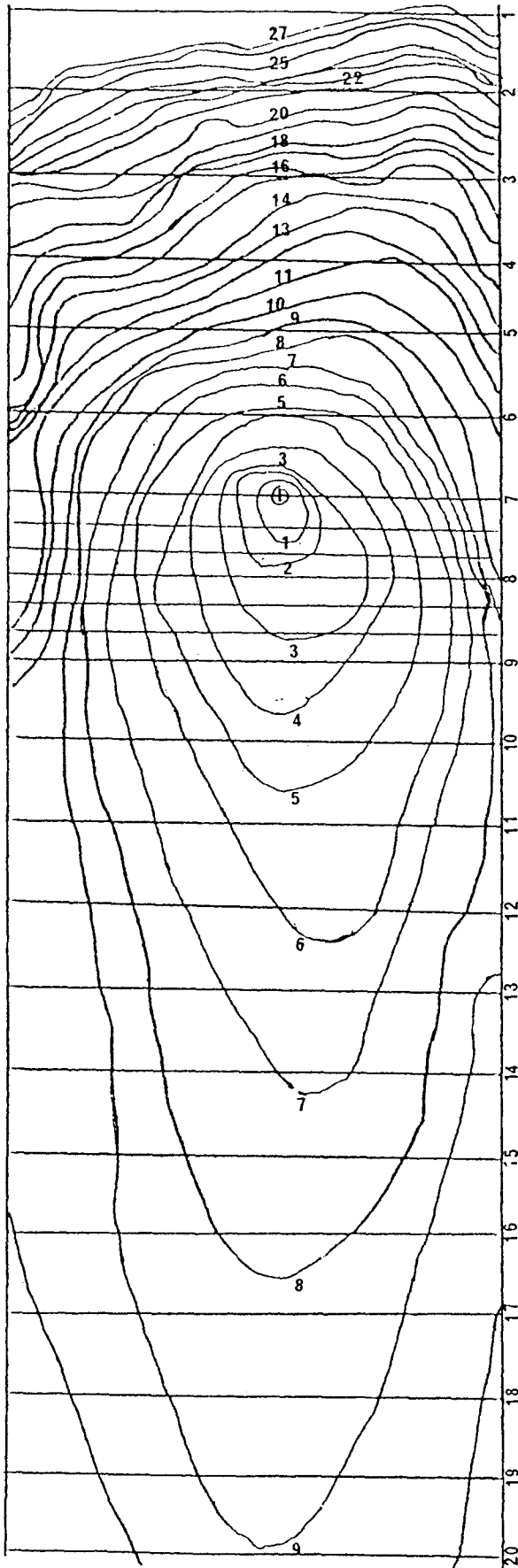
Perimeter Line Number	Elapsed Time (min:sec)
1	0:09
2	0:34
3	0:49
4	1:04
5	1:19
6	1:34
7	1:49
8	2:04
9	2:19
10	2:34
11	2:50
12	3:04
13	3:19
14	3:34
15	3:49
16	4:04
17	4:19
18	4:34
19	4:50
20	5:04
21	5:19
22	5:34
23	5:49
24	6:04



↓ Wind Direction

+ Ignition Point

Straight, horizontal ...



Burn No.: 8
 Fuel: Needles
 Loading: 2 kg/m²
 Wind Speed: 8.0 km/h
 Temp.: 27.0 °C
 % RH: 21.3
 Fuel Moist.: 8.4 %


Perimeter Line Number	Elapsed Time (min:sec)
1	0:14
2	0:24
3	0:34
4	0:44
5	0:54
6	1:04
7	1:14
8	1:24
9	1:34
10	1:44
11	1:54
12	2:04
13	2:14
14	2:24
15	2:34
16	2:44
17	2:54
18	3:04
19	3:14
20	3:24
21	3:34
22	3:44
23	3:54
24	4:04
25	4:14
26	4:24
27	4:34
28	4:44

↓ Wind Direction
 + Ignition Point

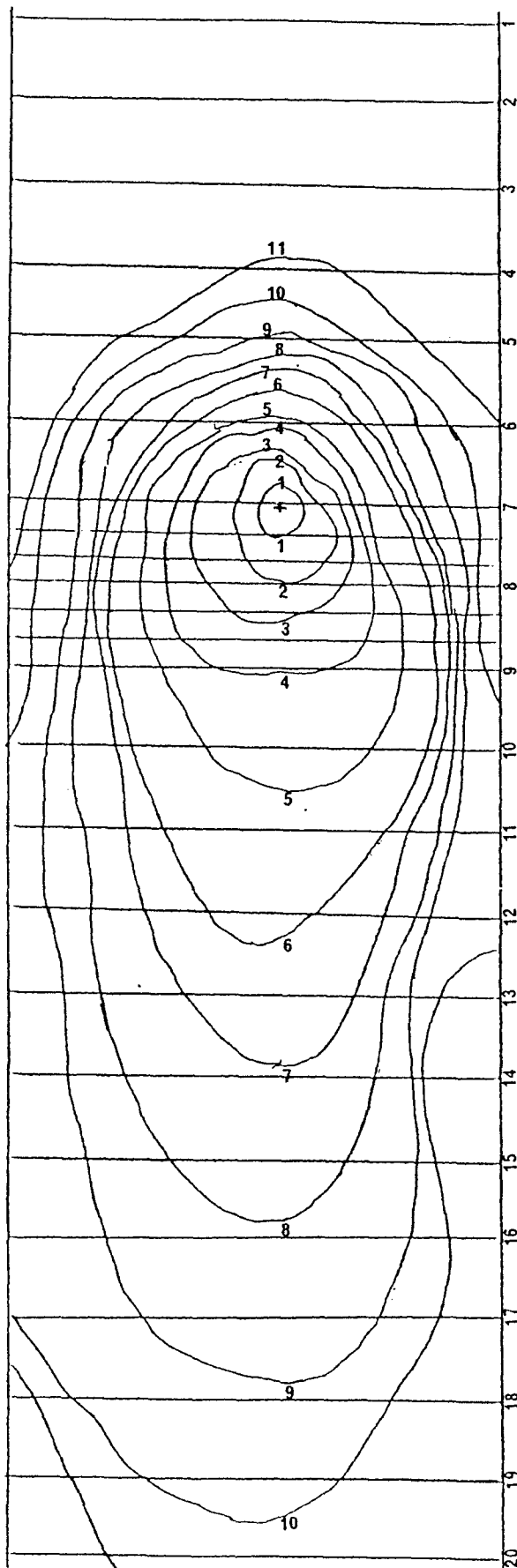
Straight, horizontal ...

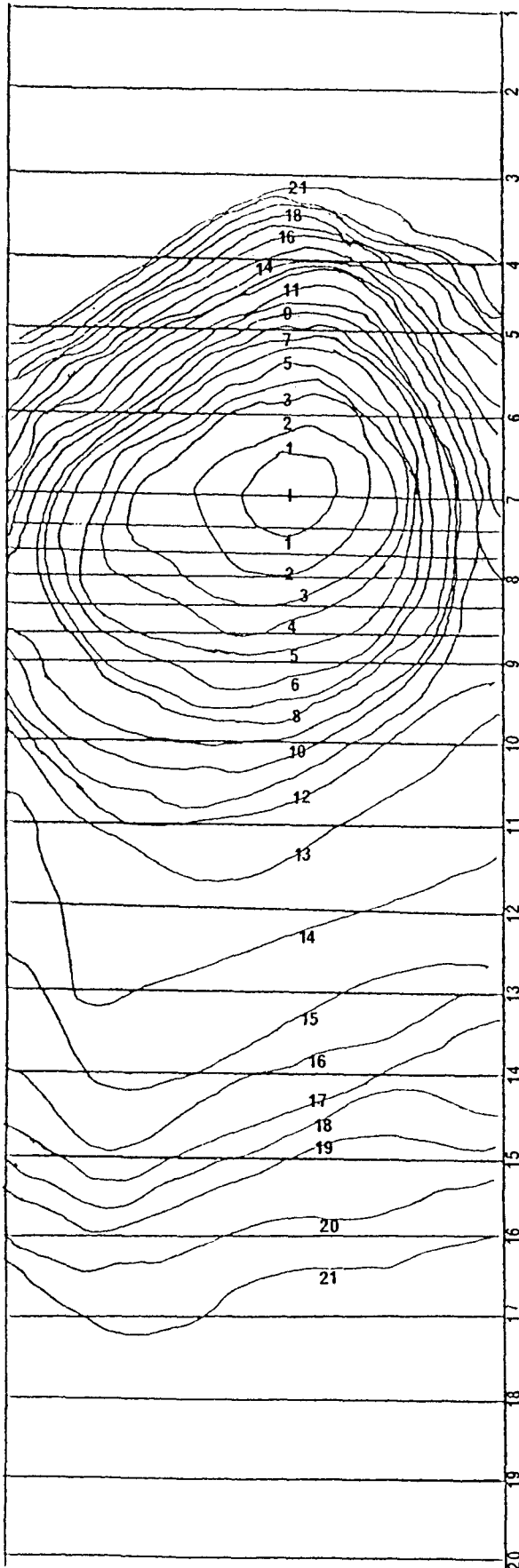
Burn No.: 9
 Fuel: Needles
 Loading: 2 kg/m²
 Wind Speed: 8.0 km/h
 Temp.: 27.8 °C
 % RH: 19.7
 Fuel Moist.: 8.3 %

Perimeter Line Number	Elapsed Time (min:sec)
1	0:08
2	0:26
3	0:36
4	0:46
5	0:56
6	1:06
7	1:16
8	1:26
9	1:36
10	1:46
11	1:56

 Wind Direction
 + Ignition Point

Straight, horizontal
 lines represent string
 lines stretched across
 each fuel bed at 15 cm
 intervals. Between lines
 7 and 9, lines are at 5
 cm intervals.



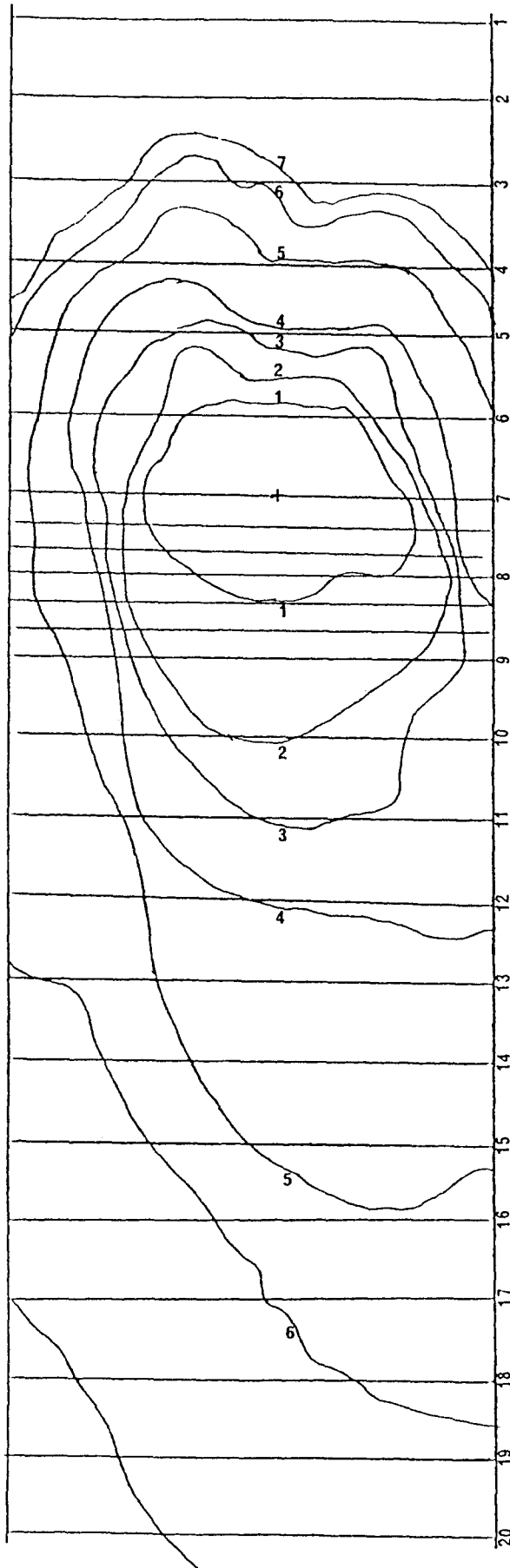


Burn No.: 10
 Fuel: Excelsior
 Loading: 0.277 kg/m²
 Wind Speed: 1.6 km/h
 Temp.: 27.2 °C
 % RH: 21.3
 Fuel Moist.: 7.1 %

Perimeter Line Number	Elapsed Time (min:sec)
1	0:09
2	0:15
3	0:19
4	0:21
5	0:24
6	0:25
7	0:27
8	0:28
9	0:29
10	0:30
11	0:32
12	0:33
13	0:34
14	0:36
15	0:37
16	0:39
17	0:40
18	0:42
19	0:43
20	0:45
21	0:48

↓ Wind Direction
 + Ignition Point

Straight, horizontal
 lines represent string
 lines stretched across
 each fuel bed at 15 cm
 intervals. Between lines
 7 and 9, lines are at 5
 cm intervals.



Burn No.: 11
 Fuel: Excelsior
 Loading: 0.277 kg/m²
 Wind Speed: 4.8 km/h
 Temp.: 27.0 °C
 % RH: 20.4
 Fuel Moist.: 6.4 %

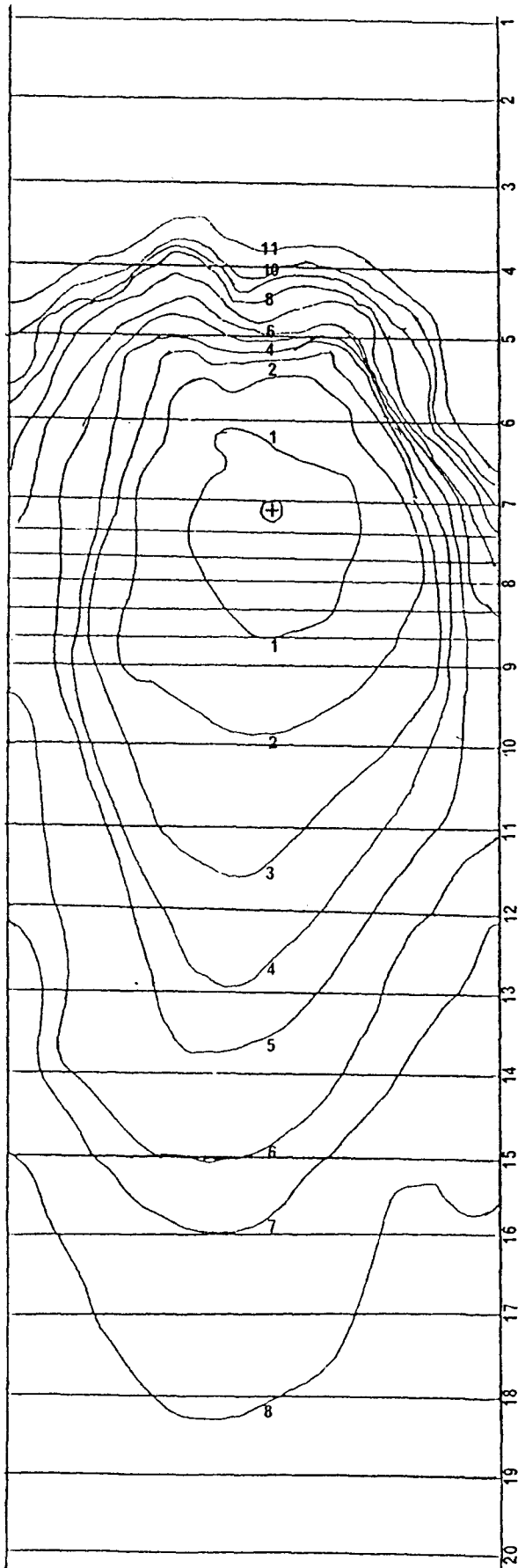
Perimeter Line Number	Elapsed Time (min:sec)
1	0:10
2	0:14
3	0:17
4	0:20
5	0:25
6	0:29
7	0:31

↓ Wind Direction
 + Ignition Point

Straight, horizontal lines represent string lines stretched across each fuel bed at 15 cm intervals. Between lines 7 and 9, lines are at 5 cm intervals.

Burn No.: 12
 Fuel: Excelsior
 Loading: 0.277 kg/m²
 Wind Speed: 8.0 km/h
 Temp.: 27.2 °C
 % RH: 19.9
 Fuel Moist.: 6.4 %

Perimeter Line Number	Elapsed Time (min:sec)
1	0:06
2	0:09
3	0:11
4	0:12
5	0:14
6	0:16
7	0:17
8	0:19
9	0:20
10	0:22
11	0:24



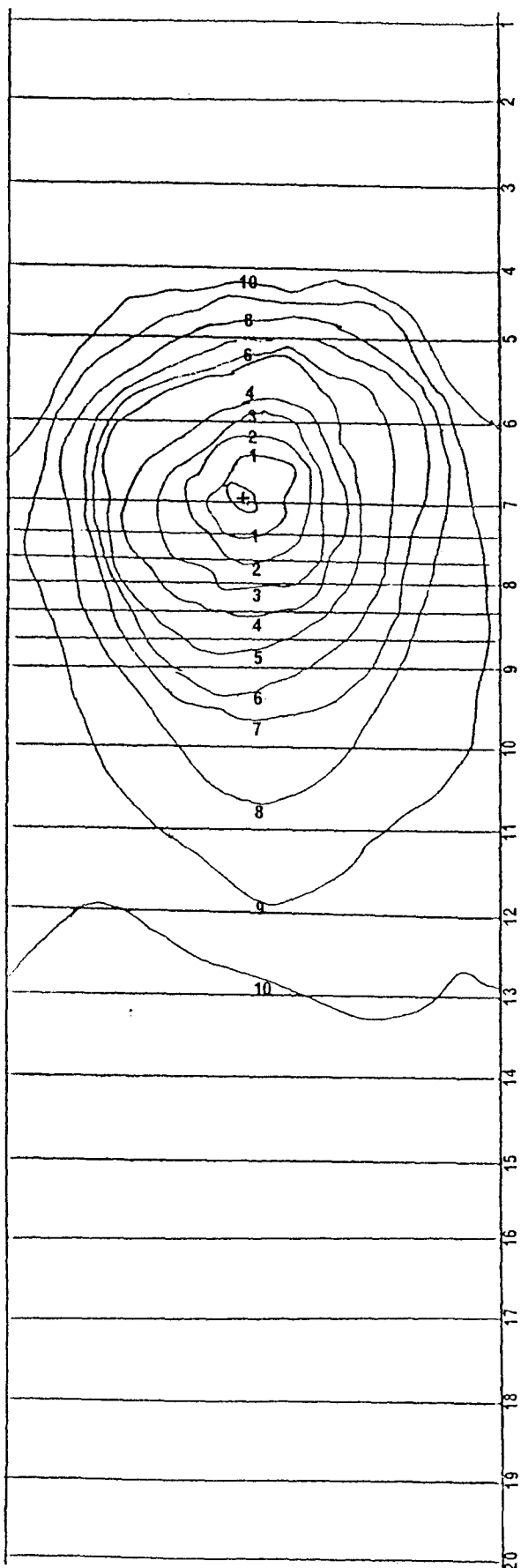
↓
 Wind Direction

+ Ignition Point

Straight, horizontal lines represent string lines stretched across each fuel bed at 15 cm intervals. Between lines 7 and 9, lines are at 5 cm intervals.

Burn No.: 13
 Fuel: Excelsior
 Loading: 0.277 kg/m²
 Wind Speed: 1.6 km/h
 Temp.: 27.3 °C
 % RH: 21.3
 Fuel Moist.: 6.6 %

Perimeter Line Number	Elapsed Time (min:sec)
1	0:08
2	0:13
3	0:18
4	0:22
5	0:26
6	0:30
7	0:33
8	0:37
9	0:41
10	0:46



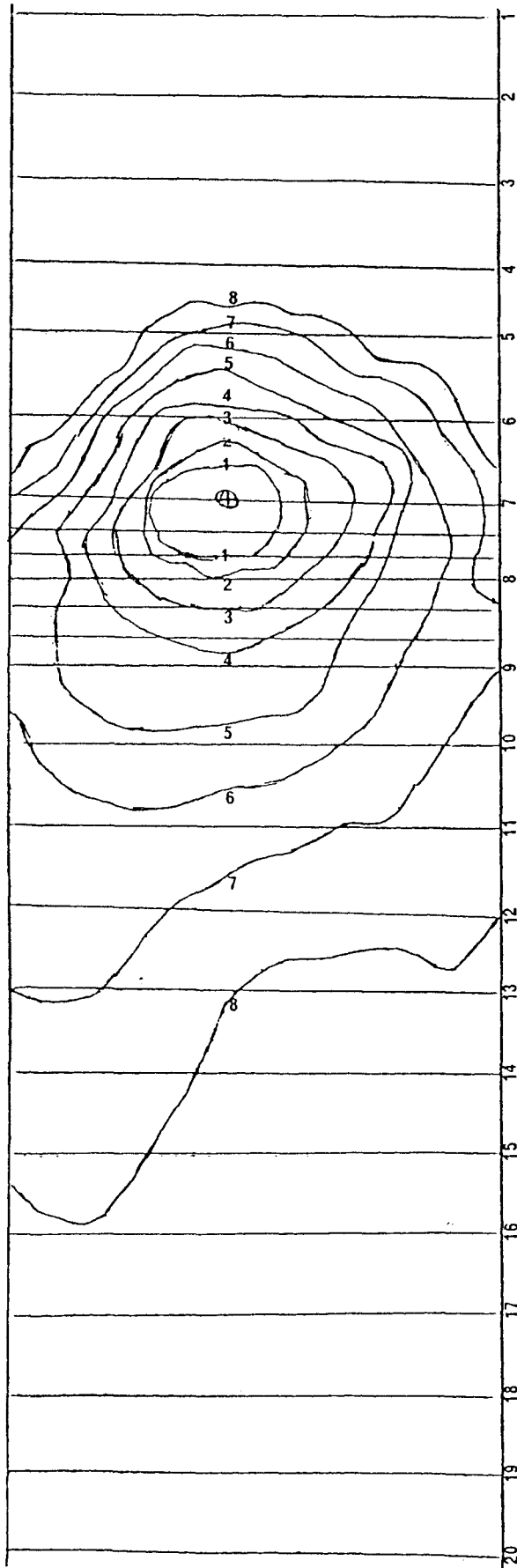
↓ Wind Direction

+ Ignition Point

Straight, horizontal lines represent string lines stretched across each fuel bed at 15 cm intervals. Between lines 7 and 9, lines are at 5 cm intervals.

Burn No.: 14
 Fuel: Excelsior
 Loading: 0.277 kg/m²
 Wind Speed: 1.6 km/h
 Temp.: 27.9 °C
 % RH: 20.1
 Fuel Moist.: 5.6 %

Perimeter Line Number	Elapsed Time (min:sec)
1	0:08
2	0:12
3	0:17
4	0:21
5	0:25
6	0:29
7	0:32
8	0:36



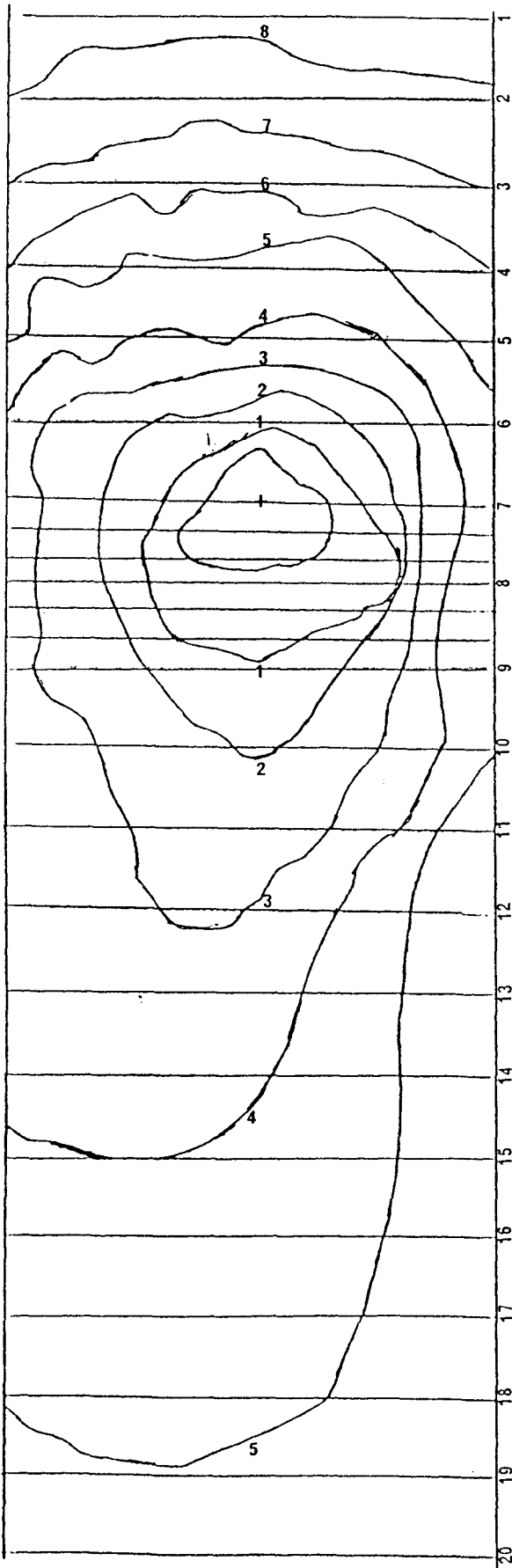
↓ Wind Direction

+ Ignition Point

Straight, horizontal lines represent string lines stretched across each fuel bed at 15 cm intervals. Between lines 7 and 9, lines are at 5 cm intervals.

Burn No.: 15
 Fuel: Excelsior
 Loading: 0.277 kg/m²
 Wind Speed: 4.8 km/h
 Temp.: 27.3 °C
 % RH: 20.4
 Fuel Moist.: 6.2 %

Perimeter Line Number	Elapsed Time (min:sec)
1	0:12
2	0:16
3	0:21
4	0:25
5	0:31
6	0:41
7	1:07
8	1:27

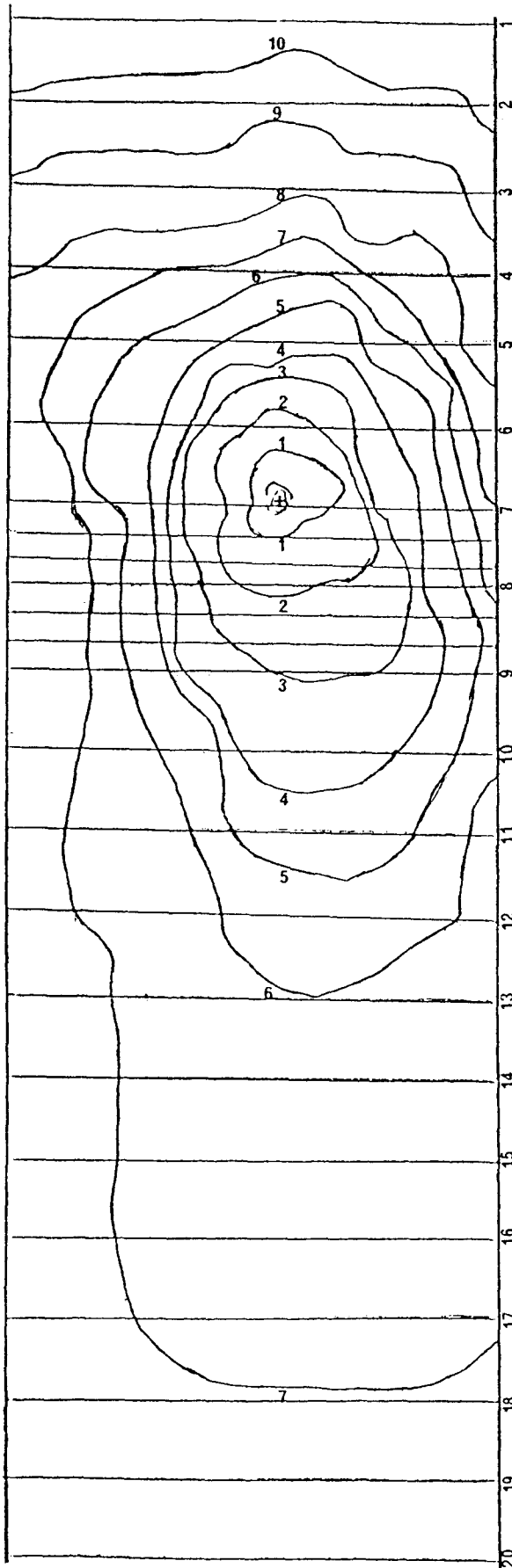


↓ Wind Direction
 + Ignition Point

Straight, horizontal lines represent string lines stretched across each fuel bed at 15 cm intervals. Between lines 7 and 9, lines are at 5 cm intervals.

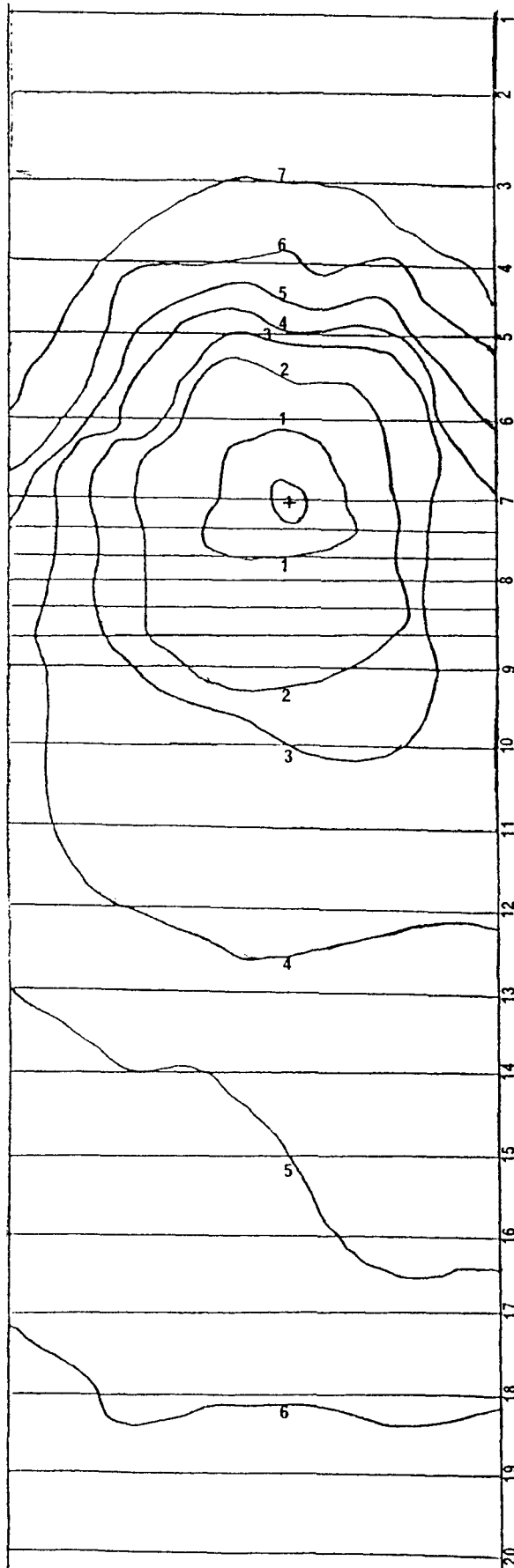
Burn No.: 16
 Fuel: Excelsior
 Loading: 0.277 kg/m²
 Wind Speed: 4.8 km/h
 Temp.: 27.4 °C
 % RH: 20.8
 Fuel Moist.: 5.5 %

Perimeter Line Number	Elapsed Time (min:sec)
1	0:07
2	0:11
3	0:15
4	0:19
5	0:23
6	0:28
7	0:33
8	0:41
9	0:54
10	1:10




↓ Wind Direction
 + Ignition Point

Straight, horizontal lines represent string lines stretched across each fuel bed at 15 cm intervals. Between lines 7 and 9, lines are at 5 cm intervals.



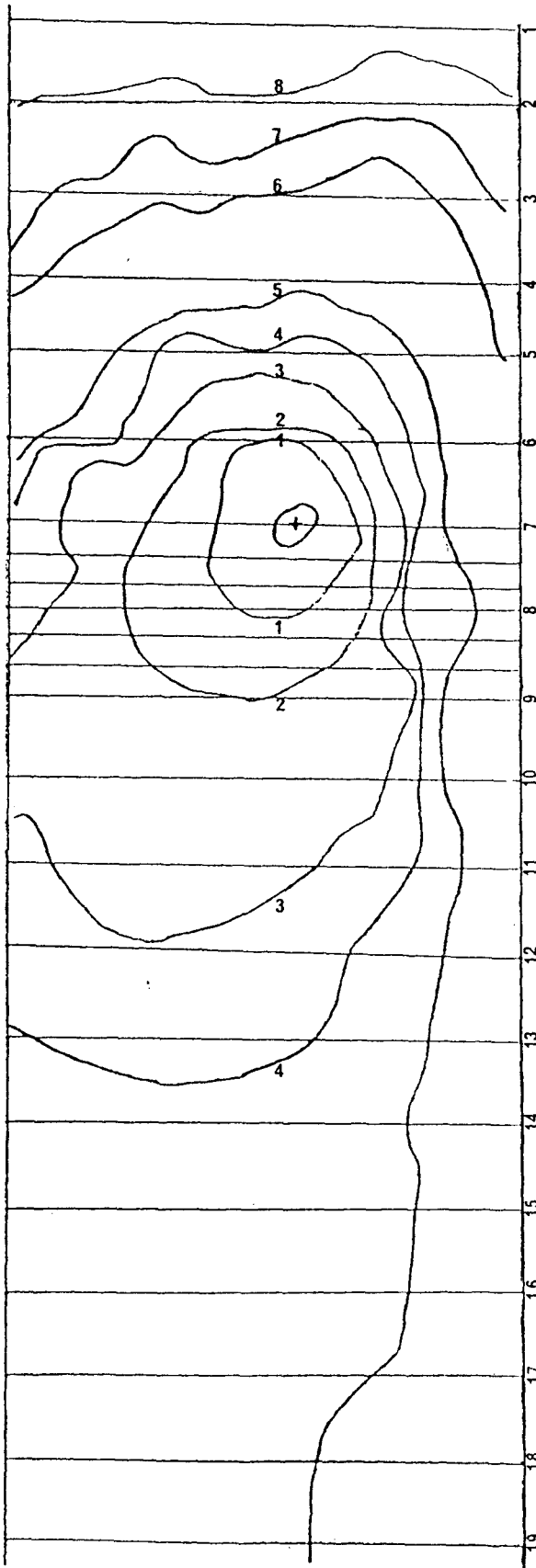
Burn No.: 17
 Fuel: Excelsior
 Loading: 0.277 kg/m²
 Wind Speed: 8.0 km/h
 Temp.: 27.3 °C
 % RH: 19.6
 Fuel Moist.: 5.4 %

Perimeter Line Number	Elapsed Time (min:sec)
1	0:06
2	0:11
3	0:14
4	0:16
5	0:19
6	0:22
7	0:25

 Wind Direction

 + Ignition Point

Straight, horizontal
 lines represent string
 lines stretched across
 each fuel bed at 15 cm
 intervals. Between lines
 7 and 9, lines are at 5
 cm intervals.

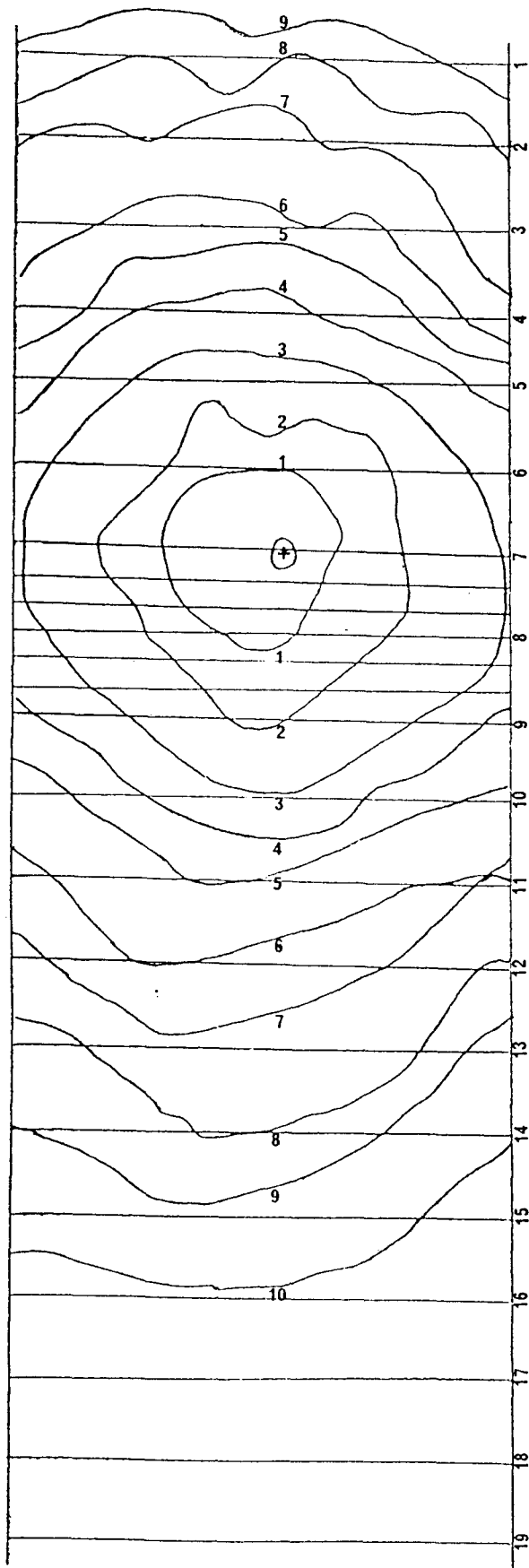


Burn No.: 18
 Fuel: Excelsior
 Loading: 0.277 kg/m²
 Wind Speed: 8.0 km/h
 Temp.: 27.6 °C
 % RH: 19.9
 Fuel Moist.: 6.7 %

Perimeter Line Number	Elapsed Time (min:sec)
1	0:05
2	0:11
3	0:14
4	0:17
5	0:23
6	0:39
7	0:53
8	1:15

↓ Wind Direction
 + Ignition Point

Straight, horizontal
 lines represent string
 lines stretched across
 each fuel bed at 15 cm
 intervals. Between lines
 7 and 9, lines are at 5
 cm intervals.

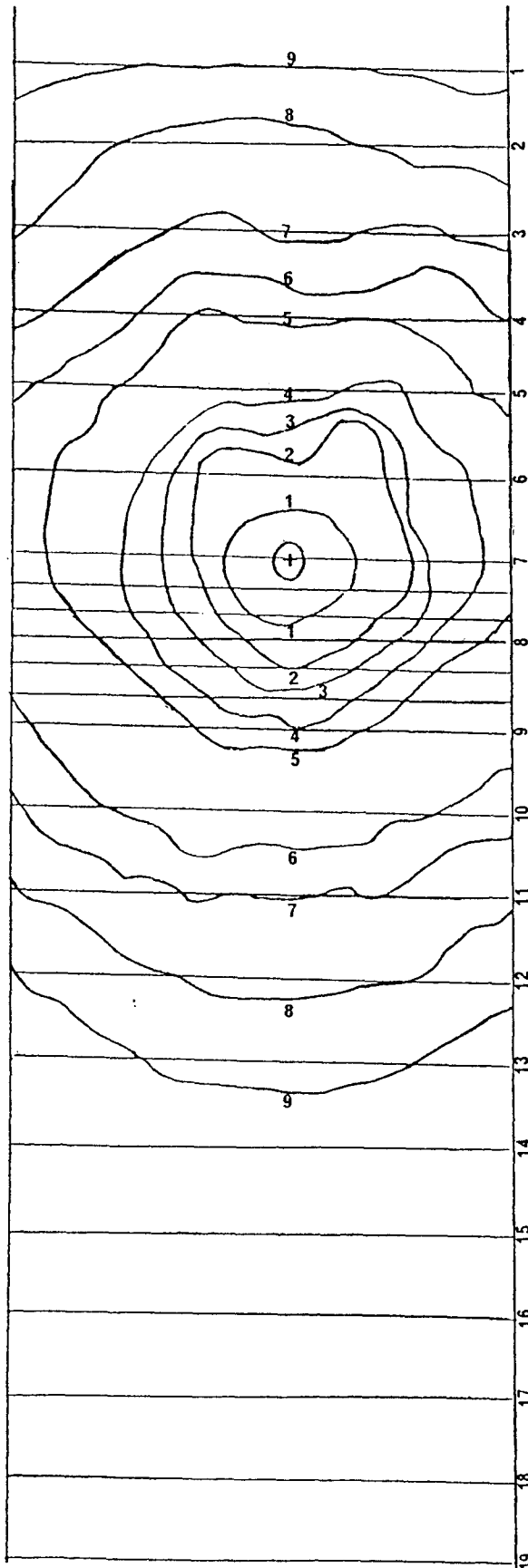


Burn No.: 19
 Fuel: Excelsior
 Loading: 0.277 kg/m²
 Wind Speed: 0.0 km/h
 Temp.: 27.6 °C
 % RH: 20.8
 Fuel Moist.: 5.5 %

Perimeter Line Number	Elapsed Time (min:sec)
1	0:15
2	0:25
3	0:34
4	0:43
5	0:51
6	1:01
7	1:10
8	1:21
9	1:29
10	1:40

↓ Wind Direction
 + Ignition Point

Straight, horizontal lines represent string lines stretched across each fuel bed at 15 cm intervals. Between lines 7 and 9, lines are at 5 cm intervals.



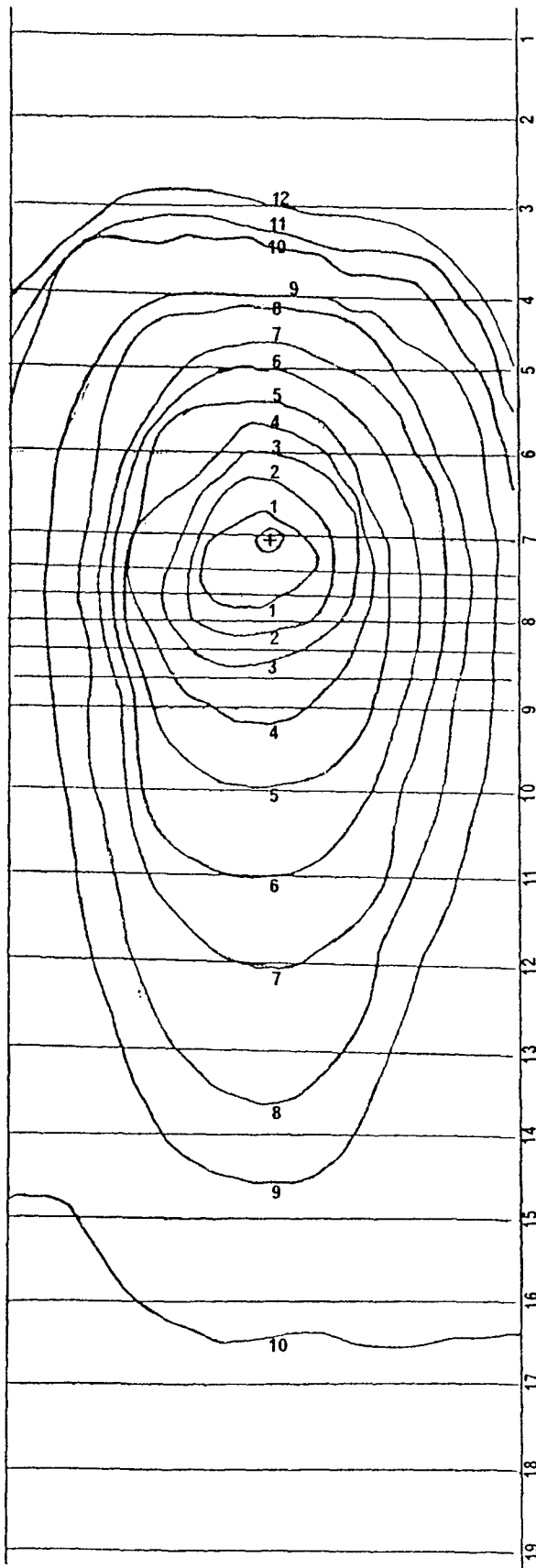
Burn No.: 20
 Fuel: Excelsior
 Loading: 0.277 kg/m²
 Wind Speed: 0.0 km/h
 Temp.: 26.9 °C
 % RH: 20.8
 Fuel Moist.: 6.9 %

Perimeter Line Number	Elapsed Time (min:sec)
1	0:10
2	0:18
3	0:23
4	0:29
5	0:39
6	0:53
7	1:03
8	1:18
9	1:33

↓
 Wind Direction

+ Ignition Point

Straight, horizontal lines represent string lines stretched across each fuel bed at 15 cm intervals. Between lines 7 and 9, lines are at 5 cm intervals.

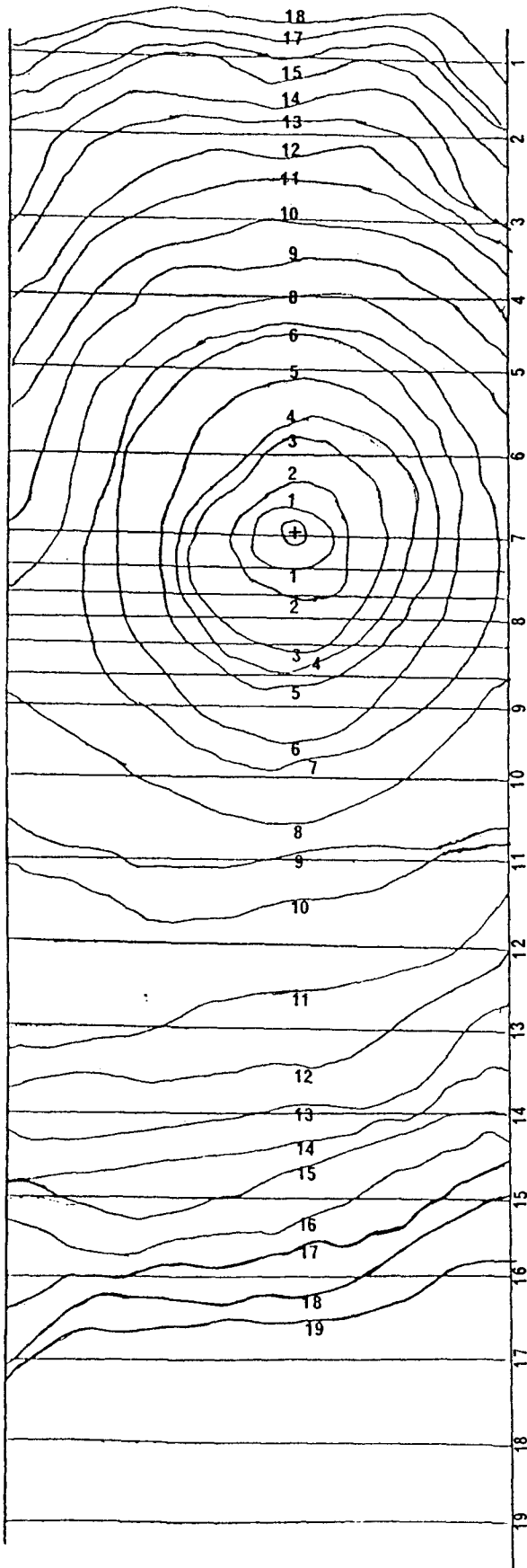


Burn No.: 23
 Fuel: Needles
 Loading: 1 kg/m²
 Wind Speed: 4.8 km/h
 Temp.: 27.6 °C
 % RH: 21.2
 Fuel Moist.: 8.7 %

Perimeter Line Number	Elapsed Time (min:sec)
1	0:15
2	0:25
3	0:35
4	0:45
5	0:55
6	1:05
7	1:14
8	1:30
9	1:45
10	2:00
11	2:15
12	2:30

↓ Wind Direction
 + Ignition Point

Straight, horizontal lines represent string lines stretched across each fuel bed at 15 cm intervals. Between lines 7 and 9, lines are at 5 cm intervals.

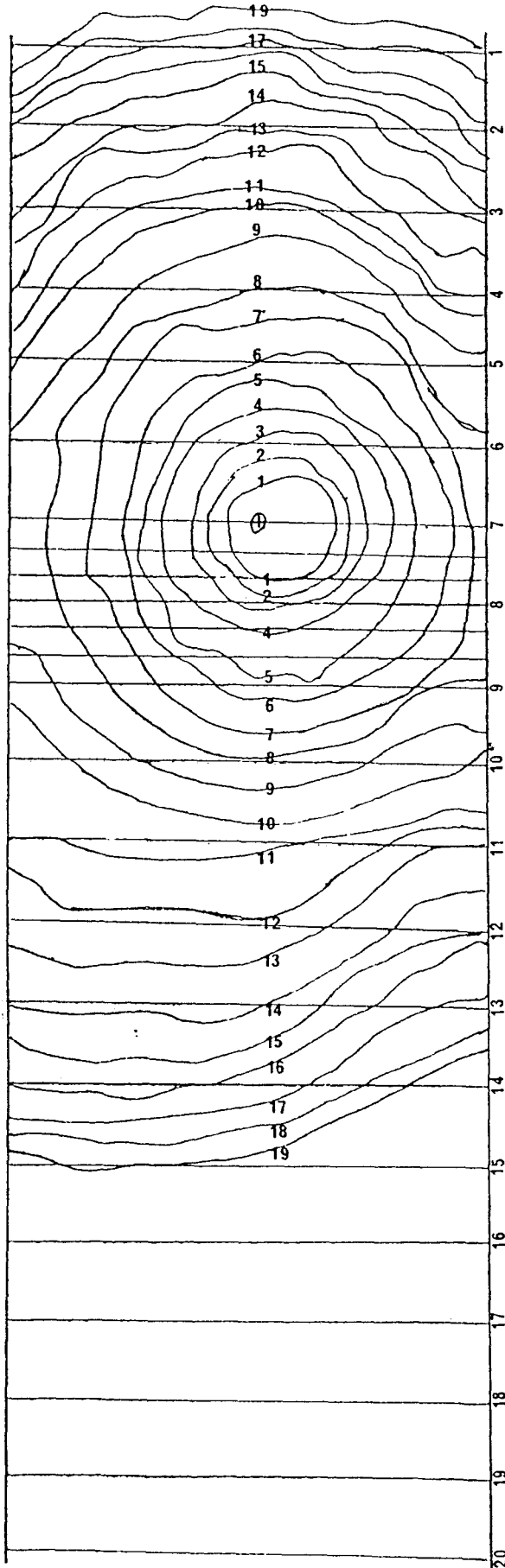


Burn No.: 24
 Fuel: Needles
 Loading: 2 kg/m²
 Wind Speed: 0.0 km/h
 Temp.: 27.4 °C
 % RH: 20.4
 Fuel Moist.: 9.97 %

Perimeter Line Number	Elapsed Time (min:sec)
1	0:17
2	0:32
3	0:47
4	1:02
5	1:19
6	1:32
7	1:47
8	2:02
9	2:17
10	2:32
11	2:47
12	3:02
13	3:17
14	3:32
15	3:47
16	4:02
17	4:17
18	4:32
19	4:47

↓ Wind Direction
 + Ignition Point

Straight, horizontal lines represent string lines stretched across each fuel bed at 15 cm intervals. Between lines 7 and 9, lines are at 5 cm intervals.

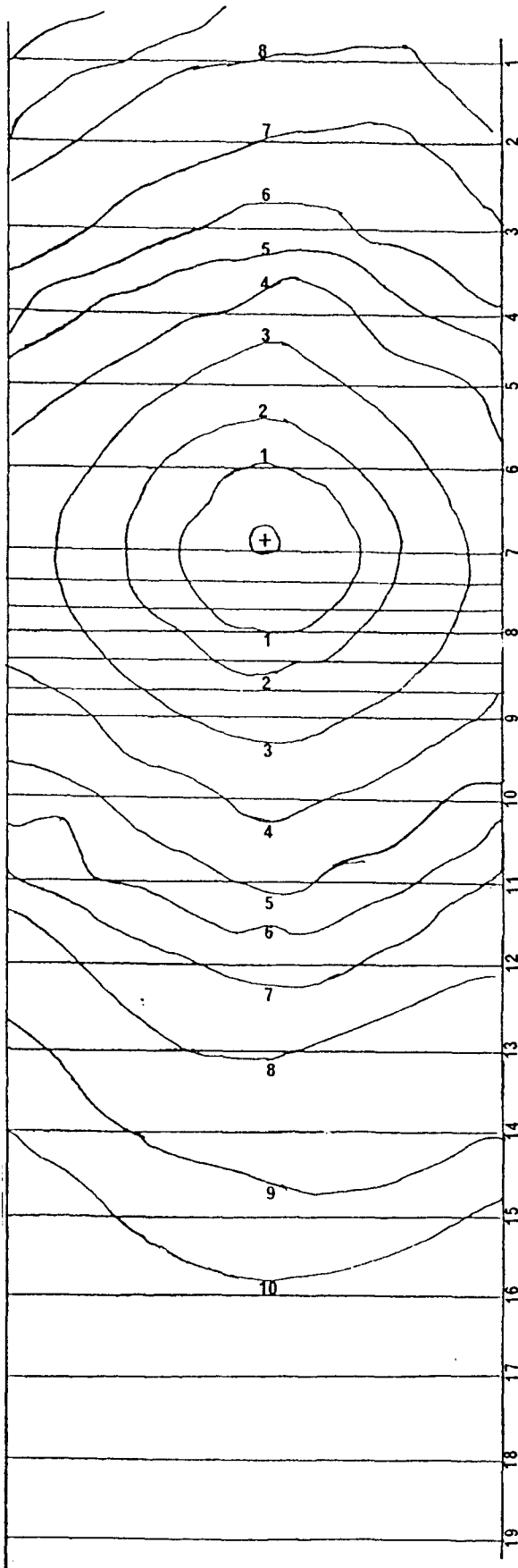


Burn No.: 25
 Fuel: Needles
 Loading: 2 kg/m²
 Wind Speed: 0.0 km/h
 Temp.: 27.1 °C
 % RH: 20.9
 Fuel Moist.: 9.4 %

Perimeter Line Number	Elapsed Time (min:sec)
1	0:59
2	1:14
3	1:29
4	1:44
5	2:02
6	2:14
7	2:29
8	2:44
9	2:59
10	3:14
11	3:29
12	3:44
13	3:59
14	4:15
15	4:29
16	4:44
17	4:59
18	5:14
19	5:29

↓ Wind Direction
 + Ignition Point

Straight, horizontal lines represent string lines stretched across each fuel bed at 15 cm intervals. Between lines 7 and 9, lines are at 5 cm intervals.



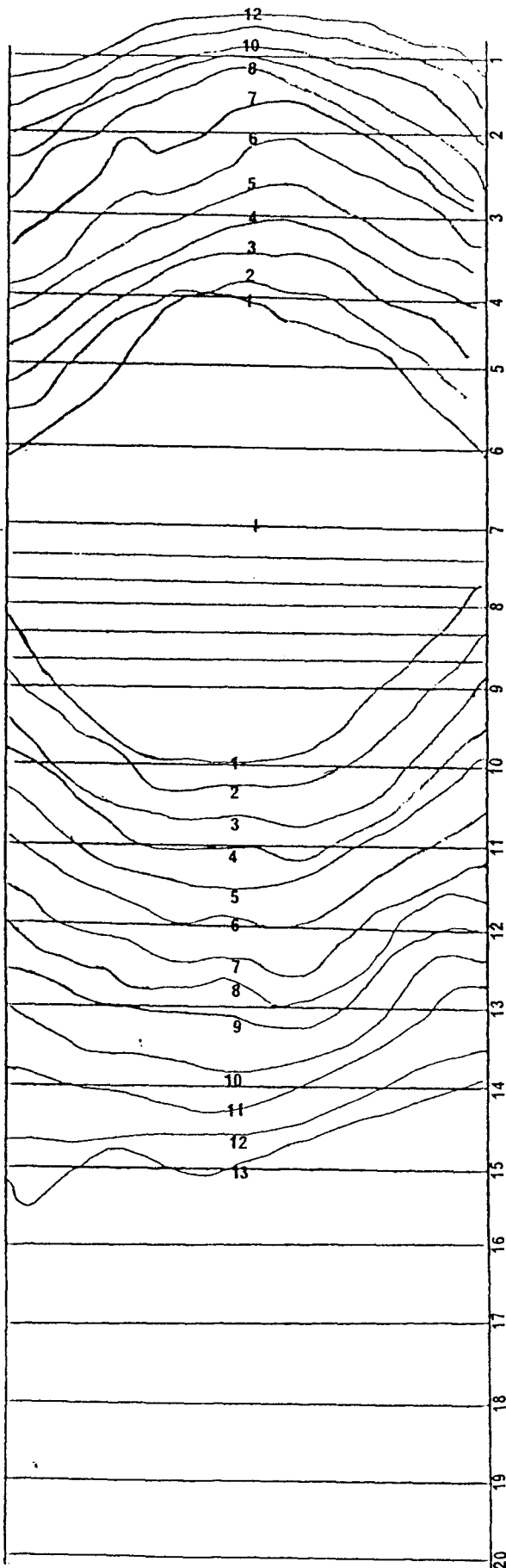
Burn No.: 26
 Fuel: Excelsior
 Loading: 0.277 kg/m²
 Wind Speed: 0.0 km/h
 Temp.: 27.3 °C
 % RH: 21.0
 Fuel Moist.: 8.6 %

Perimeter Line Number	Elapsed Time (min:sec)
1	0:17
2	0:24
3	0:34
4	0:44
5	0:54
6	1:01
7	1:09
8	1:19
9	1:29
10	1:40

↓
 Wind Direction

+ Ignition Point

Straight, horizontal lines represent string lines stretched across each fuel bed at 15 cm intervals. Between lines 7 and 9, lines are at 5 cm intervals.



Burn No.: 27
 Fuel: Needles
 Loading: 2 kg/m²
 Wind Speed: 0.0 km/h
 Temp.: 27.0 °C
 % RH: 21.4
 Fuel Moist.: 8.7 %

Perimeter Line Number	Elapsed Time (min:sec)
1	2:31
2	2:46
3	3:01
4	3:16
5	3:32
6	3:46
7	4:01
8	4:17
9	4:31
10	4:46
11	5:01
12	5:16
13	5:31

↓
 Wind Direction

+ Ignition Point

Straight, horizontal lines represent string lines stretched across each fuel bed at 15 cm intervals. Between lines 7 and 9, lines are at 5 cm intervals.